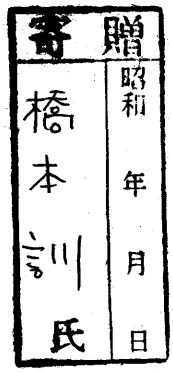

STUDIES ON CHEMICAL REACTIONS BY USE OF MATRIX ISOLATION SPECTROSCOPY

CT Excited Photochemical Reactions of Unsaturated Organic Molecules in Cryogenic Oxygen Matrices

and

The Direct Spectroscopic Detection of HSO_x Radicals as Reaction Intermediates of Atmospheric Importance

by

SATOSHI HASHIMOTO

PREFACE

The matrix isolation method has been actively developed in the last 30 years. Nowadays, it has become to be one of a standard technique widely used in the field of spectroscopy. By use of this method, many transient species and unstable molecules have been investigated with interest mainly in the molecular structures. In these studies, the matrix is used as an inert media in which the trapped species is hoped to be isolated energetically from other molecules. Low temperature efficiently prevent thermal decomposition and isomerization of the trapped species. On the other hand, it has become to be of interest in the last 10 years that use of low temperature matrix as a field of chemical reactions. For this approach, reactive materials are used as matrix molecules as well as nonreactive compounds. Many investigations have been reported, some of which were found to be specific reactions in the cryogenic matrix. Thus, low temperature matrix could be used either for preventing and for promoting chemical reactions.

Here, application of these two different characters of matrix to study chemical reactions will be investigated. One is that matrix is used as a reaction field and also a reagent for reaction with guest molecules: studies on the charge transfer band excited photochemical reaction of unsaturated organic molecules in cryogenic oxygen matrices is the theme. The other study is that matrices are used as inert solvents in which reaction intermediates are trapped: the direct spectroscopic detection of HSO_X radicals has been studeed.

This is a dissertation submitted to the University of Tsukuba in partial fulfillment of the requirements for the doctoral degree.

The author is grateful to Dr. Hajime Akimoto for his invaluable discussion and advises for this research. The help and suggestion of Prof. W. Ando, Prof. K. Tokumaru, Dr. N. Washida, Dr. G. Inoue and Prof. H. Sakuragi are also gratefully acknowledged. All ab initio calculations in CHAPTER V were carried out by Prof. Shigeru Nagase of Yokohama National University at the Computer Center of the Institute for Molecular Science using the GAUSSIAN 80 and GAUSSIAN 82 programs in the center library program package. The author also indebted to Dr. H. Bandow, Dr. S. Hatakeyama, Dr. F. Sakamaki and Mr. M. Suzuki for their kind advises.

September, 1988 S. Hashimoto

CONTENTS

CHAPTER I

THE MATRIX ISOLATION TECHNIQUE

1. Introductory Survey

The matrix isolation technique is a useful method for the preparation and observation of small molecules, atoms, and free radicals. It has been developed in order to investigate properties of unstable molecule and transient species in some chemical reaction. An interested chemical species is trapped and isolated in chemically inert solid or matrix typically of a rare gas at cryogenic temperature, below about 20K. This idea is based on an expectation that the chemical species act as energetically isolated molecule as in gas phase when it is isolated in an inert material, and on an estimation that any chemical reaction with an activation energy greater than a few kJ/mol should efficiently be prevent at cryogenic temperature.

In the middle of 1950's, the pioneering work in the field were performed[1] by G. C. Pimentel and his coworkers. N_3[1b] radical, and also small molecules such as H_2O[1c] and CH_3OH[1d] were isolated in matrices of inert gases at temperature around 20K by using liquid hydrogen as the refrigerant. They measured infrared spectra of these chemical species with relatively higher resolution than in solutions or organic matrices. At about the same time, the systematization of the matrix isolation technique was made by I. Norman and G. Porter[2], and after that S. N. Foner[3] applied the inert gas matrix isolation method for the electron spin resonance spectroscopy.

CHAPTER I

Matrix isolation has now become to be one of the standard technique which is widely used[4] in the field of spectroscopy: UV-VIS, IR, Raman, Mössbauer, photoelectron, ESR, NMR, and any other spectroscopy. Many transient species, free radicals, ions, and unstable molecules which are very important to study chemical reactions have been investigated[1~5] by use of this method. Chemical species to be studied are not only transient species but also stable molecules, metal atoms and its coagulates, molecular complexes, and clusters, etc.

In most of these studies, the main interest is in the structure of the trapped species or the guest molecules, while some photochemical reactions are used for preparation of radicals or unstable molecules. Combination of the discharge flow method and the matrix technique should give some important information of reactions if a intact reaction mixture could be frizzed to make it a matrix.

In the last 10 years, many studies have been made[6~9] with interests of chemical reactions of itself in cryogenic matrices. There are two types of studies according to degree of interaction between a guest and matrix molecules. One of the most characteristic phenomenon with negligible interaction is the single IR photon photochemical reaction[7], which includes conformational isomerization of some organic molecules, and addition reaction caused by vibrational excitation. IR induced reaction in matrix is also found in the structural changing of coordination in an inorganic molecular complex[8]. The energy barrier which is negligible at room temperature increases its

importance at cryogenic temperature. On the other hand, several studies are reported in the strong interaction systems. In such a case, reactive material, O_2, CO, etc., are used as matrix material. For example, 2,5-dimethylfuran[9] in oxygen matrix forms an endoperoxide by excitation within 8000 ~ 17300 cm^{-1} corresponding to direct excitation to singlet states ($^1\Delta_g$ and $^3\Sigma_g^+$) excitaion of oxygen molecules.

Studies on chemical reactions by use of the low temperature matrix method is an interesting subject. There are two main theme in this dissertation. One is the study on the reaction in strong interaction system of cryogenic matrices. The photochemical reaction of alkenes, arenes, and ketene derivatives in cryogenic oxygen matrix will be discussed in CHAPTER IV. The reaction found to be specific in the oxygen matrix. In advance of the study on the reaction, the charge transfer interaction between organic molecules and oxygen will be revealed in CHAPTER III. The other theme is of the investigation of some reaction intermediate. The structure of $HOSO_2$ will be disclosed by the direct spectroscopic detection using the matrix isolation method, assignment of whose spectrum is supported by the ab initio calculation in CHAPTER V. These radicals are of importance in the oxidation of SO_2 to H_2SO_4 in the atmosphere.

2. Matrix Effect

(a) Chemical Species in Low Temperature Matrix

Low temperature matrices is an environment for the guest molecule closely resemble as in vacuum at low temperature except limitation in the movement in the matrix lattice if the interaction between guest and matrix molecules is negligible. This is true in almost cases, especially in the matrix of rare gas, but the environment is never the same as in vacuum. In analyzing of spectroscopic data, consideration about the perturbation of matrix molecules to interested chemical species is very important. Strong or weak or negligible interaction should exist between a guest and the matrix, and also a guest and another guest. The interaction specific in matrix is inclusively called the matrix effect. The effect will found in spectroscopic difference form measured in gas or liquid phase. One who use the low temperature matrix method should consider about the matrix effect.

The environment of a trapped species[4c] mainly depends on preparation conditions materials of the matrix. It could be regard that the guest molecule has nearly no orientation in almost cases. The solution cage, not unique usually, has a few or several different types of sites, then matrix spectra often contain fine structure due to absorptions from the different sites. When matrices are soft enough for small guest molecules to diffuse, dimers and aggregates complicate the interpretation of spectra. When relatively low M/R ratio (ratio of matrix to guest, i.e. radical or reactant) is applied, guest-guest inte-

ractions between nearest neighbors, and even next-nearest neighbors, must be considered for a finer interpretation of spectral detail.

Even rare gas (Rg) matrices are not always inert ("inert" means non-perturbation to guest molecules, in this stage), especially heavy one is used and the measurement is based on electronic transition. Emission and excitation spectra of OH radical[10] in Ne matrix is similar those of in vacuum, that shows free rotation of OH with almost no perturbation. However, Brus[10,11] et al. reported spectroscopic property of $OH(A^1\Sigma)$, mixing of valence and charge transfer state $[Rg^+OH^-]$ in Ar, Kr, and Xe matrices. Broad bands without rotational structure was observed in spectra. The 0-0 bands in Ne matrix at 307 nm very close to that in vacuum (307 nm) shifts to 340, 363, and 440 nm in Ar, Kr, and Xe, respectively. Goodman and Brus[11] concluded that OH in these matrices makes a linear molecule Rg-HO, and the mixing of $OH(A^3\Sigma)$ with the CT state $[Rg^+HO^-]$ enhances the strength of Rg-OH bonding. Degree of the mixing is depends on the difference of these two energy levels. When ionization potential of rare gas, which is the lower the heavier, of Rg is lower than Ar the CT level is down to near the OH level. This is suggestive observation for measurement and photochemistry of matrices in the UV-VIS region.

(b) Matrix Effects in IR spectra

Matrix effect in infrared absorption spectrum is important because the spectrum is usually measured for tracing of any

reaction occur in the matrix. Indeed, it is one of the most usual spectroscopic measurement for matrix samples since the spectra give many information for molecular structure and also environment of trapped species. The matrix effect result in shift or splitting of bands of trapped species in IR absorption spectra. When the interaction between matrix molecule and a trapped species is negligible, the spectrum will show a little or negligible shift meaning that the vibronic energy transfer from the species to the lattice of the matrix is slower then the intramolecular relaxation. On the other hand, if the interaction is strong, obvious shift, multiple bands, and band broadening will be found, which makes the interpretation of the spectrum complicate. Several effects are well known[4b] as follows.

(i) Vibrational shift: in matrices, as in any condensed phase, the band center is shifted form its gas phase value, normally to lower frequency. This is a kind of 'solvent' shift.

(ii) Multiple trapping sites: in a matrix a molecule may be trapped in two or more distinct sites, each of which will give rise to a different vibrational shift, and thus several bands will appear in the spectrum.

(iii) Rotational motion: at the cryogenic temperatures, few rotational levels will be populated but nevertheless several absorptions could result from this effect. Rotation has been observed for a number of small molecules and radicals. Inversion (NH_3) and nuclear spin conversion (H_2O and CH_4) complicate the rotational spectra of certain molecules in

matrices.

(iv) Aggregation: even where the interaction between two solute molecules is small, a group of two or more solute molecules will give rise to a frequency slightly different from that of the isolated monomer. In the case of hydrogen-binding materials, the shift may be very large.

(v) Splitting of degenerate frequencies, or the appearance of infrared inactive bands: the matrix cage may perturb the solute solute molecules sufficiently to lift the degeneracy of two levels, or to induce IR inactive bands, for example the O=O stretching frequency of O_2. Also the low temperature, and the isolation of monomeric solute molecules, often cause near-degenerate bands to be resolved.

3. Photochemical Reactions in Low Temperature Matrices

(a) Reactions in Reactive Matrices

Rare gas matrices are not always inert ("inert" means non reactive or no effect for chemical reaction, in this stage) also in the case. Strong interactions related to some chemical reactions have been found in electronically excited states of a guest molecule in rare gas heavier than argon when the excited energy grater than 7 eV, in vacuum UV (VUV) region. Tylor[12] and his coworkers studied emission spectra of RgO form with atomic $O(^1D,^1S)$ formed from VUV excitation of N_2O, CO_2, O_2, and OCS in rare gas matrices. When the atomic O forms through the harpooning reaction mechanism, which is a charge transfer from the exciton of Rg to the guest molecule, the guest will

photolytically decompose with non-resonant and higher exciton energy than that of thermodynamical dissociation of the guest molecule. The emission from KrO of CO_2 in Kr matrix[12d] with the excitation threshold about 10 eV was explained with this mechanism.

Among many studies on reactions in reactive matrix reported in recent years, one of the most important in the relation of our studies is that by Frei and Pimentel[9] on the reaction of 2,5-dimethylfuran (DMF), methylfuran (MF) and furan in O_2/Ar matrices. The direct excitation of O_2 ($^1\Delta_g$ and $^3\Sigma_g^+$, v'=0 and 1 for each) and also $(O_2)_2$ ($^1\Delta_g$, $^1\Delta_g$) states in near infrared region induced formation of endoperoxides. The DMF + O_2 reaction is a single photon process with unit quantum yield for all vibronic level. Quantum yields for MF + $O_2(^1\Delta_g, v' = 0)$ and furan + $O_2(^1\Delta_g, v' = 0)$ was found to be ~0.6 and 0.4, and latter reaction rate showed an $^{18}O_2$ isotope effect 0.78 $\pm$ 0.15, which they conclude that it is in terms of quantum mechanical tunneling on the lowest singlet hyper-surface.

In matrices of oxygen, strong charge transfer interactions could be found as the decrease of ionization potential of the 0guest. Photo-excitation to these electronic states could follow new specific chemical reaction channels.

(b) IR Induced Reaction in Matrices

IR (single photon) induce reaction in matrices, which itself is very important and one of the most characteristic phenomenon in inert matrices, should be considered when any IR spectrum of

matrix sample is measured since the probe IR beam might cause some chemical reaction.

Pimentel et al. reported[7b] cis-trans photo-isomerization of HONO in N_2 matrix, which is the first investigation that single IR photon could proceed chemical reaction. This reaction induced by irradiation at 3650 ~ 3200 cm^{-1} region corresponding to the absorption band of OH stretching (st.) mode of HONO, and proceeds whichever cis to tans and trans to cis with faster rate of the former than of the latter. Following this, Shirk et al.[13] found the mode selectivity in the reaction: isomerization of cis to trans excited at cis-ν_1 and $2\nu_2$ of HONO is 200 and 10 times faster than that of trans to cis at trans-ν_1 mode. Here ν_1 and ν_2 are OH st. and N=O st. modes of HONO, these are at 3407/3552 and 3236/3345 cm^{-1} for the cis/trans forms, respectively. They conclude that energy randomization among vibronic levels in the molecule is slow, and energy transfer of the cis form is faster than trans form in that from the ν_1 and the ν_2 modes to $5\nu_6$ mode (twist) above the energy barrier of the isomerization .

Hauge et al.[14] found ethene and acetylene could trapped in F_2/Ar matrices without thermal reaction, and IR (2500 ~ 10000 cm^{-1}) irradiation induced reactions of these compounds with F_2. The products from ethene with F_2 were 1,2-gauche-CH_2FCH_2F, trans-CH_2FCH_2F, CH_2CHF, and HF. After that, Frei and Pimentel[9,15] studied the reaction of ethene and F_2 in N_2 matrices using CO_2, CO, F-centered lasers. Obvious mode selectivity was not found in this system, and the quantum yield of the reaction efficiently increases as excitation energy increases. No randomization of

vibronic energy could occur in such low energy area, and the vibration could relax through a cascading mechanism with frequent energy transfer to the matrix lattice the molecule. They concluded that the energy dependence is because of the cascading relaxation: highly vibrationally excited molecule could pass many vibrational levels each of which have some probability to react.

As discussed in section 2.(b), IR spectrum often shows multiple band of a guest corresponding to multiple sites. Poliakoff[16] reported a site selective reaction induced by IR irradiation. $Fe(CO)_4$ in a specific site in Ar matrices reacted with CO selectively by irradiation at 1973.7 cm^{-1} from CO laser. Resulted absorption spectrum after the laser irradiation showed a "hole" with 0.3 cm^{-1} width in the CO band of $Fe(CO)_4$ indicating the selective reaction. The spectrum also depicts the formation of $Fe(CO)_5$ and retention of $Fe(CO)_4$ in other sites.

Single photon IR photochemistry in low temperature matrices is interesting still apart from the caution for tracing chemical reaction by IR spectroscopy. The excellent selectivity could make many chemical and physical applications.

Reference

1) (a) Whittle, E.; Dows, D.A. and Pimentel, G.C. J. Chem. Phys. **1954**, 22, 1943. (b) Milligan, D.E.; Brown, H.W. and Pimentel, G.C. ibid., **1956**, 25, 1080. (c) Van Thiel, M.; Becker, E.D. and Pimentel, G.C. ibid., **1957**, 27, 486. (d) Van Thiel, M.; Becker, E.D. and Pimentel, G.C. ibid., **1957**, 27, 95.

2) Norman, I. and Porter, G. Nature, **1954**, 174, 508.

3) Foner, S.N.; Jen C.K.; Cochran E.L. and Bowers V.A. J. Chem. Phys., **1958**, 28, 751.

4) (a) Meyer, B. "Low Temperture Spectroscopy", Elsevier, New York, **1971**. (b) Halman, H.E.; Ed., "Vibrational Spectroscopy of Trapped Species", John Wiley & Sons, London, **1973**. (c) Barns, A.J.; Orville-Thomas, J.; Muller, A. and Gaufres, R. "Matrix Isolation Spectroscopy", Reidel, **1981**. (d) Dunkin, I.R. Chem. Soc. Rev., **1980**, 9, 1.

5 (a) Bass, A.M. and Broida, H.P.; Eds., "Formation and Trapping of Free Radicals", Academic Press, London, **1960**. (b) Jacox, M.E. Rev. Chem. Intermed., **1978**, 2, 1.

6) (a) Poliakoff, M. and Turner, J.J. Chem. Biochem. Appl. Lasers, **1980**, 5, 155. (b) Perutz, R.N. Chem. Rev., **1985**, 85, 77. (c) ibid., **1985**, 85, 97.

7) (a) Frei, H. and Pimentel, G.C. Ann. Rev. Phys. Chem., **1985**, 36, 491. (b) Hall, R.T.; Pimentel, G.C. J. Chem. Phys. **1963**, 38, 1889.

8) (a) Davies, B.; McNeish, A.; Poliakoff, M.; Tranquille, M.; Turner, J.J. J. Chem. Soc. Chem. Commun. **1978**, 36. (b)

Poliakoff, M.; Breedom, N.; Davies, B.; McNeish, A.; Turner, J.J. Chem. Phys. Lett. 1978, 56, 474.

9) Frei, H. and Pimentel, G.C. J. Chem. Phys. 1983, 79, 3307.

10) Brus, L.E.; Bondybey, V.E. J. Chem. Phys. 1975, 63, 786.

11) Goodman, J.; Brus, L.E. J. Chem. Phys. 1977, 67, 4858.

12) (a) Tylor, R.V.; Walker, W.C. J. Chem. Phys. 1979, 70, 284. (b) Tylor, R.V.; Walker, W.C. Appl. Phys. Lett. 1979, 35, 359. (c) Tylor, R.V.; Walker, W.C.; Monahan, K.M; Rehn, V. J. Chem. Phys. 1980, 72, 6743. (d) Tylor, R.V.; Scott, W.; Findley, P.R.; Wu, Z.; Walker, W.C. J. Chem. Phys. 1981, 74, 3718.

13) (a) McDonald, D.A.; Shirk, J.S. J. Chem. Phys. 1982, 77, 2355. (b) Shirk, A.E.; Shirk, J.S. Chem. Phys. Lett. 1983, 97, 549.

14) Hauge, R.H.; Grausden, S.; Wang, J.L.F.; Margrave, J.L. J. Am. Chem. Soc. 1979, 101, 6950.

15) (a) Frei, H.; Fredin, L.; Pimentel, G.C. J. Chem. Phys., 1981, 74, 397. (b) Frei, H. J. Chem. Phys. 1983, 79, 748.

16) Poliakoff, M. Chem. Phys. Lett. 1981, 78, 1.

CHAPTER II

EXPERIMENTAL APPARATUS AND METHOD

1. Cryostat

(a) Refrigeration

In a low temperature matrix experiment, temperature of an objective sample must be held low enough to keep the material rigid and the vapor pressure negligible. For example in the case of argon matrix desirable temperature is below 20K. Cryostat used for this kind of experiment is one can hold the sample temperature between 4 to about 15 K at the lowest temperature depend on the type of refrigeration method.

Several kind of cryostat have been used[1] for cryogenic experiments. From the view of refrigeration method, three major types of cryostat are used nowadays. The double Dewar cryostat is a apparatus to use with liquid helium or hydrogen. In 1960's the use of liquid helium to obtain low temperature became prevalent in labolatories. The spread of the matrix isolation technique owed to that liquid helium became easy to use. This classical apparatus has simple structure and has been used for a long time. The temperature of the sample in the cryostat depend on the boiling point of refrigerant liquid. It can cool samples down to 4K when liquid helium is used at 1 atm. By evacuating liquid helium, temperature near 1 K may be realized. This equipment itself is a cheapest between the three types but it consumes several litters of liquid helium for every cooling, and that is normally bulky, difficult to handle, and not so easy to

control temperature.

Other one is the Joule-Thomson open cycle cooling system. This system has a simple structure and consists of no mechanically moving part. To operate the system continuous refrigerant gas flow is needed, but temperature of cryostat can be easily controlled within 4~300 K simply by regulating the gas flow. "Cryo-Tip" (Air Products and Chemicals Inc.) is commercially available one of this type.

Another one is the closed loop system based on the Stirling refrigeration cycle. This is more useful system than double Dewar and Joule-Thomson type. The cryostat used in this study consists of this type of refrigerator. The cycle works by reversal sequence of four stages of the Stirling cycle, which is one of heat engines. Fig.2.1 (a) shows a conceptual schematic diagram of the Stirling refrigerator. Five sections consist of the system: compression space, cooler, regenerator, freezer, and expansion space. The refrigeration cycle works by reversal sequence of four successive thermodynamical stages in the Stirling cycle. These stages are took place, as follows, by change of a volume in the engine running out-of-phase operation of two pistons.

(i) The fluid gas near at room temperature is compressed by upper movement of the right piston. In this stage, the left piston is at the upper side. The the fluid passes through the cooler to dissipate the heat of the compression. The fluid then goes through the regenerator and finally the freezer. The fluid is cooled by exchanging of heat in the regenerator down near to

refrigeration temperature. This process is corresponds to changing of state (2) to (1) in the p-v diagram of the Stirling cycle as shown in Fig.2.1. (b).

(ii) The fluid is expanded into the expansion space which is enlarged by downward movement of the left piston while the right piston is standing at the upper side that has followed by its upward movement. Further cooling of the fluid gas will occur in this stage. Fig.2.1 (a) shows a situation that this adiabatic expansion in the expansion space having been exceeded. This process corresponds to (1) to (4) in the p-v diagram.

(iii) As the right piston moves to the lower side, the total volume of the system is maximized. Temperature and pressure of the fluid in the compression space decrease. This corresponds to (4) to (3) in the p-v diagram.

(iv) As the left piston moves upward again while the right piston is at the lower side, the fluid back to the compression space. When the fluid passes through the freezer, it adsorbs heat of the system that is being cooled. The fluid then flows through the regenerator where it get back the heat stored in the present heat exchange. Finally, the fluid return back into the compression space and the cycle re-start. This process correspond to (3) to (2) in the p-v diagram.

In practice, the right piston, the right cylinder, the compression space, and the cooler can replaced by a closed cycle compressor supplying and returning of the fluid, and a valve system. The left piston, cylinder, and the expansion space also can replace by a displacer in a cylinder. This cylinder also

contains a freezer and a regenerator. The displacer in the unit moves reciprocally by pressure difference of the fluid form and to the compressor. In ordinal system, the displacer, regenerator, and the valve system are combined into a unit called "cold head". The cold head is connected to a compressor with a pair of flexible gas lines made from stainless steel. One of these lines is supplying, and the other is returning, which make a closed system. These flexible gas lines efficiently isolate the vibration of the compressor. The compressor has an adsorber to remove impurity in the refrigerant fluid, for which helium gas is used for ordinal purpose. The valve system is driven by an electric motor with a cam on the cold head. The flow of gas introduced into the cold head is controlled the valve system to ensure the Stirling cooling cycle.

In our cryostat, a commercial closed cycle refrigerator, CTI-Cryogenics Model-21, is used for refrigeration. This has been originally designated for cryo pump system. The cold head of this refrigerator has two set of displacer-regenerator unit, so it is called two stage closed cycle refrigerator. At the first cold stage, helium gas is pre-cooled near liquid N_2 temperature. Then, at the second stage the gas is cooled further to keep the top of the cold head, on which a sample holder is mounted, below 15 K in ordinal system. In our system temperature of a matrix sample can be held at 10~11K with no heat load. If 1W of heat is loaded at the second cold stage, the temperature increases by 6~7K. The helium gas in the second stage passes to the first cold stage again to exchange the heat and return to the

compressor through the returning flexible gas line.

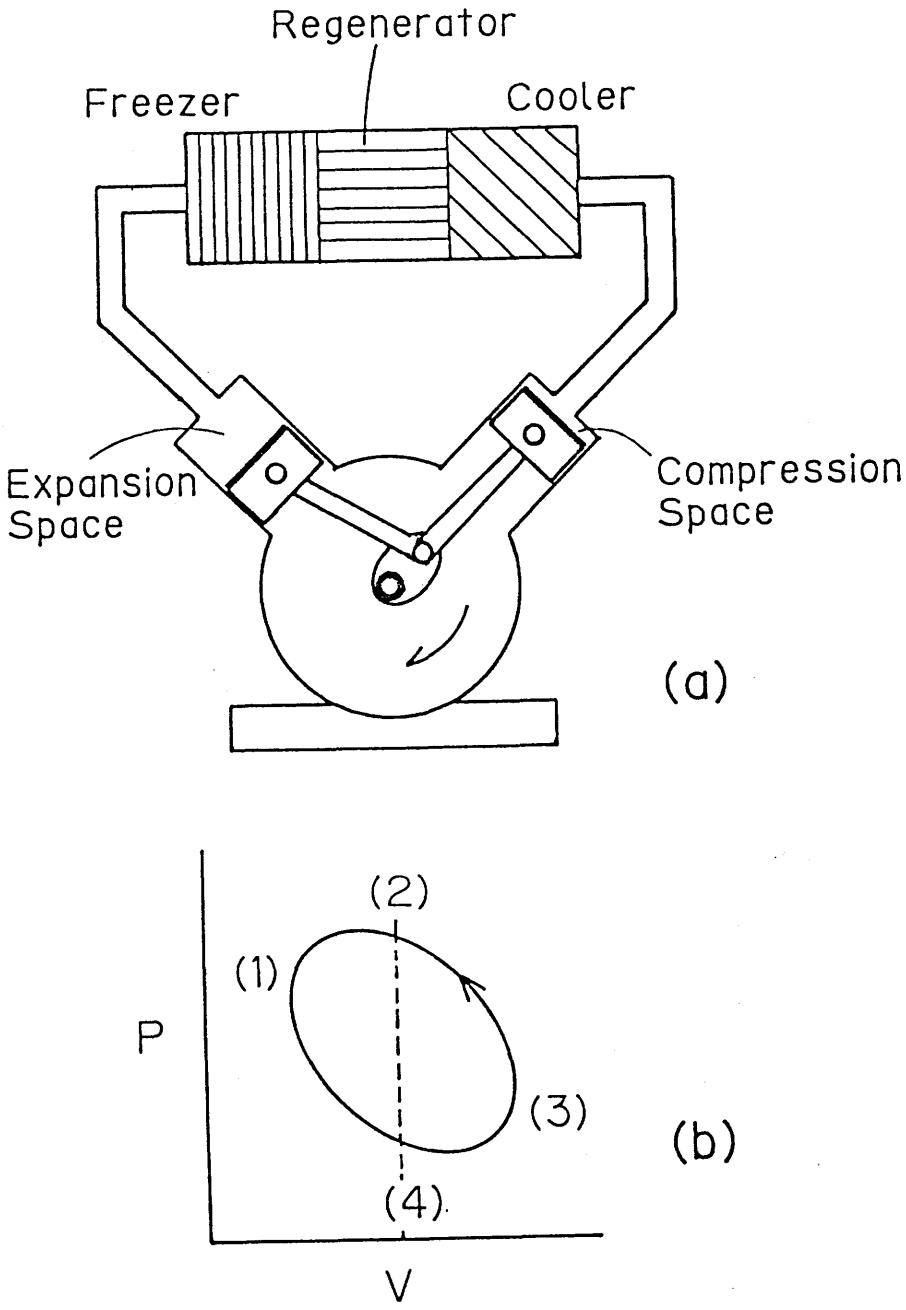

Fig.2.1. (a) Schematic diagram of the Stirling refrigerator. The refrigeration cycle works by reversal sequence of four successive thermodynamical stages in the Stirling cycle. (b) The p-v diagram of the Stirling cycle. The arrow depicts the direction for refrigeration sequence.

(b) Detail of the Cryostat Used

Fig.2.2 shows a cross section of our cryostat. A sample plate holder made of a copper block has a base as a heat buffer, **C**, is mounted on the second stage, **CS2**, of the cold head of the closed cycle refrigerator (CTI-Cryogenics Model-21). A sample plate, **P**, made of sapphire for UV-VIS or of CsI for IR measurement having 2 mm thickens is screwed on the sample plate holder together with a copper backup plate. The sample plate is positioned at the angles of 45 degree toward both directions of the probe beam and the irradiating light for photolysis. The geometry is illustrated in Fig.2.3, which shows a typical set-up for an experiment of photochemical reaction in matrices. Indium metal sheet is used at each contact surface in order to ensure good heat conductivity.

The sample temperature is monitored by a silicon diode sensor, **D**, on the edge of the sample plate holder. The diode is wired to a digital thermometer module, DIGI-K Model DI-8 of Lakeshore Inc. The base of the sample plate holder was fitted with a resistance heater to control the temperature of the sample plate window between 10 to 100 K within $\pm$1 K accuracy. The power to the heater is govern by the tripping alarm signal from the thermometer module. The wiring of the diode and the heater are coiled round the cold head rod (cold finger) to avoid thermal leakage form higher temperature part to the sample plate. These wiring are led out from the vessel thorough a hermetic shielded connector.

There are two lines of stainless tubing to introduce sample

gas mixtures into the cryostat and jetted from the nozzles, N, to deposit on the sample plate. The nozzles are located 10~15 mm over the sample plate. The other end of the tubing are connected to a sample gas feeding systems thorough a feed-thorough on a vacuum flange. A sample gas mixture prepared in a graceless gas handling line are stored in a glass bulb. The gas mixture flows through a diaphragm metering valve to control the rate and passes one of the stainless tubing in the cryostat. The gas mixture is then jetted from the nozzle and deposited on the sample plate. The other stainless tubing is also connected another set of a gas handling line..

All cryogenic parts of the system are installed in a vacuum vessel made of cylindrical stainless steel with 102 mm inner diameter and 265 mm long, which is composed of three parts: a cylindrical body, a connecting flange, and a head cylinder with five window ports. The vacuum is shielded by Viton (copolymer of vinyliden fluoride and hexafluoropropylene) O-rings. One pair of the ports at opposite position are fitted with KBr windows through which IR spectra of a matrix sample on the sample plate surface are measured. Another pair of the port is fitted with quartz plates for UV-VIS measurement or irradiation from out side. The head cylinder can rotate around the sample plate capable to pass the probe beam through whichever pair of the windows. The port on the top (left end in Fig.2.2) of the head cylinder is a view port fitted with a Pyrex window.

The cryostat chamber is maintained at ~10^{-6} torr before each cooling cycle. In each scheme, an evacuation port of the

cryostat chamber is closed below 100K, and deposition and irradiation of the sample were made at 10~11 K without evacuation in order to avoid back diffusion of contaminants otherwise noted.

(c) Optional Apparatus for the Cryostat

In some experiments optional apparatus are fitted on the head cylinder. As shown in Fig.2.4, an electrodeless discharge resonance lamp for photolysis of H_2O_2 is installed on the cryostat. This optional set have been used for the detection of $HOSO_2$ radical, which will be discussed in CHAPTER V. In this case, Pyrex plate of the view port is replaced with a metal plate with a feed-thorough glass tubing to introduce H_2O_2/Ar gas mixture. An all-glass deposition line with a PTFE nozzle is installed in order to minimize the decomposition of hydrogen-peroxide. This glass-PTFE line is also used to deposit some other unstable samples. For example, to obtain IR spectrum of tetramethyl-1,2-dioxetane in an oxygen matrix the glass-PTFE deposition line was used as will be discussed in CHAPTER IV. In this case the authentic dioxetane was vaporized at 255~260 K from a sample tube connected about 40 cm before the PTFE nozzle, and the vapor was swept into the cryostat with oxygen gas flow.

Fig.2.5 shows another optional set for a matrix experiment combined with a discharge flow system. The flow tube is made from Pyrex except quartz tubing for discharge area. The inner and outer tube have 8/10 and 22/25 mm in ID/OD. A mixture of radical source in Ar is microwave (2.45 GHz) discharged though a cavity. Reactant gas is added downstream, and a part of the

reaction mixture is deposited on the sample plate surface through a pinhole of ca. 0.3 mm in diameter. Resident gas mixture is then pumped out by a mechanical vacuum pump with a liquid N_2 cooled cold trap. Transient species formed in the discharge flow will be trapped in the matrix. This system was used to study the reaction of the H-atom and SO_2 as will be discussed in CHAPTER V.

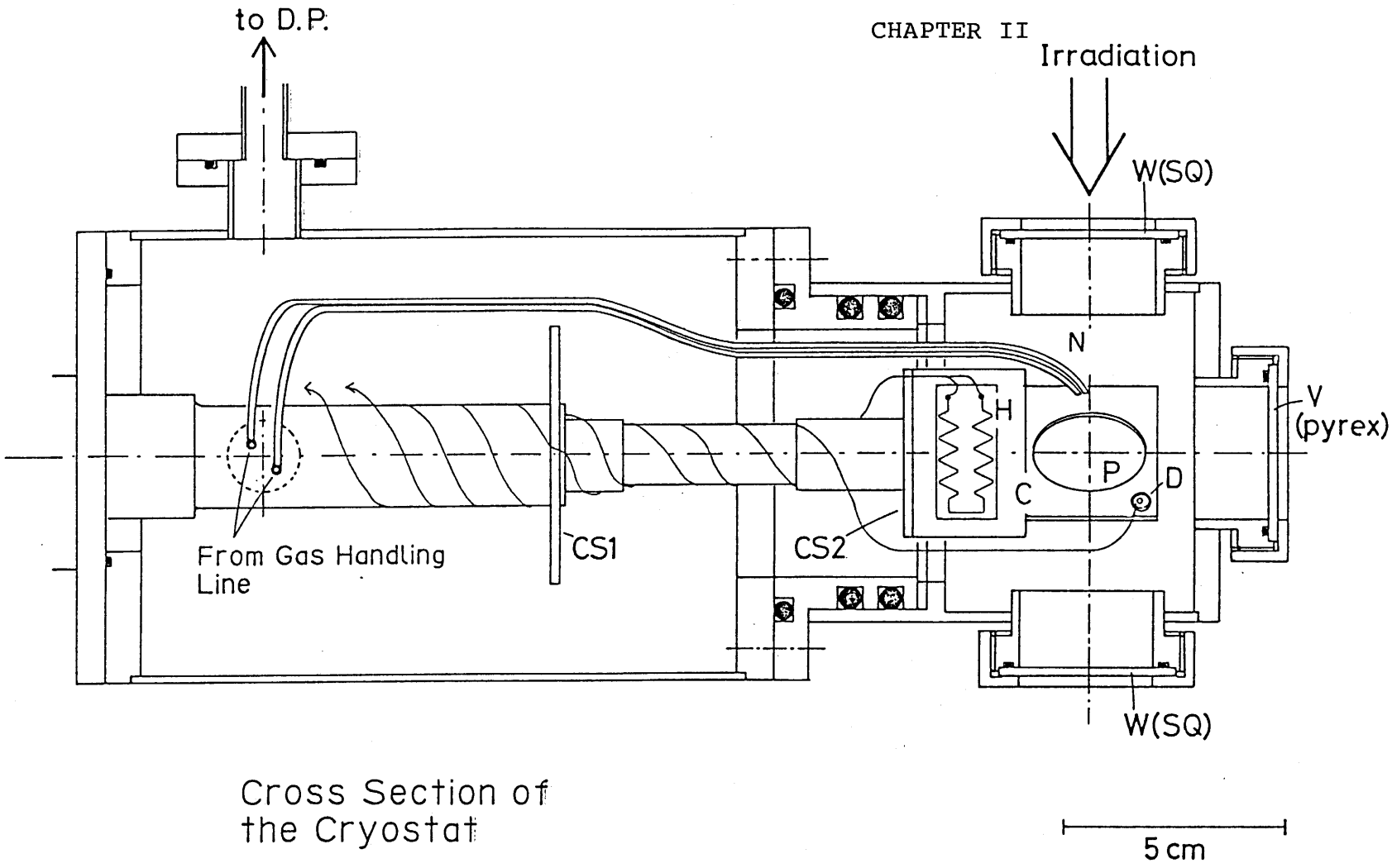

Fig.2.2. Cross section (side view) of the cryostat: **C** Copper sample plate holder block, **CS1** Cold Stage-1, **CS2** Cold Stage-2, **D** silicon Diode thermal sensor, **N** Nozzle of the stainless tubing (0.7/1.0 mm ID/OD), **P** sample Plate (CsI or sappier), **V** View port (Pyrex), and **W** Window (supurasil quartz) for irradiation and UV-VIS measurement.

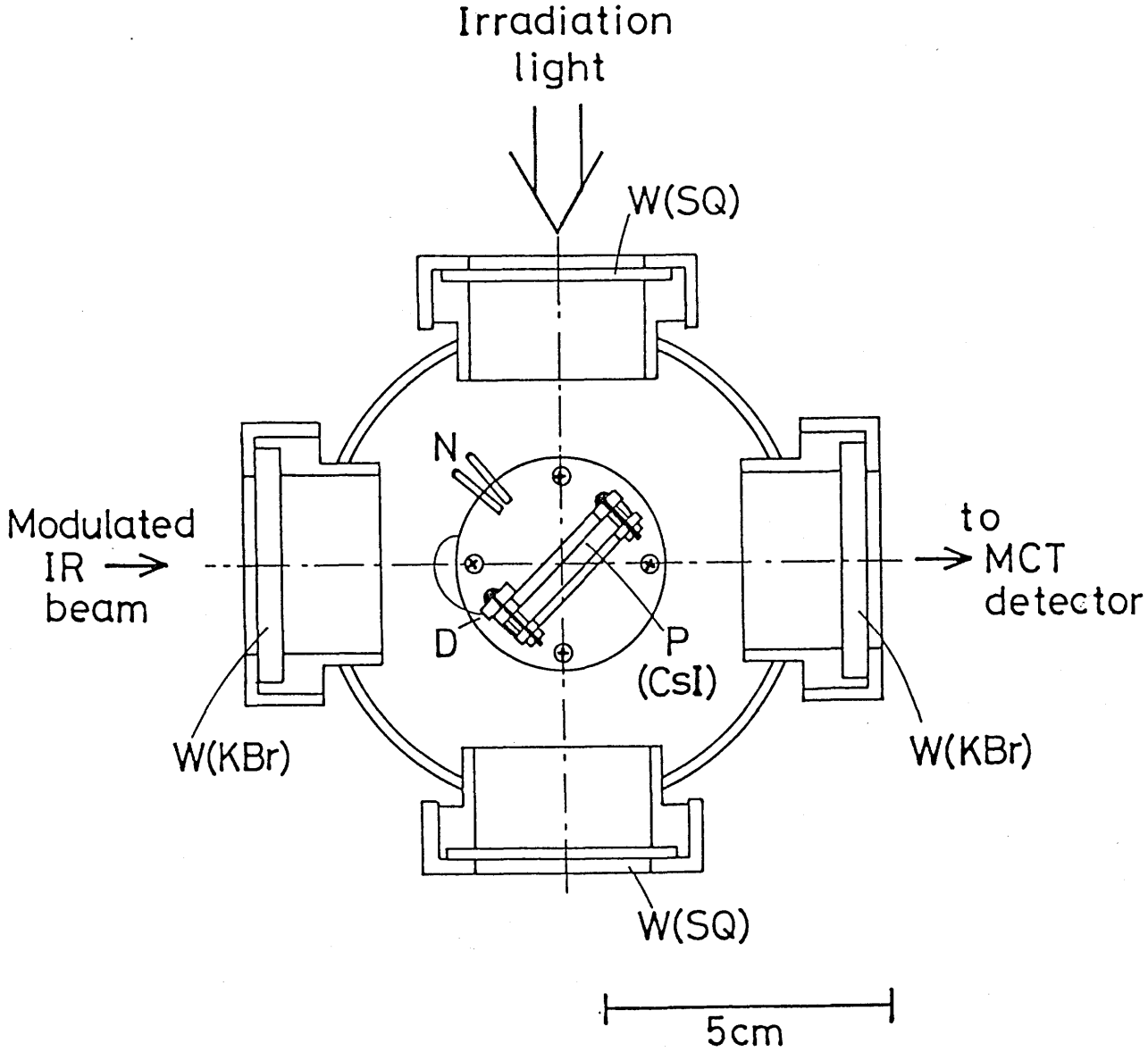

Fig.2.3. Cross section of the head of the cryostat. View from the right side of Fig.2.2.

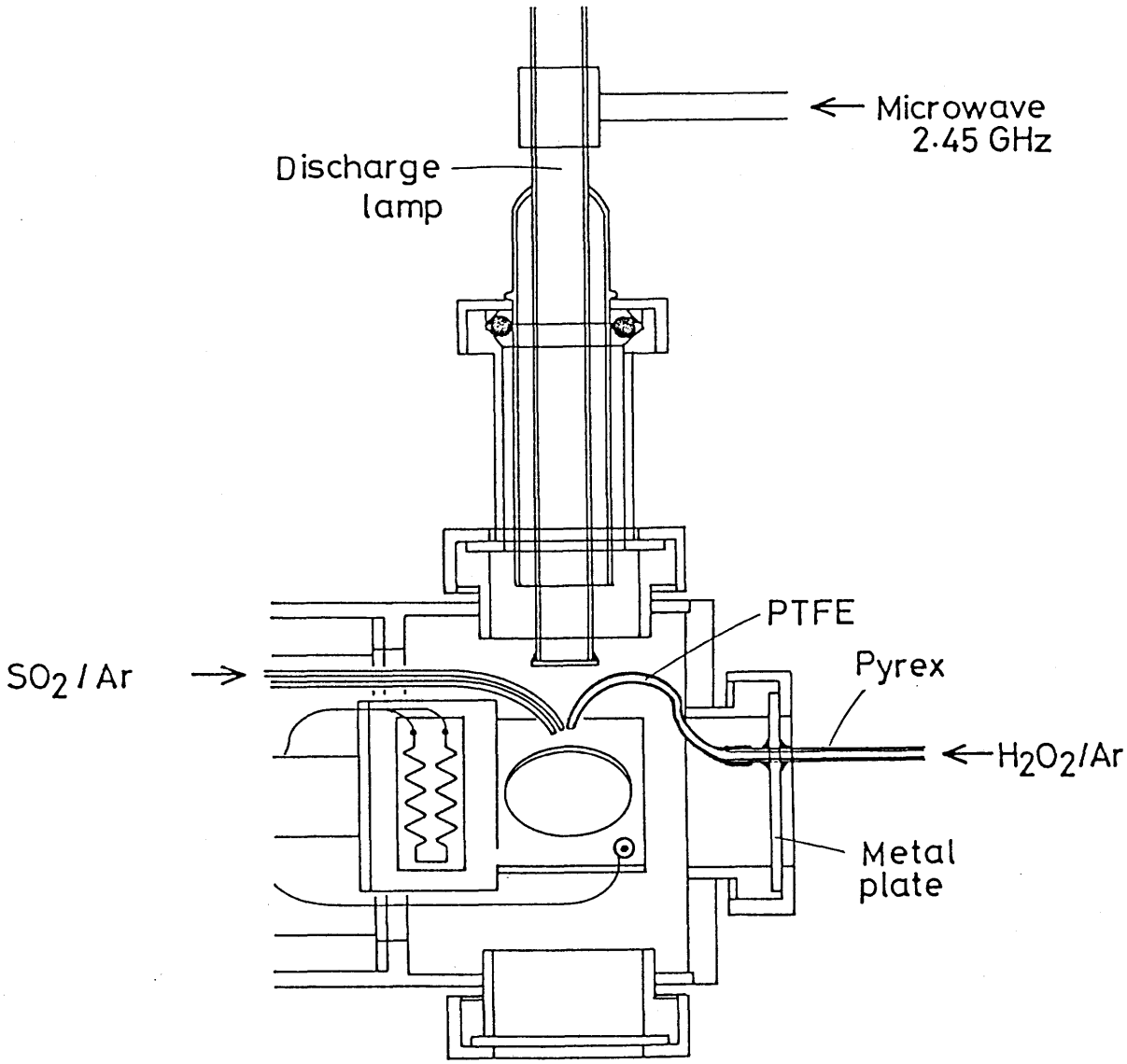

Fig.2.4 An electrodeless discharge lamp is mounted on the head cylinder perpendicular to the probe beam over the sample plate for the photolysis. The third inlet tubing (glass-PTFE) to introduce sample gas containing H_2O_2 or other reactive reagent is also illustrated.

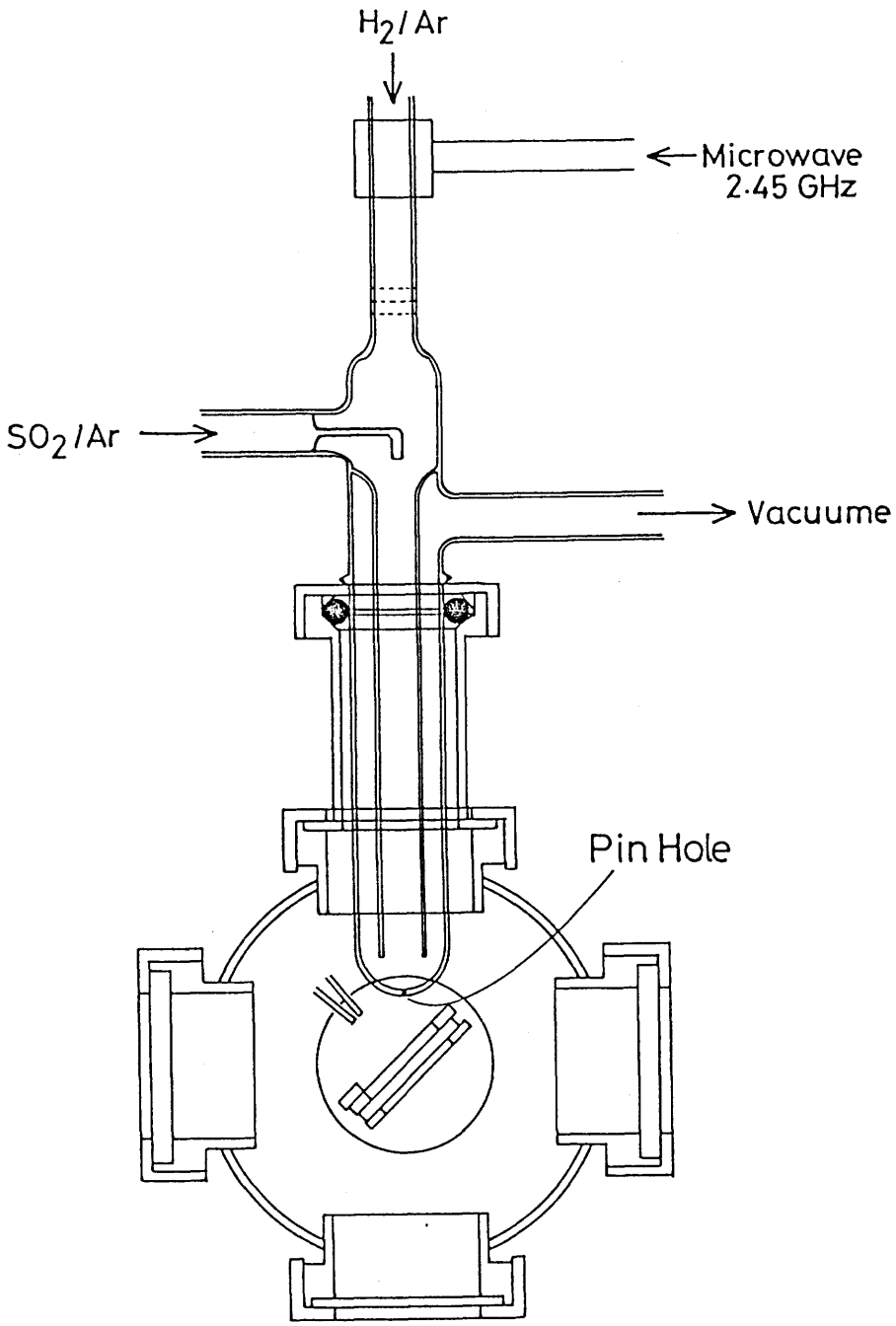

Fig.2.5 An optional set for a matrix experiment combined with a discharge flow system. The flow tube is made from Pyrex except quartz tubing for discharge area. The inner and outer tube have 8/10 and 22/25 mm in ID/OD. Reaction mixture is deposited on the sample plate surface through a pinhole of ca. 0.3 mm in diameter at the bottom of the flow tube.

2. Fourier Transform Infrared Spectroscopy (FT-IR)

(a) Advantages of the FT-IR

The Fourier transform infrared spectroscopy has several important advantages over ordinal dispersion spectroscopy[2,3]. A much larger beam diameter may be used than the grating spectrometer (throughput advantage or Jacquinot's advantage) although the beam diameter must be stepped down as resolution gets higher. Concurrent measurement of the detector signal all over the spectrum rage (multiplex advantage or Fellgett's advantage). Above two advantages make the signal-to-noise ratio (S/N) higher for spectra obtained under condition of the same measurement time. Further, by the concurrent nature of the spectrum shows one to get an average spectrum in the measuring time when data are collected during photochemical reaction of matrix sample. High S/N ratio is helpful to detect very small amount of transient species and unstable species formed in the matrices. This also makes easier to measure spectra at higher resolution. To monitor of proceeding of reactions, 0.25 cm^{-1} or higher resolution can be used practically.

Stray light does not affect the detector since all information is modulated to audio frequencies. As the sample is placed after the beamsplitter and is subject to only audio frequencies, any emission of infrared radiation by the sample will not be detected by the audio frequency detector. Rapid scan speeds (about 0.5 sec/scan) allow an interferometer system to monitor samples undergoing rapid change. Use of He-Ne laser provides frequency accuracy better than 0.01 cm^{-1} (laser

reference advantage or Connes advantage).

(b) Principle of the FT-IR

A system of FT-IR requires an IR source, an Michelson interferometer, an IR detector, mirror optics, spectrometer body, an analog-to-digital converter (ADC), and a computer. Fig.2.6. shows a simplified schematic diagram of the spectrometer. The Michelson interferometer is the most important device in the spectrometer. This consists of a fixed mirror (M_F) and a movable mirror (M_M) and a beam splitter (BS). A part of the IR source radiation is reflected by BS, goes to M_F, and back through BS to the detector. The resident of the radiation is transmitted by the BS, goes to M_M and back to BS, where a portion of it is reflected and also reaches the detector. The ratio of reflected/transmitted intensity of the radiation is 1/1 in ideal case. When the distance between M_F and BS, and that between M_M and BS of the interferometer are of equal length, the two beams interfere constructively. If M_M is displaced in either direction by the 1/4 distance of a specific wavelength of a component of the radiation from IR source, the two beams of the specific light interfere fully destructively since the path between BS and M_M (also M_F) is twice of the distance. The difference in the optical path in the distances between BS-M_M and BS-M_F in the interferometer is called "retardation". The maximum retardation of the IR interferometer typically 2~30 cm. As M_M moves, signal from the detector should show cosine wave form if the radiation is monochromatic. In such case, the signal intensity of the

detector I(x) is given as

$$I(x) = B(\nu)\cos(2\pi x\nu) \qquad (2\text{-}1).$$

Where x is the reterdation in centimeters and $B(\nu)$ represents the intensity of the source as a function of frequency ν in cm^{-1}. As the IR source is polychromatic, the detector will respond the sum of all the cosine waves of the components of the radiation:

$$I(x) = \int_{-\infty}^{\infty} B(\nu)\cos(2\pi x\nu)d\nu \qquad (2\text{-}2).$$

This signal will be essentially constant over most positions of the movable mirror if the source is perfectly polychromatic and nothing absorbs the radiation in the spectrometer and the responsibility of the detector is flat for all frequency region. However, when the position of M_M is at the zero retardation point, all the cosine wave should be in phase and the detector will give strong signals called center burst. Equation 2-2 is one-half of a cosine Fourier transform pair. The other is

$$B(\nu) = \int_{-\infty}^{\infty} I(x)\cos(2\pi x\nu)dx \qquad (2\text{-}3).$$

These two equations define the relationship between the interferogram and the spectrum. The transformation of the interferogram into a spectrum is done by a computer by the fast Fourier transformation (FFT) algorithm which was proposed by Cooly and Tukey[4]. At 1 cm^{-1} resolution and for 8192 cm^{-1} of band width, 16384 data points are used for the calculation. Equations (2-2) and (2-3) mean a complete interferogram must have infinite

length. In practice, the interferogram cannot be infinite. If FFT is made for a truncated interferogram, a specific peak in the resulted spectrum appears with side lobes. The apodization is a technique to suppress the side lobes to multiply the interferogram by a function before FFT calculation. Several functions are known for apodization: triangular, cosine, trapezoidal, Happ-Genzel(Humming), and boxcar(unapodizing). Any apodization decrease resolution. The use of Happ-Genzel apodization function has been found to be desirable for most spectral work, except when the maximum instrument resolution is required. This apodization function is given by

$$I'(x) = (0.54 + 0.46\cos(\pi x/2x_{max}))I(x) \qquad (2\text{-}4)$$

where $I'(x)$ is the apodized interferogram, and x_{max} is the maximum reterdation in cm.

(c) Nicolet 7199 FT-IR

Fig.2.7 shows the optical layout of Nicolet 7199 FT-IR with the cryostat. The IR beam originates at the source S which is a water cooled Globar source used for mid IR operation. The IR beam from the source is focused by spherical mirror M1 upon the aperture wheel A. There are three aperture on the wheel these diameter of 6.3, 2.3 and 1.1 mm. In the typical case, the aperture of 2.3 mm diameter is used. After the apertures, the IR beam is collimated at 2" diameter spherical mirror M2 and brought to the beamsplitter BS coated by Ge on KBr substrate. The collimated radiation is partially reflected and partially transmitted by the beamsplitter. The reflected beam is reflected

from the flat fixed mirror M4 while the transmitted beam is reflected from flat movable mirror M5 mounted on the movable mirror assembly. The assembly which rides on dual air bearings, is driven by a linear induction motor with a large magnetic field strength controlled by a digital designated servo loop. Essentially only the movable mirror is in motion during an experiment. It should be noted that the FT-IR is basically free from many mechanical problems by elimination of cams, synchronized choppers, servo-driven combs, slit programs, gear shifts, etc. as used in the grating spectrometer. This makes the reliability of the FT-IR higher than dispersion spectrometer. The beams are recombined at the beamsplitter. Thus BS and the mirrors M4 and M5 compose a Michelson interferometer resulting a modulated IR beam. Velocity of the mirror M5 movement is chosen as the modulation frequencies to be in audio range. The collimated and modulated beam is reflected at flat mirror M6 and M7 into the sample compartment. The beam is focused at off-axis parabolic mirror M8 and passing thorough the cryostat, and then collimated again at off-axis parabolic mirror M9 and reflected at flat mirrors M10 and M11. Finally, the beam is focused on the MCT detector D by off-axis parabolic mirror M12. Mirrors M13 and M14, and a small beam splitter for white light WBS constitute a small interferometer. M14 is mounted on the same moving mirror assembly as M5. Visible light form a white light source WS is modulated by the small interferometer. Then the modulated white light is detected by a silicon diode detector WD. Signal from WD will cause a center burst by every passing of M14 to the zero

retardation point. Thus the zero retardation can easily be known. An He-Ne laser L is located on the interferometer body. The beam from L is reflected by a small prism P and passes to the main interferometer coaxially to the IR beam to a diode detector LD. Signal from LD has a cosine form according to the traveling of M5. By counting of the waves beginning at the zero retardation point, absolute retardation can be known.

The analog signals (IR signals) from D is filtered electronically and converted to digital form by 15-bit ADC triggered by the modulated laser signal. Then the digital data transferred to a host mini-computer Nicolet 1180 which is a 20-bit word machine with 40k word of RAM and a hard disc drive (5MB x 2 planes).

The functions of Nicolet 7199 FT-IR system is listed in Table II-I.

TABLE II-I: THE FUNCTIONS OF NICOLET 7199 FT-IR SYSTEM

Interferometer	Michelson type (dual air bearing)
Maximum Scan Length (half of retardations)	16.59 cm
Mirror Velocity	5.5 ~ 31.3 mm/sec (40 steps)
Maximum Resolution	0.06 cm^{-1} (unapodized)
Aperture	1.14, 2.31, 6.35 mm
Available Measurement Area	700 ~ 4,000 cm^{-1} (mid IR) 10 ~ 25,000 cm^{-1} (optional)
Wave Numbers Accuracy	better than 0.01 cm^{-1}
ADC	15 bit 100k Hz
Host Computer	Nicolet 1180 (20 bit/W x 40kW RAM)
Maximum Sampling Rate	100k Hz (on RAM, depending on the ADC ability) 30k Hz (with disk acquisition)

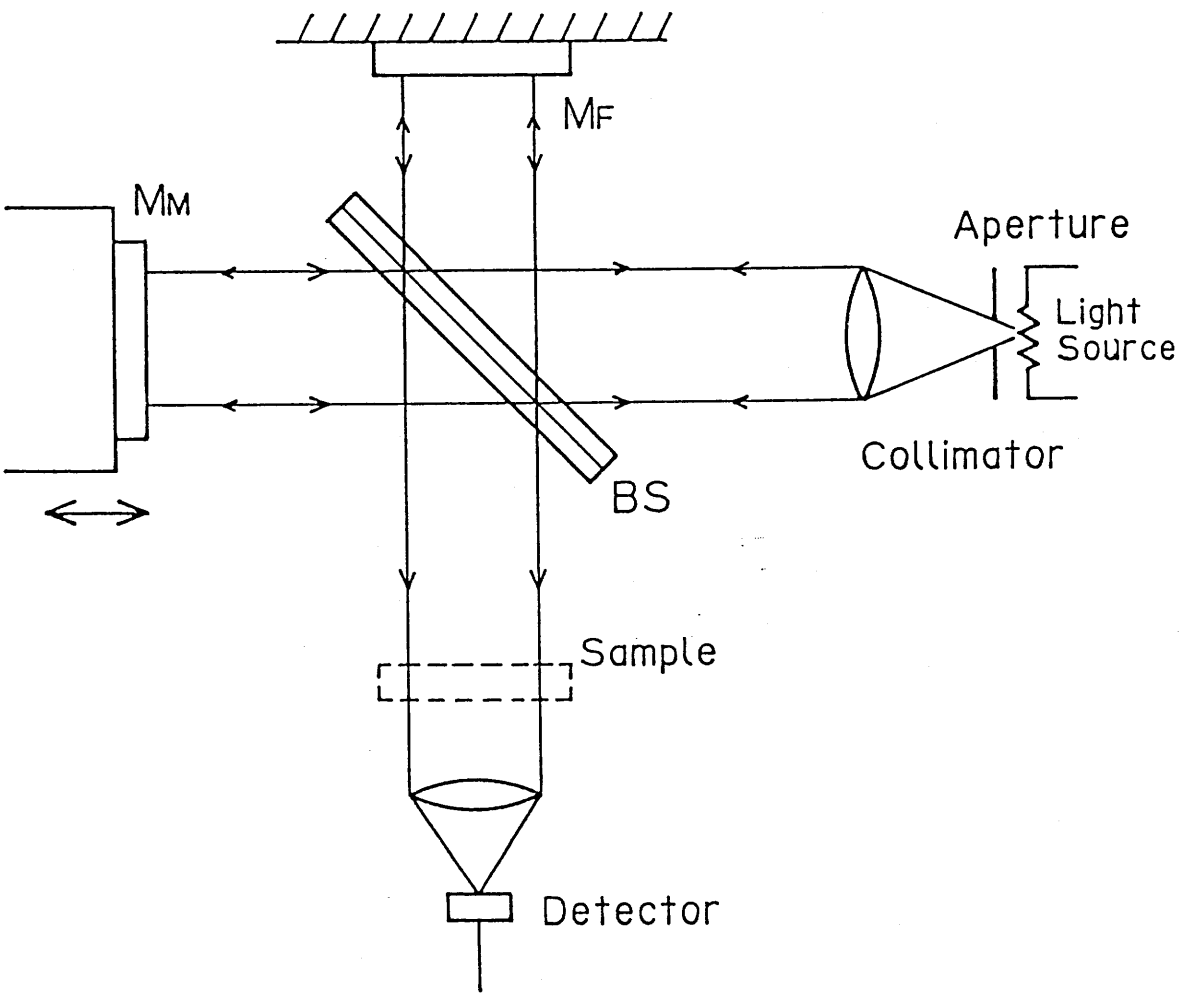

Fig.2.6. Simplified diagram of the optical system of a Fourier transform infrared spectrometer.

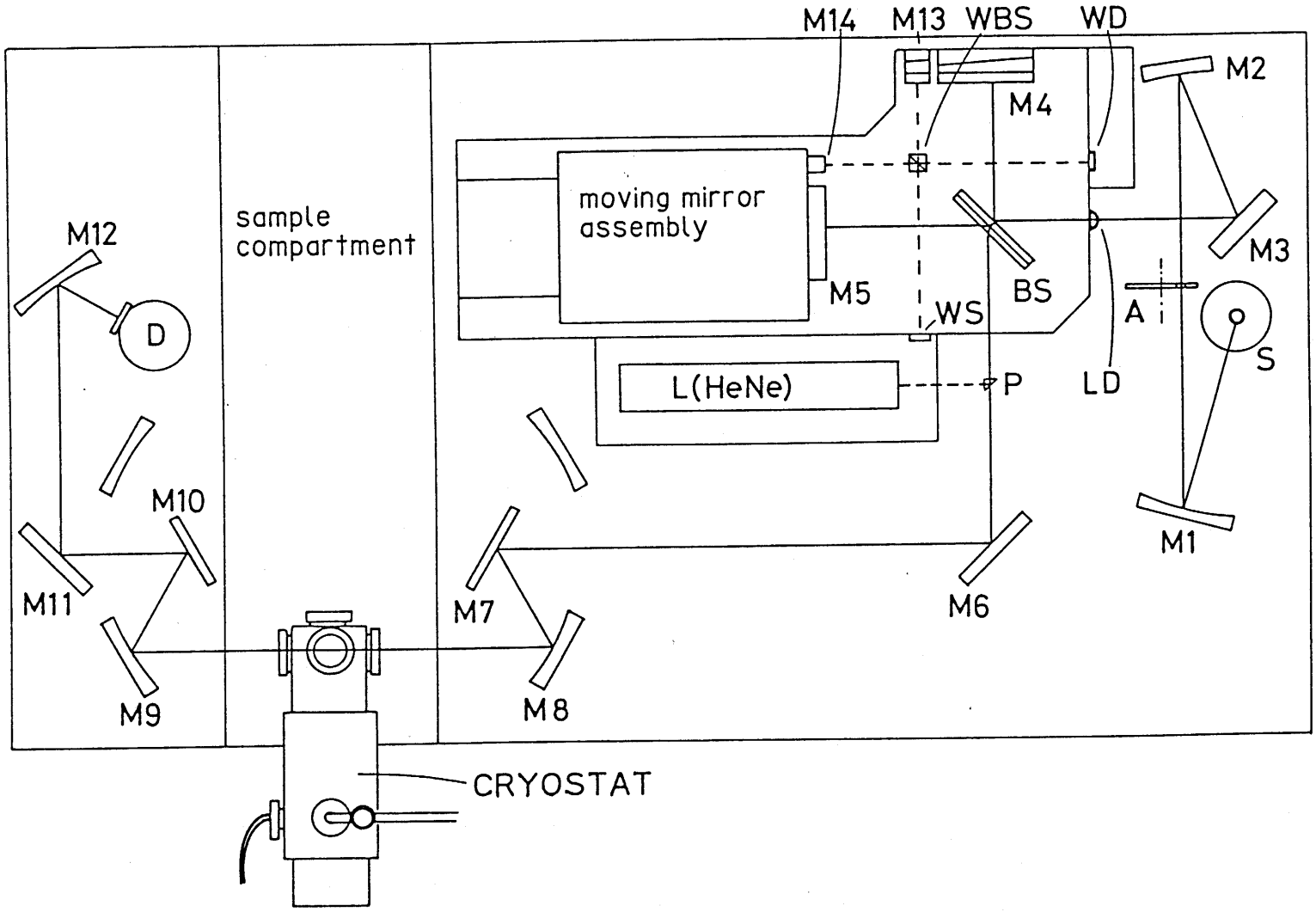

Fig.2.7. The optics of the Nicolet 7199 FT-IR. The cryostat is installed in the sample compartment of the spectrometer.

3. UV-VIS Spectrometer and Data Processor

A double beam UV-VIS spectrophotometer, HITACHI 220A, and a personal computer (PC), PC-9801 VM2 were used to measure UV-VIS spectra of matrix samples and to analyze the measured spectra. The functions of the spectrophotometer are listed in Table II-II.

The light from a source selected automatically between a D_2 ($\lambda \leq$ 350 nm) and a tungsten (λ > 350 nm) lamp is monochromated by a grating and a suitable optical filter and a slit. Then the beam is chopped and separated into a probe and a reference beam by a rotating sector mirror. The probe beam passes thorough a matrix sample on the sapphire sample plate of the cryostat in the sample compartment of the spectrophotometer. Finally, the sample beam focused into a photomultiplier together with the reference beam. The signal from the photomultiplier is amplified and digitized in the spectrometer system. The digital data are transported bit-serially and asynchronously to the PC thorough a communication interface based on RS-232C standard. Control signals for and status informations from the spectrometer are also communicating with the PC. A program for control of the spectrophotometer, measurement of spectra, transport, storage, display, subtraction, and plotting of spectral data for the present study have been written in N88-BASIC (NEC) language.

TABLE II-II: THE FUNCTIONS OF HITACHI 220A

Available Measurement Area	190 ~ 900 nm
Wave Length Accuracy	±0.3 nm
Wave Length Reproducibility	±0.1 nm
Stray Light	lower than 0.02%
Signal Accuracy	±0.004 Abs.
Baseline Stability	lower than 4×10^{-4} Abs./h
Available Band Pass	0.1, 0.2, 0.5, 1, 2, 4 nm
Light Source	tungsten and D_2 lamp

4. Method.

(a) Preparation of Matrices

Matrix samples are usually prepared by deposition of a mixture of matrix gas and guest molecule on a low temperature target at 10~15K. It is recognized[1] that the target temperature should be chosen below 0.3Tm K, where Tm is the matrix melting point, in order to keep the diffusion of the cold host remains negligible. The M/R ratio is between 10^2 and 10^5 as guest-guest interactions could be negligible. The required sample amount depends on the oscillator strength of the optical transition of an interest. For allowed electronic transitions, only micro-mole quantities of guests are necessary. For infrared or forbidden visible transitions, a milli-mole or more might be necessary. Any material which can be vaporize without decomposition can be embedded in a matrix by deposition of the gas mixture. Some chemical species can be synthesized in situ by diffusion controlled chemical reaction. Another species are prepared by photolysis of vaporized reagent. The concentration of impurities depends on the origin and preparation method of the sample. In the case of chemically or photolytically prepared guests, the impurities might actually outnumber the desired product by a large factor.

Typical matrix materials are the rare gases, H_2, SF_6, lighter hydrocarbons, and nitrogen. SF_6 can be deposited at 77K. N_2 yields clearly transparent solid, making it especially suitable for thick matrices. The rare gases are optically transparent from the ultraviolet. SF_6, CH_4 and other matrices

have infrared absorption which reduce their usefulness for IR work. More reactive materials, for example, O_2, CO, and CO_2 are also used in some case. The useful temperature range is from 1.5K to about 0.6Tm. Above this temperature, the vapor pressure of the matrix leads to vacuum breakdown, diffusion becomes significant, and phase separation can occur.

In our photochemical experiments, typically, about 1 mmol of a gas mixture of organic compound and O_2 (M/R = between 250/1 to 1000/1; M is O_2) has been deposited at 10~11K on the CsI target with a flow rate about 1 mmol/h. For the detection of HSO_x radicals, gas mixtures of SO_2 in Ar (M/R = 250/1; M is Ar) and that of H_2O_2 in Ar (M/R = 1/250 also) have been deposited on the CsI plate at 11K. In all case matrices formed just after depositions have been colorless and clear. Oxygen matrices for UV-VIS measurement were prepared by "pulse deposition method". The detail will be discussed in CHAPTER II.

(b) UV-VIS Spectral Measurement of Organic Molecules Isolated in Oxygen Matrices

The UV-VIS spectrum of a matrix sample was measured through the quartz window with the UV-VIS spectrophotometer communicating with the data processing system. The spectral range measured was 200~900 nm with resolution of 2 nm. A spectrum of pure solid oxygen prepared under the same condition was also measured as a reference. The apparent optical densities of the pure oxygen reference were 1.71, 1.06, 0.60 and 0.27 at 200, 220, 250 and 300 nm, respectively. Besides the Herzberg band absorption of O_2

(<270 nm)[5], surface scattering contributes to the optical density particularly in the shorter wavelength region. Difference spectra were obtained by numerical subtractions of the pure oxygen reference from those of the matrix samples. The resultant spectra are thought to be reliable in the range between 230 to 900 nm. Fig.2.8 shows an example of spectra set of before and after subtracted spectra and a oxygen reference. 2,3-dimethyl-2-butene in oxygen matrix shows spectrum **(a)**, and pure oxygen reference is **(b)**. Spectrum **(c)** is the subtracted **(b)** from **(a)** shows 'net' absorption band.

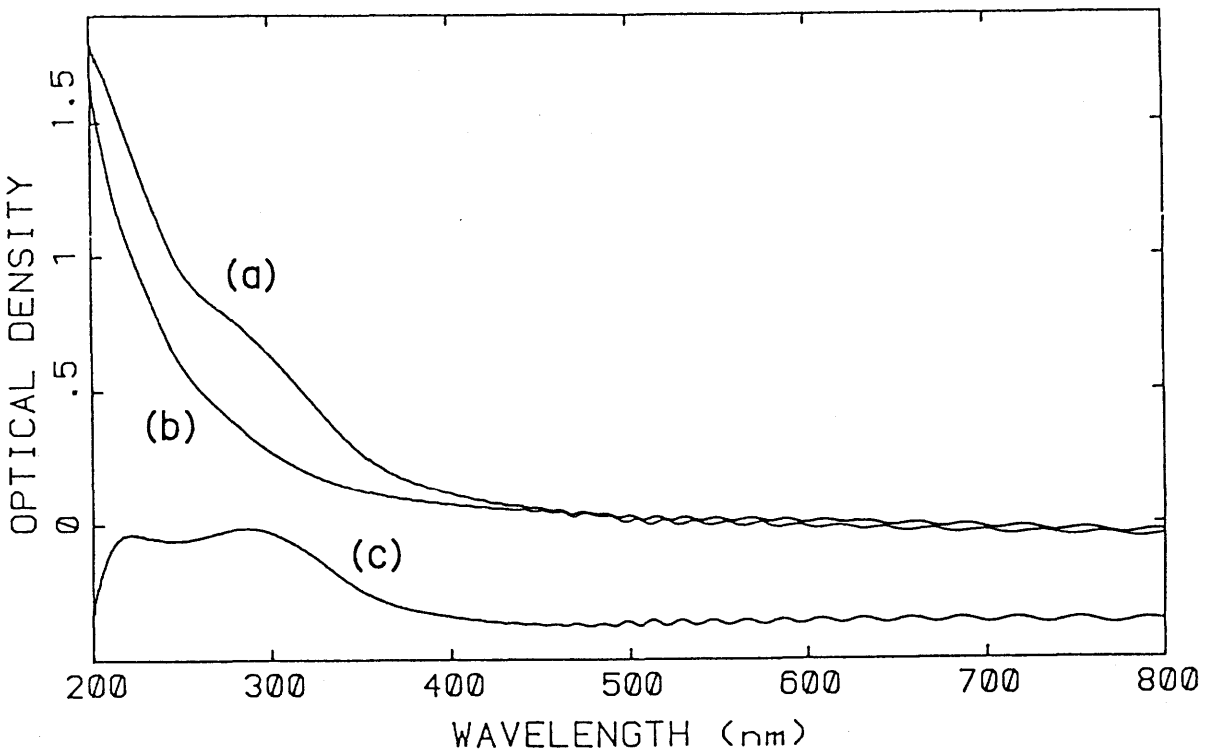

Fig.2.8. UV-VIS absorption spectra of before and after subtracted spectra and a oxygen reference. (a) 2,3-dimethyl-2-butene in oxygen matrix shows spectrum (M/R = 1/250 at 10K), (b) pure oxygen reference, and (c) is the subtracted (b) from (a).

(c) Photochemical Experiments

For the photochemical experiments, a 500-W high pressure mercury arc lamp was used as a light source. A water cell (15 cm in length) with a pair of Supurasil quartz windows and an interference band pass filter combined with a suitable cut filter were used to remove the infrared radiation and to isolate an appropriate wavelength region for excitation. If necessary, to correct relative decay rate constant of a sample under each irradiation condition, the irradiance for each specific excitation wavelength was measured by a thermopile.

About 1 mmol of O_2 with organic compound (M/R = between 250/1 to 1000/1) was deposited on the CsI plate at 10~11K with a flow rate of 1 mmol/h for each photochemical run. IR absorption spectra were measured before and after each irradiation by FT-IR (Nicolet, 7199 system) under the condition of 0.5~1 cm^{-1} of resolution with a liquid N_2 cooled HgCdTe detector; the spectrum range studied was 4000~700 cm^{-1} (type A) or 4000~600 cm^{-1} (type B) depend on the character of the detector used. Type A is a highly sensitive detector, but available bandwidth is narrower. The sensitivity steeply drops below 800 cm^{-1}. Type B has more wide bandwidth than type A, but the peak responsibility is lower than type A. These were used depending on the interested spectral regions.

The irradiation time was chosen so that the decrement of reactants should not exceed 1/3 of initial amount. Product spectra were obtained by partial subtraction of the reactant spectra from those of reaction mixtures after irradiation at the

specified excitation wavelengths. Wavy base-line caused by optical interference were corrected numerically.

CHAPTER II

Reference

1) (a) Hallam, H.E.; Ed. "Vibrational Spectroscopy of Trapped Species", John Wiley & Sons, London, 1973. (b) Barnes, A.J.; Orville-Thomas, W.J.; Muller, A.; Gaufres, R. "Matrix Isolation Spectroscopy", D. Reidel Publication Company, Dordrecht Holland, 1981

2) Griffiths, P.R. "Chemical Analysis Vol. 3: Chemical Infrared Fourier Transform Spectroscopy", John Wiley & Sons, London, 1975.

3) Ferraro, J.R. and Basile, L.J.; Eds. "Fourier Transform Infrared Spectroscopy" Vol. 1., Academic Press, London, 1978.

4) Cooley, J.W. and Tukey, J.W. Math. Comput., 1965, 19, 297.

5) Busschmann, H.W. Ber. Bunsenges. Phys. Chem. 1974, 78, 1344.

CHAPTER III

UV-VIS ABSORPTION SPECTRA OF CONTACT CHARGE TRANSFER BANDS OF SELECTED UNSATURATED ORGANIC MOLECULES IN CRYOGENIC OXYGEN MATRICES

1. INTRODUCTION

The ultraviolet and visible absorption spectra caused by the interaction of organic molecules with O_2 have been well known since the study of Tsubomura and Mulliken[1]. The phenomena has been establishes as charge transfer (CT) interaction. When the ground state of donor-acceptor is a contact pear, whose interaction energy is negligible, it is more restrictively called as contact charge transfer (CCT) interaction. The interaction of O_2 molecule with simple alkenes have well been known as CCT: these have been found in systems of 2-methyl-2-butene and 2,3-dimethyl-2-butene in the oxygen-saturated liquid[2] and propene, 2-methyl-propene, t-2-butene, 2-methyl-2-butene, and 2,3-dimethyl-2-butene in the vapor phase[3] at 70 atm of O_2. CCT absorption also found in many other organic solvent saturated with O_2[1,4].

However, the vertical energy of these CCT transition of contact pairs have not been known since the maxima of the CCT tend to overlap the absorption of original transition of the large majority of solvent molecules free from CCT interaction. When a organic molecule is isolated in oxygen matrix, almost of guests will be surrounded and perturbed by O_2 molecules, then the maximum of CCT band could be shown.

In this chapter, CCT interaction of a series of simple

alkene, arenes and ketenes in solid oxygen at 10K will be discussed with measurements of the absorption maxima in UV-VIS region. The character of electronically excited states of these unsaturated organic compounds in cryogenic oxygen matrix will be investigated.

2. Theoretical Aspects of the Contact Charge Transfer (CCT) Interaction

Considering the charge transfer interaction, the energy of vertical transition, E_{CT}, obtained from the energy of absorption maxima can be expressed as

$$E_{CT} = IP(D) - C_1 + C_2/(IP(D) - C_1), \qquad (3\text{-}1)$$

when the second-order perturbation theory[5] is applied. Here IP(D) is the ionization potential of the donor, and C_1 and C_2 are approximately constant for a series of donor with the same acceptor. A series of donors are benzene and its derivatives which have different numbers of methyl substituents, for an example. The value of C_1 approximately the sum of the electron affinity of the acceptor, EA(A), and the electro static energy between the molecules in the CT state (E_E). C_2 reflects the interaction between the ionic state and non-configurations. When the O_2 is the electron acceptor and some hydrocarbon is the donor (D), the ground state D-O_2 pair is a very weak complex or only a contact pair. In such a case, C_2 thought to be negligible. If the Coulombic attraction energy is almost same over a series of D, E_{CT} should correlate to IP(D) with a slope near unity since the electron affinity of O_2 is constant ($EA(O_2)$ = 0.440±0.008

eV[6]). In such a case, eq. (3-1) can be simplified as

$$E_{CT} \simeq IP(D) - EA(A) - E_E \qquad (3\text{-}2).$$

3. Experimental

Optical transparency of matrices are important to obtain UV-VIS spectra with higher S/N ratio. The ordinal slow deposition method produces a matrix with low transmittance due to optical scattering especially in the UV region. This tendency is not so serious in the Ar matrix, but is a problem in the oxygen matrix. To minimize the optical scattering, the pulsed deposition method similar to those used by Perutz and Turner[7], and Rest at al.[8] was employed. Ten portions of a sample/oxygen gas mixture (M/R = 250/1 for olefins, ketenes, benzene and methyl substituted benzenes, 1000/1 for styrene and naphthalene) in a few cm^3 volume loaded from a 4-liter glass bulb at pressure of 80~100 torr were deposited successively on the sapphire plate at 10K. The total amount of the mixture deposited was ca. 0.25 mmol. Each deposition took 30 seconds with a 90 seconds interval. No temperature increase was observed during the deposition. Spectra were measured in the rage of 200~900 nm with resolution of 2 nm.

Gas samples, ethene, propene, methylpropene, c-2-butene, t-2-butene, CO and CO_2 (all from Takachiho, research grade), were used after degassing. Liquid reagents, 2-methyl-2-butene (Wako), 2,3-dimethyl-2-butene (Aldrich), benzene, toluene, p-xylene, mesitylene and styrene (Wako) were, degassed and purified by trap to trap distillation in vacuum. Naphthalene and durene (Wako) were purified by sublimation in vacuum. Ketene, methylketene and

dimethylketene were synthesized from these dimer (ketene and dimethylketene) or 2-butanone (methylketene) by pyrolysis as discussed in the experimental section in CHAPTER IV. Oxygen and argon (Nippon Sanso) were passed thorough a spiral glass tube at liquid nitrogen temperature just before use. All these reagents and gases were of research grade purity.

4. CCT Absorption in Cryogenic Oxygen Matrices

(a) Simple Alkenes

Fig.3.1 depicts "net" absorption spectra of the simple alkenes in the oxygen matrix (M/R = 250/1) when 0.25±0.01 mmol of each sample was deposited. The spectra were obtained by subtracting the reference spectrum of pure oxygen to remove the contribution of Herzberg band ($A^3\Sigma_u^+ \leftarrow X^3\Sigma_g^-$) absorption of oxygen molecule (<270 nm)[9] and also surface scattering of oxygen matrix. Fig.3.1 demonstrates the CCT bands of the alkene-O_2 pairs in solid oxygen as will be discussed later. The absorption maxima are clearly seen at 218 nm (optical density, 0.16) for propene, 243 nm (0.14) for 2-methylpropene, 234 nm (0.20) for CB, 235 nm (0.24) for t-2-butene, 263 nm (0.17) for 2-methyl-2-butene and 287 nm (0.36) for 2,3-dimethyl-2-butene. In the case of 2,3-dimethyl-2-butene, long tail extending into the VIS region to about 550 nm was observed.

The oscillatory structures in long wavelength part as shown in Fig.3.1 are artifact of the optical fringe caused by interference. The thickness of the matrix can be estimated from the intervals of the fringe. The average thickness of matrices thus estimated is 5.61±0.06 μm. Assuming that the sample plate of 2.0 cm diameter is covered evenly, the amount of sample actually deposited on the plate is estimated to be 0.078 mmol from the thickness and the density of solid oxygen (d=1.426 at 21K), which can be compared with the total amount of deposition of 0.25 mmol. Thus, the deposition efficiency is calculated to be 31%. The concentration of alkene in solid O_2 can be

calculated to be 0.178 mol/l from the M/R ratio and the density. Then, the molar absorption coefficients (ε) of the CCT bands at their absorption maxima can be estimated from the thickness of the matrix and the concentration of alkene in solid oxygen using the absorbance given in Fig.3.1: propene, 1.5×10^3; CB, 1.8×10^3; t-2-butene, 2.2×10^3; 2-methyl-2-butene, 1.5×10^3; and 2,3-dimethyl-2-butene, 3.3×10^3 l $mol^{-1}cm^{-1}$, respectively.

Therefore, when we plot E_{CT} (in eV) against IP(D) (in eV) for the series of alkenes studied, the correlation is expected to be linear with a slope of unity if eq. (3-2) could be applyed. In such condition, the upper state is a charge transfer state with a potential characterized by a pure coulombic attraction. Fig.3.2 demonstrates the linear correlation between the experimental values of E_{CT} and the literature values of IP(D) (given in Table III-I) with a slope of 0.96 ± 0.11. Thus, the CCT character of the observed bands in the present study has been established and the upper states are found to be purely coulombic ion pair states.

The main features of the CCT bands of 2,3-dimethyl-2-butene in the oxygen-saturated liquid[2] are similar to those obtained in the present study but a long tail of absorption extending to >500 nm was observed in solid oxygen. In the vapor phase spectra[3], only a long wavelength edge of the oxygen enhanced absorption has been observed. They were assigned to the T ← N transition for propene, 2-methylpropene and t-2-butene, and to the CCT absorption for 2-methyl-2-butene and 2,3-dimethyl-2-butene.

The CCT absorption spectra for some arenes in oxygen

matrices have been reported by Rest et al.[8] In their experiments, singlet-triplet absorption bands of benzene and toluene have been observed overlapping to the CCT bands. On the contrary, no oxygen-enhanced singlet-triplet absorption[3,10] accompanying a vibrational structure was clearly observed in the range of 280~350 nm for either alkene (2-methyl-2-butene or 2,3-dimethyl-2-butene) under our experimental conditions. This result agrees well with the previous data[1,11] that the oxygen-enhanced singlet-triplet absorption bands have much smaller transition moment than those of the CCT bands.

Table III-I gives the estimated values of Coulombic attraction energy (E_E) calculated from eq. (3-2) using the values of IP(D) and E_{CT} cited in the table. Further, the energy of formation of an electric dipole pair from two elementary charges is given by Birks et al.[12] as,

$$\Delta W \simeq E_E = \frac{14.41}{R_{DA}} \quad eV \qquad (3\text{-}4)$$

where R_{DA} is the charge separation in A. R_{DA} values thus calculated from the ΔW values are also given in Table III-I. Using the van der Waals radii of oxygen atom (1.40A) and carbon-carbon double bond plane (1.70A), the separation between the dipole pair may be estimated to be 3.1 or 4.5A when the O_2 molecule lies parallel or perpendicular to the plane, respectively. The observed value of 4.1 $\pm$ 0.2A, being nearly independent of the number of methyl substituents, lies between these values, suggesting that the O_2 molecule lies on the tilt to the double bond plane in the ground state. The long-wavelength

tail of the CCT band for 2,3-dimethyl-2-butene might be due to the 2,3-dimethyl-2-butene-O_2 pair in which O_2 lies parallel to the double bond plane. For such a CCT pair with a different geometric configuration, the upper state potential surface would also be different.

Table III-I. Parameters for the CCT pair of the alkene-O_2 system

alkene	IP(D)/eV[a]	E_{CT}/eV[b]	ΔW/eV[c]	R_{DA}/A[c]
ethene	10.51	-	-	-
propene	9.73	5.68	3.61	3.99
2-methylpropene	9.23	5.11	3.68	3.92
c-2-butene	9.13	5.30	3.39	4.25
t-2-butene	9.13	5.28	3.41	4.23
2-methyl-2-butene	8.67	4.71	3.52	4.09
2,3-dimethyl-2-butene	8.30	4.32	3.54	4.07

a. Data from reference 13). Values determined by a photoionization technique are adopted. Associated errors are typically $\pm$0.02 eV.
b. Determined from the absorption maxima of the CCT bands shown in Fig.3.1. Associated errors are typically $\pm$0.07 eV.
c. Associated errors for ΔW and R_{DA} are estimated to be $\pm$0.1 eV and $\pm$0.12 A.

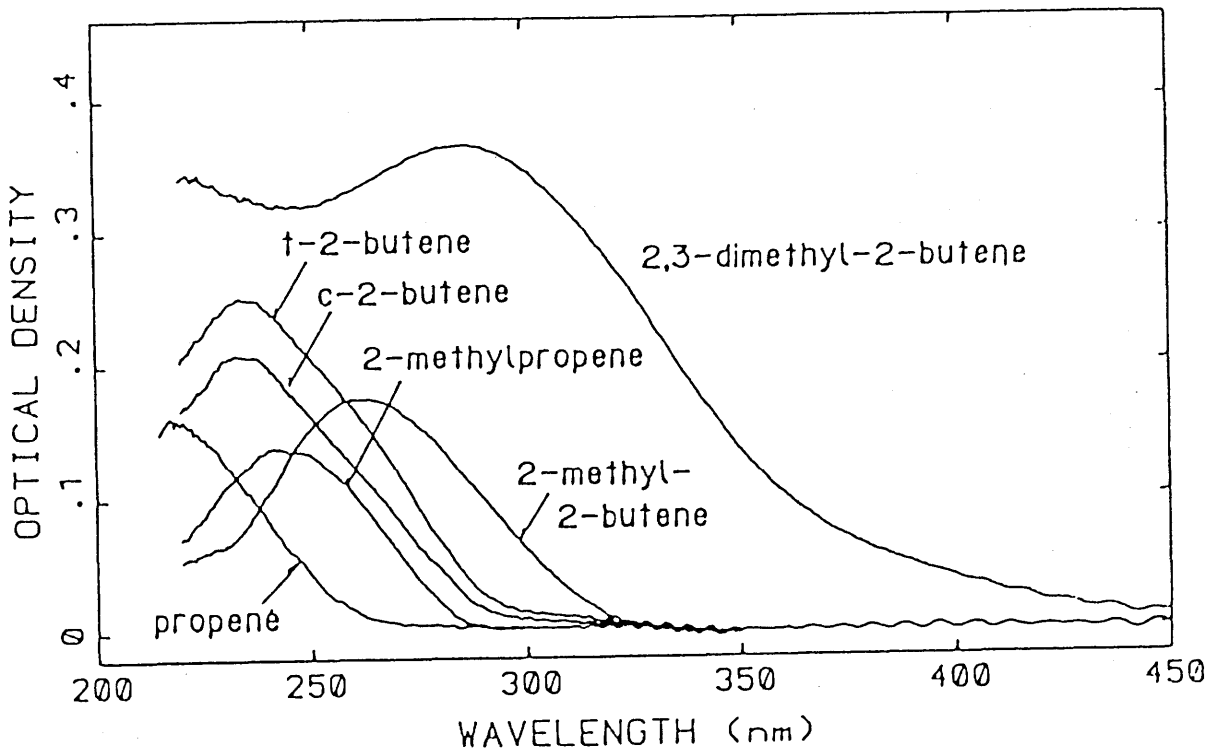

Fig.3.1. UV-VIS absorption spectra of alkene-O_2 systems (M/R = 250/1) at 10K, obtained by subtracting a pure oxygen reference from original spectra.

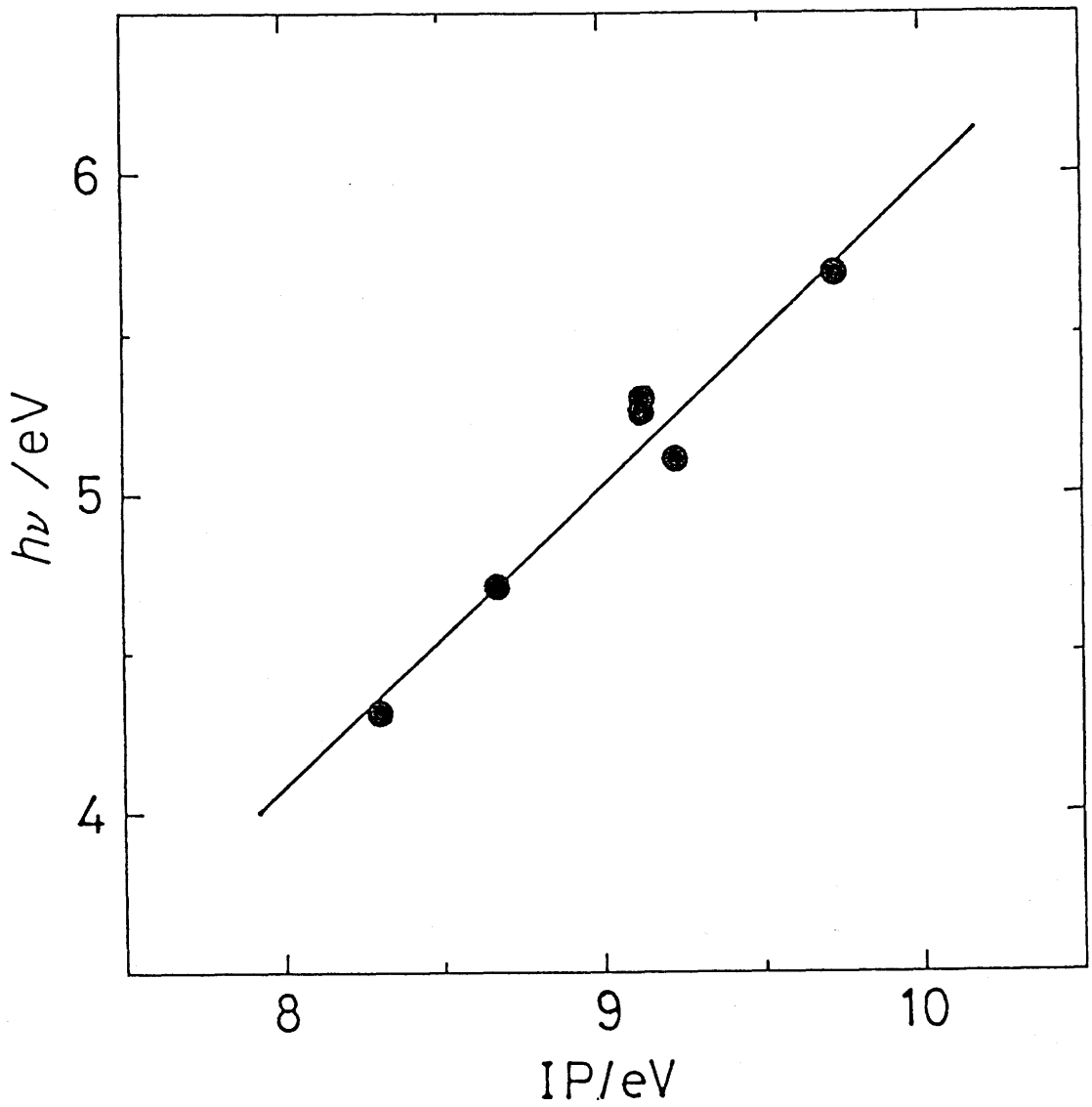

Fig.3.2. The correlation of the energy of absorption maxima of the CCT spectra of the alkene-O_2 systems against the ionization potential of alkenes. The slope is 0.96 ± 0.11.

(b) Simple Arenes

The CCT absorption spectra of arene-O_2 pairs has attracted much interest since Evans[4a] reported oxygen-enhanced absorption spectra of oxygen-saturated liquid benzene, toluene, styrene, and several other arenes in 1953, although the reported absorption maxima were later ascribed to an instrumental error[4b,14]. In 1960's several studies[11,14~16] were reported on the CCT absorption spectra of arene-O_2 system in the liquid phase. In all these studies, however, only enhanced absorptions overlapping the long wavelength tails of the first singlet symmetry-forbidden bands were generally observed, and no well-resolved absorption maximum was revealed. Only for benzene, Lim and Kowalski[14] presented the spectrum of the CCT absorption in liquid phase as a difference spectrum between with and without pressurized oxygen, which showed the absorption maximum at around 220 nm. Birks and coworkers[17] later reported the absorption maximum for the benzene-O_2 charge transfer band in the vapor phase at 219 nm. More recently, Rest et al.[8] studied the absorption bands of benzene, toluene, styrene and indene in the cryogenic solid phase at low mixing ratios (between 10/1 to 1/60). They presented the difference spectra between those obtained in the O_2 and Ar mixture as the CCT bands with O_2. The absorption maximum of benzene-O_2 (M/R = 1/1) system reported was 235 nm.

Absorption Spectra. Fig.3.3 shows the observed UV absorption spectra of (1) benzene, (2) toluene and (3) p-xylene in the oxygen matrices (M/R = 250/1) comparing with those in the argon matrices (M/R = 250/1). The spectra in the oxygen matrices

were obtained by subtracting the reference spectrum of pure oxygen. The vertical scale of the spectra in both matrices are the same for each compound. Fig.3.4 presents similar comparison of the spectra for (1) styrene and (2) naphthalene in oxygen and argon matrixes (M/R = 1000/1). The UV absorption spectra of benzene, toluene, p-xylene, mesitylene and durene in oxygen matrices (M/R = 250/1) are depicted in Fig.3.5 illustrating the spectral shift and change of the spectral shape of the absorption bands as the number of methyl substituents increases.

The absorption coefficients (ε) of these bands at their absorption maxima can be estimated by same manner as applyed to alkene-O_2 measurement. From the absorbance, the thickness of the matrix (5.6 μm) and the concentration of arenes in solid oxygen (180 mmol/l for M/R = 250/1, 45 mmol/l for M/R = 1000/1). The absorption maxima and the estimated absorption coefficients (in parentheses) are as follows: 238 nm (5.4×10^3) for benzene, 247 nm (3.4×10^3) for toluene, 255 nm (3.0×10^3) for p-xylene, 263 nm (2.8×10^3) for mesitylene, 266 nm (2.8×10^3) for durene, 238 nm (2.4×10^4) for styrene, around 260 nm (8×10^3, very broad) for naphthalene.

Figs.3.3~5 show that all these absorption bands have a long tail for longer wavelength side. Except the spectrum of benzene in the oxygen matrix which has a single peak, each spectrum of methyl substituted benzenes consists of two absorption bands. The spectrum of styrene has one strong peak at 238 nm with a very long tail to about 330 nm. Naphthalene has very broad absorption around 230 to 350 nm.

As seen in Fig.3.5, the UV absorption spectra of the methyl substituted benzenes seem to consist of two absorption bands. The second band at longer wavelength part is indiscernible for benzene and is apparent as a small shoulder for toluene. With the increase of the number of methyl substituents, the intensity of the second (longer wavelength) band becomes comparable to the main band. Fig.3.6 depicts the plots of the vertical transition energy corresponding to these absorption maxima of the main (shorter wavelength) band against IP(D) for a series of methyl substituted benzenes (closed circles) comparing with that for alkenes (open circles) studied previously. It should be noted that the plot for benzene lies on the slope for the series of the shorter wavelength component of the methyl substituted benzenes shows that this band of benzene constitute the main series. As seen in Fig.3.6, the correlation of the vertical transition energy against IP(D) for the methyl substituted benzenes is linear, which represents the transitions are essentially of the CT character. However, the slope is 0.46 ± 0.13, which is far from unity. This is in contrast with the case of alkenes whose slope is nearly unity (0.96 ± 0.11) as expected from equation (3-2). This means that the CT states of the methyl substituted benzenes are not characterized as pure coulombic attraction but valence interaction should also be participating.

Here it should be noticed that the intrinsic $S_1 \leftarrow S_0$ transition of the arenes lies in the close energy range to that of the CCT bands in oxygen matrix and the intensity of the former bands is never negligible as shown in Fig.3.3. The intensity of

the intrinsic band observed in the argon matrix increases as the number of substituted methyl groups increases, so as the intensity of the second band. Another evidence which should be noted is that the vibrational structure of the band observed in the argon matrix disappears in the oxygen matrix. This suggests the existence of strong perturbation to the first excited state of these compounds by surrounding O_2 molecule(s). Since the energy level of the CT state and the first excited state of the electron donor molecule are close and there is strong interaction between them, these two could be mixed to split into two levels, which should be a cause of the appearance of the two absorption band for each compound. Considering a relative intensity and excitation energy for the two bands, the main series should retain more of the nature of the original CCT bands, and the second series should be recognized as perturbed $S_1 \leftarrow S_0$ bands. It is interesting to note that the spectrum of benzene retains a vague vibrational structure of the $^1B_{2u} \leftarrow {}^1A_{1g}$ bands, which should reflect the fact the mixing of the CCT and $^1B_{1u}$ state is less significant. This is also consistent with the fact the IP(D) plot of benzene (Fig.3.6) falls on the line for alkenes whose excited state is known to be purely ionic.

For styrene, Fig.3.4 show that the spectral intensity in the argon matrix is comparable with that in oxygen. The spectrum for styrene in the argon matrix shows a strong absorption band around 230~260 nm and weak one around 270~290 nm both showing vibrational structures. The former is due to $\pi \rightarrow \pi^*$ transition of the olefinic part conjugated with the aromatic system, and the

latter is a benzenoid band. The disappearance of the vibrational structure and the enhancement of the absorption at the longer wavelength region in the oxygen matrix shows the presence of a CCT band and the strong perturbation by the CT state to these intrinsic transitions. Also for naphthalene, the bands can be interpreted as they consist of the CCT and the perturbed intrinsic transition.

Rest et al.[8] typically measured a spectrum of a 1/1 mixture of arene/oxygen, which may be characterized as a mixed crystal rather than a matrix isolated arene-O_2 pair. By subtracting the spectra of the arene in argon and of pure oxygen from that of the mixture of arene/oxygen, they reported the difference spectrum as a CCT band. Ignoring small difference of the band shape, these spectra for benzene and toluene agreed well with those observed in the present study. Reported absorption maxima at 235 and 246 nm agreed well with our values of 238 and 247 nm, respectively. They also applied the same treatment for styrene and reported the difference spectrum showing two distinct absorption maxima at 228 and 268 nm, both assigning to the CCT bands. However, judging from the strong perturbation and the comparable intensity between the intrinsic and CCT bands of styrene shown in Fig.3.4, subtraction of the spectrum in argon from that in solid oxygen should not be justified to obtain the CCT spectrum. Thus, their "CCT spectrum" must have suffered substantial distortion and the reported one of unusual band shape with a sharp edge should be an artifact. This is also the case for indene whose intrinsic absorption bands have comparable intensity to the CCT bands. It

is generally concluded that the complete separation of the pure CCT band from the intrinsic band is impossible for most of arenes.

The CCT absorption maximum of the liquid[14] and vapor[17] phase benzene pressurized by O_2 has been reported to be at around 220 nm, whereas the maximum in the O_2 matrix is at 238 nm as shown in 1a in Fig.3.3. Since the energy of the absorption maximum for benzene in the present study is in line with all other methyl-substituted benzenes as depicted in Fig.3.3, it may be concluded that previously reported values would have suffered from error attributable to subtraction of large absorption by unperturbed benzene.

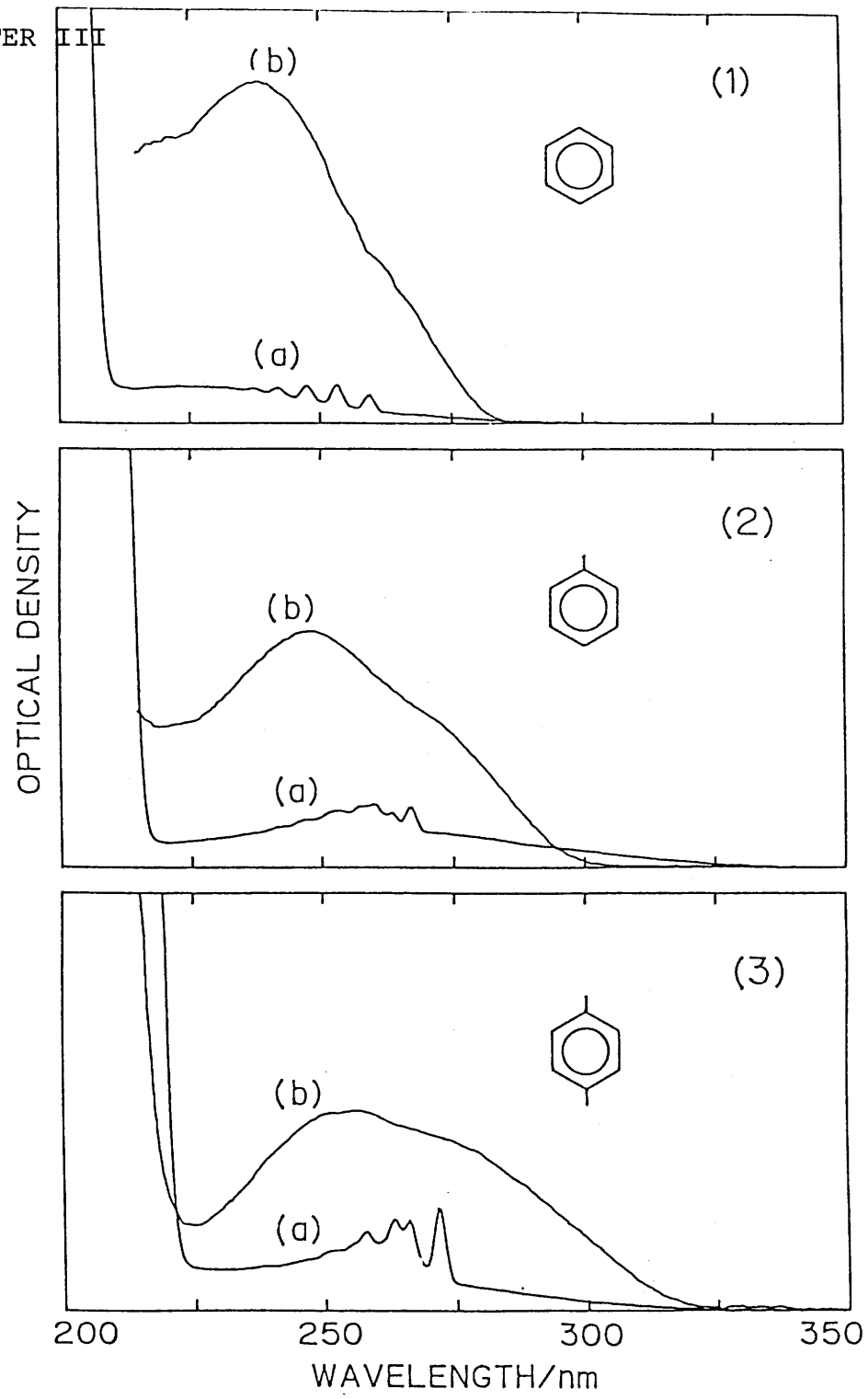

Fig.3.3 UV absorption spectra of benzene and methyl substituted benzenes with M/R = 250/1 at 11K; **(1)** benzene, (a) in argon matrix and (b) in oxygen matrix; **(2)** toluene, (a) in argon matrix and (b) in oxygen matrix; **(3)** xylene, (a) in argon matrix and (b) in oxygen matrix. Spectra measured in oxygen matrix are obtained by subtraction of a pure oxygen reference.

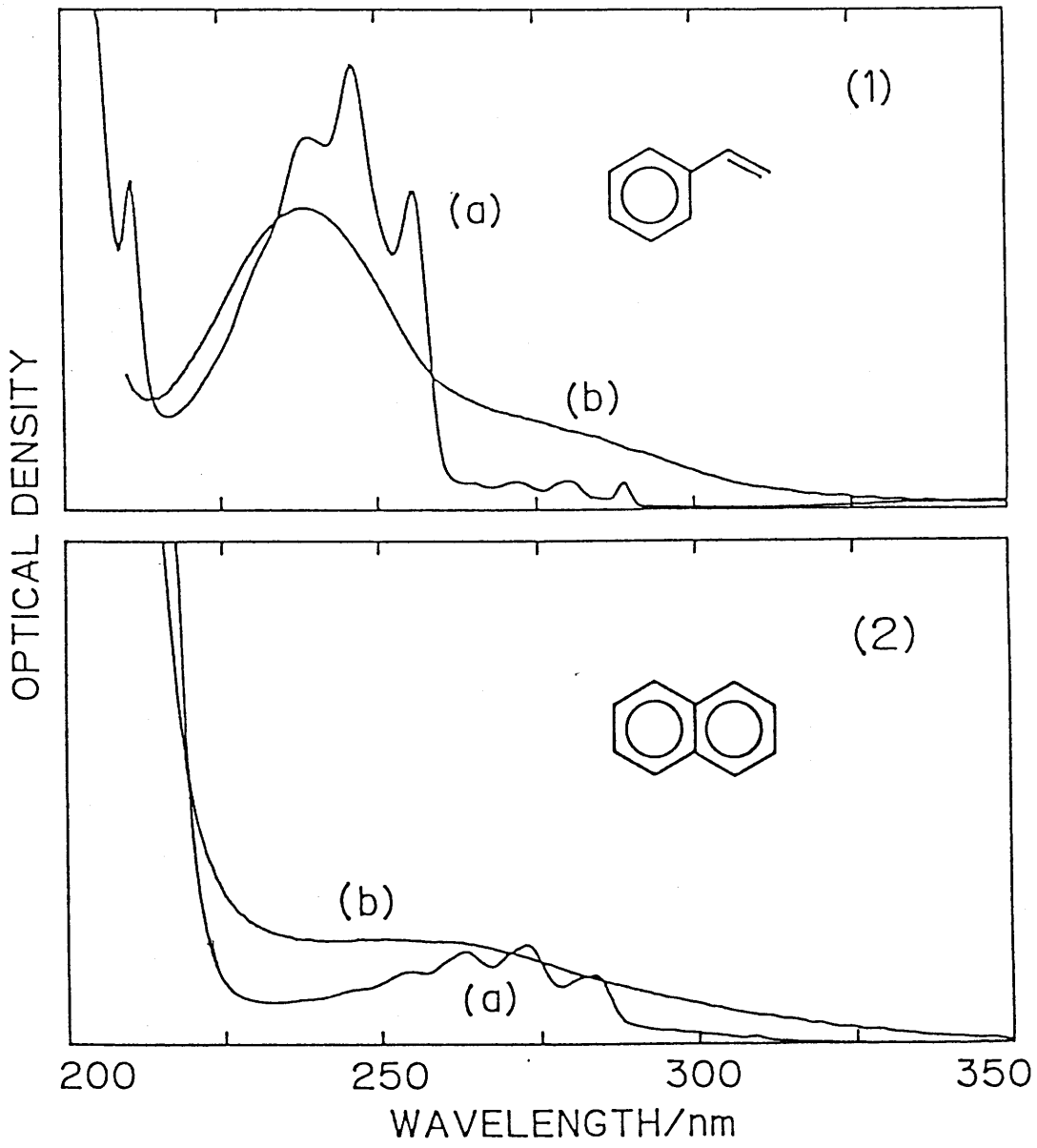

Fig.3.4. UV absorption spectra of styrene and naphthalene with M/R = 1000/1 at 11K; (1) styrene, (a) in argon matrix and (b) in oxygen matrix; (2) naphthalene, (a) in argon matrix and (b) in oxygen matrix. Spectra measured in oxygen matrix are obtained by subtraction of a pure oxygen reference.

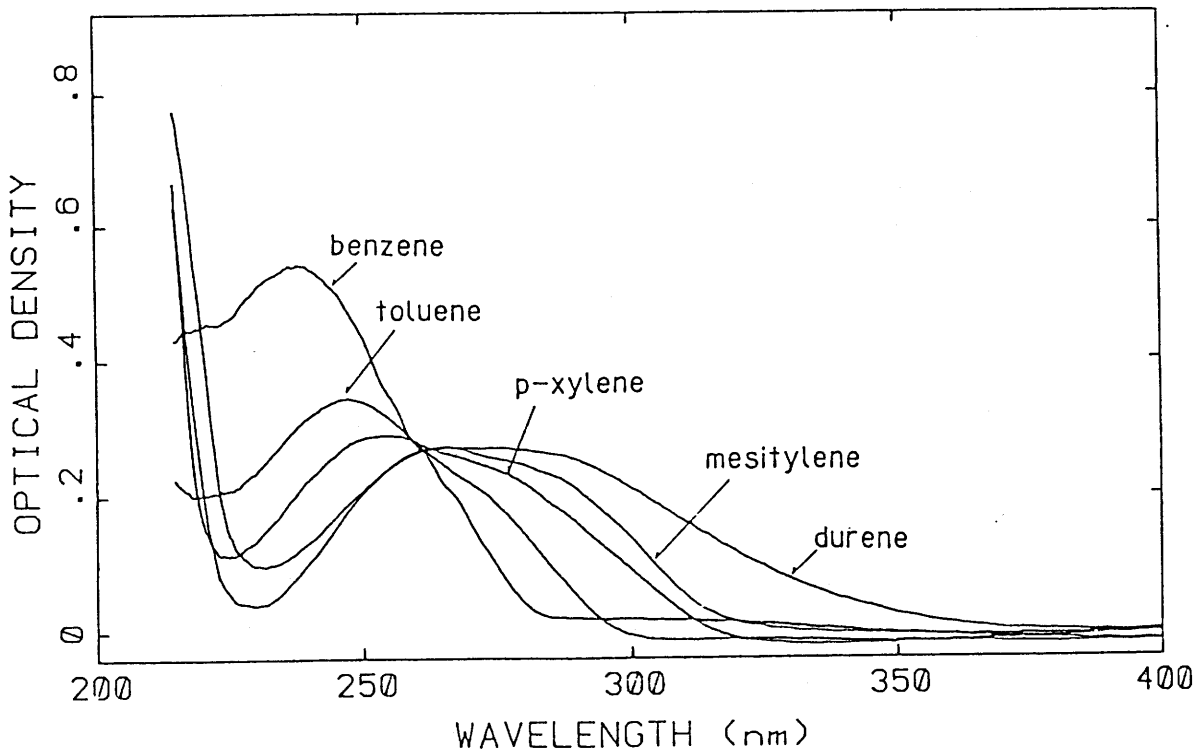

Fig.3.5. UV absorption spectra of benzene and methyl substituted benzenes in oxygen matrix with M/R = 250/1 at 11K for (a) benzene, (b) toluene, (c) xylene, (d) mesitylene and (e) durene.

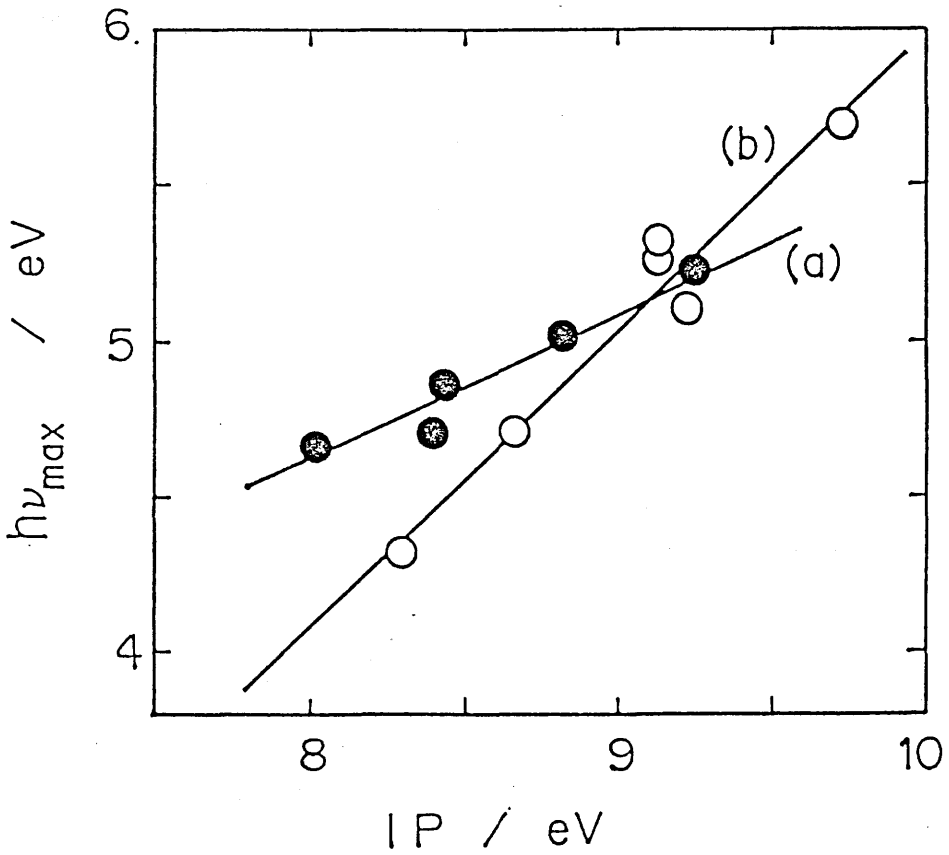

Fig.3.6. Correlation of the energy of absorption maxima of the CCT spectra against the ionization potential. (a) alkyl benzene-O_2 system (●), (b) alkene-O_2 system (O).

(c) Ketenes

Fig.3.7 shows absorption spectra of ketene a(m), methylketene b(m) and dimethylketene c(m) in oxygen matrices (M/R = 250/1, 0.25±0.01 mmol deposited) after subtraction of the pure oxygen standard. The absorption maxima are seen at <220 nm (optical density > 0.15) for ketene, 242 nm (0.14) for methylketene, 292 nm (0.12) for dimethylketene. The oscillatory structures in long wavelength part shown in c(m) is artifact as in the spectrum of 2,3-dimethyl-2-butene. The molar absorption coefficients (ε) of the CCT bands at their absorption maxima can be estimated from the thickness of the matrix and the concentration of ketene to apply the same manner as discussed in section 4.(a): $\varepsilon > 1.4 \times 10^3$ for ketene, 1.4×10^3 for methylketene and 1.1×10^3 for dimethylketene. These values of absorption coefficients are in the same range as in the case of alkene-O_2 system. The correlation of the energy of absorption maxima of the spectra of these ketene-O_2 systems against these ionization potential[13,18] (open circles and a ellipsoid) plotted over the slope (0.96±0.11) of the alkene-O_2 systems (closed circles) in Fig.3.8. The ellipsoid denotes the uncertainty in the CT energy for ketene, absorption maximum in whose spectrum is unknown. The plots for ketenes are very close to the slope for alkenes. Therefore, in the series of ketenes, the upper state of the transition is a charge transfer state with a potential characterized by a pure coulombic attraction as found in the alkene-O_2 system.

These ketenes show absorption of forbidden $n \rightarrow \pi^*$ transition

at 326, 357 and 370 nm in gas phase for ketene (Fig.3.7**a**(g)), methylketene (Fig.3.7**b**(g)) and dimethylketene (Fig.3.7**c**(g)), respectively. Intensity of these forbidden bands are around 10 in ε. Existence of intrinsic bands at longer wavelength part is a difference from the case of alkenes. Only a small part of the CT bands of ketenes and methylketene are overlapped with that of the n→π* band while the longer part of the CT band of dimethylketene are largely overlapped with the n→π* band. In the photochemical experiment, the difference can be revealed between the CT excited photochemical reaction and n→π* excited, in the case of methylketene.

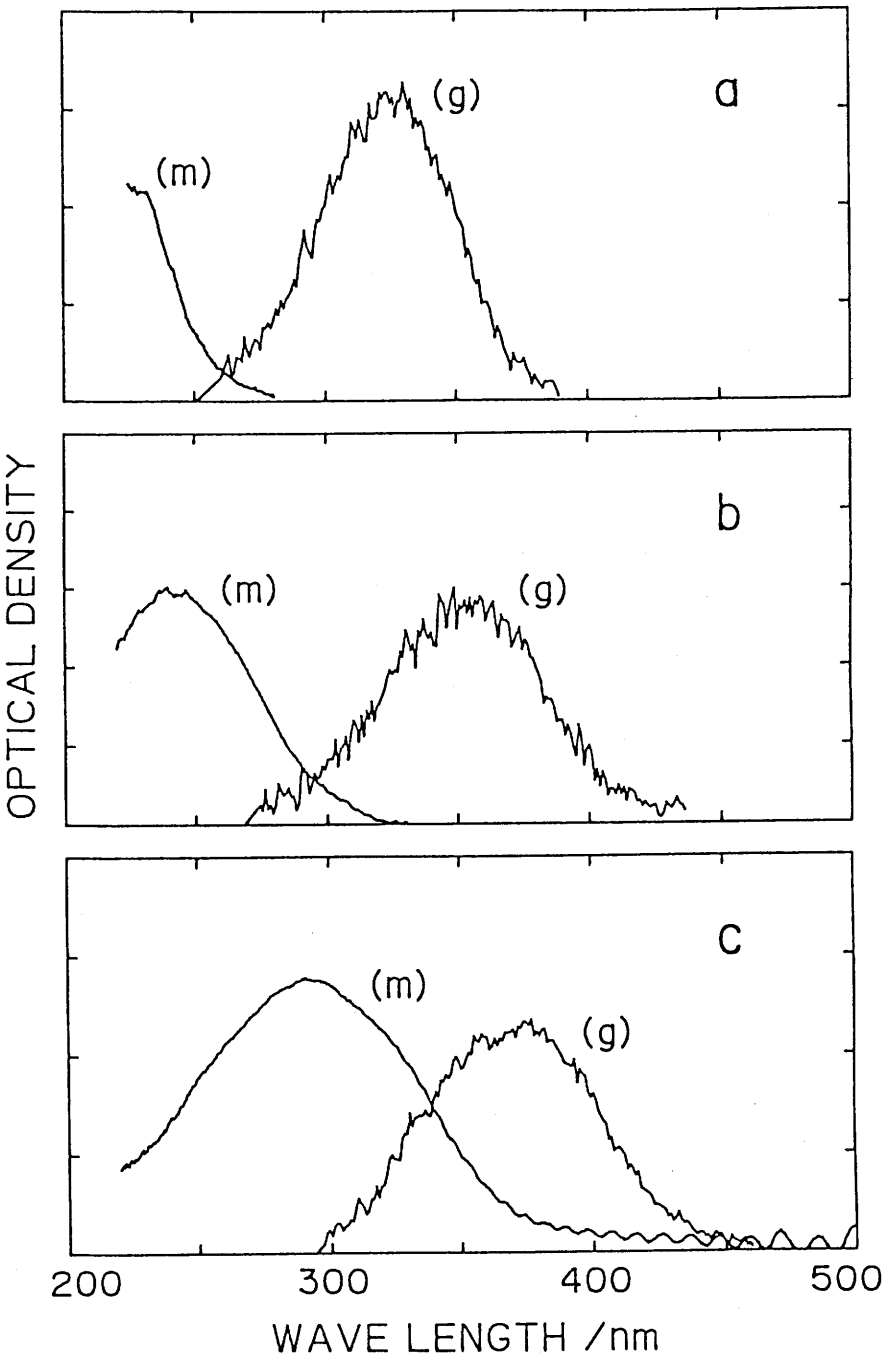

Fig.3.7. UV absorption spectra of ketene and methyl substituted ketenes: **a** ketene, (g) in gas phase and (m) in oxygen matrix; **b** methylketene, (g) in gas phase and (m) in oxygen matrix; **c** dimethylketene, (g) in gas phase and (m) in oxygen matrix. Spectra measured in oxygen matrix are obtained by subtraction of a pure oxygen reference. All matrix conditions are M/R = 250/1 at 10K. Gas phase spectra were measured at about 10 torr at room temperature in a 10 cm gas cell.

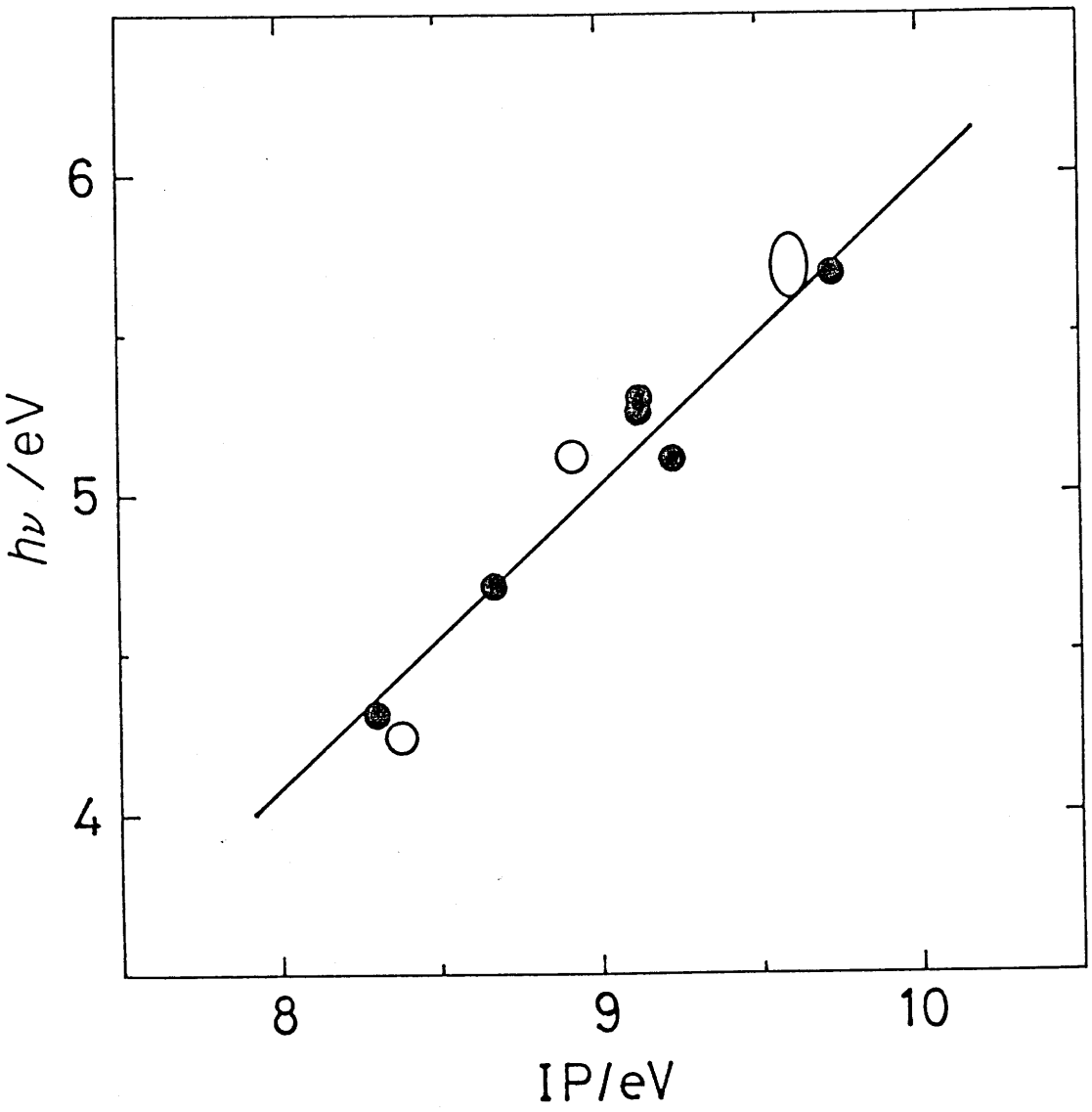

Fig.3.8. The correlation of the energy of absorption maxima of the CCT spectra of the ketene-O_2 systems against the ionization potential of ketenes (open circles and a ellipsoid). The slope 0.96 ± 0.02 is of the alkene-O_2 systems (closed circle).

5. Conclusion

The UV-VIS absorption spectra of alkene-O_2 pairs in solid oxygen at 10K was studied. The contact charge transfer (CCT) bands separated well from the intrinsic absorption bands of isolated alkenes were recorded with the maxima at 218, 243, 234, 235, 263 and 287 nm for propene, 2-methylpropene, c-2-butene, t-2-butene, 2-methyl-2-butene and 2,3-dimethyl-2-butene, respectively. The vertical transition energy correlated linearly with the ionization potential of the alkenes. .

The UV absorption spectra and photochemical properties of benzene, toluene, p-xylene, mesitylene, durene, styrene and naphthalene in solid oxygen at 11K were also studied. The well-resolved contact charge transfer (CCT) absorption spectra have been observed. Participation of valence interaction to the CT state has been discussed based on the evidence that the spectra of the methyl substituted benzenes consist of two absorption bands, and a vibrational structure of the intrinsic bands disappear. The vertical transition energy of the main CCT band against the ionization potential correlate linearly with the slope of 0.46 ± 0.13, which are far from unity.

In the series of ketenes, the plot of CT energy against these IP very close that of alkenes. The upper state of the transition is a charge transfer state with a potential characterized by a pure coulombic attraction as found in the alkene-O_2 system.

Reference

1) Tsubomura, H.; Mulliken, R.S. J. Am. Chem. Soc. **1960**, 82, 5966.

2) Coomber, J.W.; Hebert, D.M.; Kummer, W.A.; Marsh, D.G.; Pitts Jr., J.N. Environ. Sci. Technol. **1970**, 4, 1141.

3) Itoh, M.; Mulliken, R.S. J. Phys. Chem. **1969**, 73, 4332.

4) (a) Evans, D.F. J. Chem. Soc. **1953**, 345. (b) Evans, D.F. Chem. & Ind. (London) **1953**, 1061.

5) Mulliken, R.S.; Person, W.B. Ann. Rev. Phys. Chem. **1962**, 13, 107.

6) Celotta, R.J.; Bennett, R.A., Hall, J.L.; Siegel, M.W.; Levine, J. Phys. Rev. **1972**, 6, 631.

7) Perutz, R.N.; Turner, J.J. J. Chem. Soc. Faraday Trans. II, **1973**, 69, 452.

8) Rest, A.J.; Salisbury, K.; Sodeau, J.R. J. Chem. Soc. Faraday Trans. II, **1977**, 73, 265.

9) Buschmann, H.W. Ber. Bunsenges. Phys. Chem. **1974**, 78, 1344.

10) Evans, D.F. J. Chem. Soc. **1960**, 1735.

11) Chien, J.C.W. J. Phys. Chem. **1965**, 69, 4317.

12) Birks, J.B.; Pantos, E.; Hamilton, T.D.S. Chem. Phys. Lett. **1973**, 20, 544.

13) Franklin, J.L; Dillard, J.G.; Rosenstock, H.M; Herron, J.T.; Draxl, K; Field, F.H. "Ionization Potentials, Appearance Potentials, and Heats of Formation of Gaseous Positive Ions, NSRDS-NBS26 National Bureau of Standards", June **1969**.

14) Lim, E.C.; Kowalski, L.V. J. Chem. Phys. **1962**, 36, 1729.

15) Jortner, J.; Sokolov, U. J. Phys. Chem. **1961**, 65, 1633.

16) Slifkin, M.A.; Allison, A.C. Nature, **1967**, 215, 949.

17) Briks, J.B.; Pantos, E.; Hamilton, T.D.S. Chem. Phys. Lett. **1973**, 20, 544.

18) Chong, D.P.; Westwood, N.P.C.; Langhoff, S.R. J. Phys. Chem., **1984**, 88, 1479.

CHAPTER IV

CT EXISTED PHOTOCHEMICAL REACTIONS OF SELECTED UNSATURATED ORGANIC MOLECULES IN THE CRYOGENIC OXYGEN MATRICES

1. Introduction

Photochemistry in reactive low temperature matrices is of particular interest from the point that new reaction channels which are not observed in the conventional gas and liquid phase could be found. Reactions in the oxygen matrix are attractive examples, and have been investigated by E.K.C. Lee and his co-workers for formaldehyde,[1a] glyoxal[1b] and sulfur containing compounds,[1c] and by Bandow and Akimoto[2] for ketene. A photochemical reaction induced by direct excitation of the singlet oxygen bands has been reported by Frei and Pimentel[3] on the dimethylfuran in O_2/Ar matrix.

The photochemical reaction of some organic compound in an oxygen matrix could proceed via CT state by excitation at UV-VIS region since the guest molecule with the O_2 molecule shows CCT absorption band whose transition energy and intensity are depend on the ionization potential of the guest as discussed in CHAPTER III. In this chapter, at first, the novel photooxygenation reaction of simple alkenes in solid oxygen excited at the CCT band by UV-VIS light is presented.

One of the alkenes, 2,3-dimethyl-2-butene found to be react with O_2 by irradiation of visible light ($\leq 520 \pm 20$ nm) in oxygen matrix. This compound is characterized by low ionization potential (I.P. = 8.40 eV) among simple alkenes. The CCT band

with O_2 is lie in the longest wavelength region in the simple alkenes. The product is very specific and much different from that known for conventional singlet oxygen reactions. The characteristics of the CCT photochemistry of other alkenes, ethene, propene, 2-methylpropene, c-2-butene, t-2-butene, and 2-methyl-2-butene, in cryogenic oxygen matrices also will be discussed.

Along with the study of alkenes, CT excited photochemistry of a series of arenes in solid oxygen has also been studied. Benzene, toluene, p-xylene, mesitylene, durene, styrene and naphthalene were selected as electron donor molecules. Further more, photochemistry of methyl substituted ketenes, methylketene and dimethylketene, in cryogenic oxygen matrices are also studied. Discussion will be made with previous[2] investigation on the reaction of ketene-O_2 system.

It would be interesting here to compare the results of this work with those of the photochemistry of alkene-O_2 and arene-O_2 systems in gas and liquid phase, and also on surfaces.

2. Experimental

(a) Simple Alkenes

The outline of photochemical experiment have been discussed in the CHAPTER II. The 500-W high pressure mercury arc lamp, the water cell, a selected interference band pass filter together with a cut filter were used as a light source. The maximum transmission wavelength and the band width at half maximum of the filter, and the irradiance at the center of the sample plate are

as follows: >620 nm (an interference long pass filter combined with Corning 0-52, irradiance not measured), 579±11.5 nm (14.7 mW/cm^2). >500 nm (an interference long pass filter combined with Corning 0-52, irradiance not measured), 434±16 nm (14.5 mW/cm^2), 406±18 nm (9.1 mW/cm^2), 364±20 nm (6.4 mW/cm^2), 333±19.5 nm (0.90 mW/cm^2), 322±12 nm (1.3 mW/cm^2), 310±15.5 nm (5.2 mW/cm^2), 297±17.5 nm (3.8 mW/cm^2), 254±17 nm (0.54 mW/cm^2), >220 nm (Corning 9-54, irradiance not measured).

About 0.8 mmol of an alkene/O_2 ($^{16}O_2$ for all alkenes studied, $^{18}O_2$ and 1:1 mixture of $^{16}O_2$-$^{18}O_2$ only for 2,3-dimethyl-2-butene) mixture (M/R = 250/1) was deposited on the CsI plate at 10K with a flow rate of 1 mmol/h for each photochemical run. IR absorption spectra were measured before and after each irradiation by the FT-IR under the condition of 0.5 cm^{-1} of resolution with a HgCdTe detector (4000~700 cm^{-1}).

An IR absorption spectrum of tetramethyl-1,2-dioxetane in an oxygen matrix was obtained as a reference. The glass/PTFE line (see section 2.1.3 in CHAPTER II) was used in order to minimize the decomposition of the dioxetane. Authentic dioxetane was vaporized at 255~260 K from a sample tube connected about 40 cm before the PTFE nozzle. The vapor was swept into the cryostat thorough the line with oxygen gas flow.

Relative integrated absorption coefficients of c-2-butene, t-2-butene, CH_3CHO, CO, CO_2, and O_3 were determined by the spectra of standard mixtures, c-2-butene/CH_3CHO/CO/CO (5/5/5/1), O_3/CO/CO_2 (5/5/2), and c-2-butene/t-2-butene (1/1) in solid oxygen (M/R = 250/1) for the purpose of determining the yields of

products in the (c-2-butene)-O_2 system. Frequency range of the bands used for the quantitative analysis were 1387.4~1382.8 cm^{-1} (c-2-butene), 1382.8~1376.0 cm^{-1} (t-2-butene), 1780~1715 cm^{-1} (CH_3CHO), 2350~2335 cm^{-1} (CO_2), 2150~2130 cm^{-1} (CO) and 1046~1030 cm^{-1} (O_3).

Gaseous reagents, ethene, propene, 2-methylpropene, c-2-butene, t-2-butene, CO and CO_2 (all from Takachiho, research grade) were used after degassing. Two liquid alkenes, 2-methyl-2-butene (Wako) and 2,3-dimethyl-2-butene (Aldrich) were degassed and purified by trap to trap distillation. $^{18}O_2$ (Pro Chem, 99 atom%) was used without further purification. The 1:1 mixture of $^{16}O_2$ and $^{18}O_2$ was prepared by simply mixing the two gases. Authentic sample of tetramethyl-1,2-dioxetane was synthesized by the method of Kopeckey.[4] Degassed acetaldehyde (Wako, 80% aq. solution) in a sample tube cooled at about 270K was distilled trap-to-trap repeatedly to obtain water-free acetaldehyde.

(b) Simple Arenes

The method of photochemical experiment similar to that of the alkene-O_2 systems. About 0.8~1.0 mmol of an arene-O_2 mixture (M/R = 250/1 for benzene and methyl substituted benzenes; 1000/1 for styrene and naphthalene) was deposited on the sample plate (CsI) at 10K with a flow rate of 1 mmol/h for each photochemical run. IR absorption spectra were measured before and after each irradiation by FT-IR with a HgCdTe detector (4000~600 cm^{-1}) with resolution of 1 cm^{-1}.

An experiment using $Ph^{13}CH_3$ (α-^{13}C labeled toluene) in an

oxygen matrix was also done to reveal the reactivity of the substituent methyl group.

Benzene, toluene, p-xylene, mesitylene and styrene (all from Wako) were degassed and purified by trap-to-trap distillation in vacuum. $Ph^{13}CH_3$ of >99% isotopic purity (Merck) was also degassed and purified in the same manner. Naphthalene and durene (Wako) were purified by sublimation in vacuum. All these reagents and gases were of research grade purity.

(c) Methyl Substituted Ketenes

The method of photochemical experiment similar to that of the alkene-O_2 and arene-O_2 systems. About 0.8 mmol of a sample mixture (M/R = 250/1) was deposited on the CsI plate at 10K with a flow rate of 1 mmol/h for each photochemical run. Matrix oxygen was $^{16}O_2$ for both ketenes, and only for dimethyl ketene $^{18}O_2$ and 1:1 mixture of $^{16}O_2$-$^{18}O_2$ also. IR absorption spectra were measured before and after each irradiation by the FT-IR with a HgCdTe detector (4000~700 cm^{-1}) with resolution of 0.5 cm^{-1}.

Dimethylketene was prepared[5] by pyrolysis of dimethylketene dimer (Tokyo Kasei) at about 550 Centigrade in a reactor column, which was held vertically and continuous dry N_2 stream flowed up to down in. The reaction occurred on surface of small quartz tubes (about 10 mm in length, 6/4 mm in OD/ID) packed in the quartz column body (24/20 mm OD/ID). Total length of the reaction area was about 10 cm. Powder of dimethylketene dimer was successively dropped on the top of the reaction area, and dimethylketene thus formed was carried by the N_2 stream out of

the reactor, and passed a cold trap in a dryice-acetone bath to remove remaining dimer, and finally, trapped in a small flask at liquid N_2 temperature. Methylketene was also prepared[5] by pyrolysis of 2-butanone (Wako) with the same manner. Ketene, which was used in CHAPTER III, was also prepare with the same manner from the dimer. Each ketene synthesized was then degassed and purified in vacuum and quickly stored in a Pyrex tube with a graceless valve at liquid N_2 temperature. Just before use, each reagent was vaporized after degassing again and measured in a glass bulb at room temperature.

3. Results

(a) Simple Alkenes

Excitation of the alkene-O_2 systems within the absorption bands shown in Fig.3.1 induced photochemical reaction in all the cases studied. The long-wavelength thresholds of the reactions as expressed by the central wavelengths of optical filters are shown in Table IV-I and are found to coincide approximately with the absorption threshold within the range of the bandwidth of the interference filters. Table IV-I also shows the relative photolytic rates of alkenes at 254 and 297 nm normalized to the photon flux.

Figs.4.1~4 show the IR spectra sets of reactants and products for ethene and propene; c-2-butene and t-2-butene; 2-methylpropene and 2-methyl-2-butene; and 2,3-dimethyl-2-butene, respectively. The product spectra were obtained by partial subtraction of the reactant spectra from those of reaction

mixtures after irradiation at the specified excitation wavelengths. For these experiments irradiation time was controlled to cause typically 30% decrease of reactants. A standard spectrum of tetramethyl-1,2-dioxetane is also shown in Fig.4.4 (d).

Reaction products observed in the irradiation of simple alkenes in oxygen matrices are summarized in Table IV-I. Photolysis of ethene in solid oxygen occurred at >220 nm and formed CO_2, CO, HO_2 and O_3 as shown in Fig.4.1 (b). Trace peaks at 1740.1 and 1734.9 cm^{-1} should be due to formaldehyde (1740.0 cm^{-1})[6] and performic acid (1735.0 cm^{-1})[6], respectively. Other than these products, peaks at 1779.6, 1138.3 and also 872.9 cm^{-1} are discernible but remain unidentified. Trace of these peaks and O_3 were observed after the long irradiation at 254 nm but none of CO_2, CO and HO_2 was produced at this wavelength. In the case of propene (Fig.4.1 (d)), small amount of formaldehyde and acetaldehyde were observed in addition to the same fragmentary products observed for ethene.

Cis-trans isomerization was the major reaction pathway for c-2-butene and t-2-butene as seen in Fig.4.2. It should be noted in Fig.3.1 that c-2-butene and t-2-butene gave substantially different spectra; the band for t-2-butene extend to longer wavelength than that for c-2-butene giving lower threshold energy to induce photochemistry (see Table IV-I). The irradiation of t-2-butene in solid O_2 at 333 nm gives solely c-2-butene as a product while the irradiation of c-2-butene at 322 nm gives a trace amount of CH_3CHO, CO_2 and O_3 in addition to t-2-butene as a

major product. All the fragmentary products, CH_3CHO, CO_2, CO and O_3 were detected for the prolonged irradiation of both t-2-butene and c-2-butene at 297 and 254 nm, although their yields remain low as compared to the isomerization. Table IV-II cites the product distributions of reaction mixtures in the (c-2-butene)-O_2 system after the irradiation. The percentage values are based on the relative integrated absorption coefficients of the reactant and products determined for standard mixtures. Although the product yield against the decrease of c-2-butene seems very low in Table IV-II, it has been found that the thermal annealing of c-2-butene and t-2-butene at ~25K for 3~5 minutes changes their band shape and decreases the integrated absorbance of their bands by 20~30%. Since the similar change of the band shapes was observed when they were irradiated within the CCT band, their integrated absorbance is also expected to decrease as in the case of thermal annealing. This causes the apparent low percentage value of the abundances of both c-2-butene and t-2-butene in Table IV-II since the values in the table are referenced to the relative integrated absorbance of the un-annealed samples. If the corrections due to such effect are taken into account, both abundances of c-2-butene and t-2-butene after the irradiation should increase to give much higher yield of t-2-butene and thus to improve the material balance. The change of the spectral band shape and the apparent decrease of absorbance were not observed when irradiated outside the region of the CCT bands. As expected, the yield of CH_3CHO and other fragmentary products increased to much higher value after the prolonged irradiation

(see Fig.4.2 (b) and (c)). It can be noticed in Fig.4.2 (b) and (c) that the CO_2 yield relative to CH_3CHO also increases as the irradiation time increases suggesting the formation of CO_2 via the secondary photolysis of CH_3CHO.

In the case of 2-methylpropene and 2-methyl-2-butene, CH_3CHO and HCHO, and $(CH_3)_2CO$ and CH_3CHO were observed, respectively, as major products as well as other common fragmentary products (see Fig.4.3). It should also be noted that the substantial change in the spectral band shape of the reactant occurred after the irradiation as evidenced by the partially negative residue of most reactant bands in the product spectra. This feature is especially marked for 2-methylpropene as can be seen in Fig.4.3 (b). Although CO_2 is formed even at low conversion both for 2-methylpropene and 2-methyl-2-butene, its yield relative to carbonyl compounds increases as the irradiation time increases suggesting that secondary photooxygenation of the carbonyl products contributes to the CO_2 formation as in the case of c-2-butene.

Figs.4.4 (b) and (c) show the product spectra of the (2,3-dimethyl-2-butene)-O_2 system after the irradiation at >500 nm and 297 nm, respectively. The product spectra show characteristic IR bands at 3050~2800 (m), 1465.6 (m), 1377.1 (s), 1367.9 (vs), 1191.2 (s), 1173.1 (m), 1155.1 (s), 1132.0 (m), 1110.3 (s), 917.9 (w), 896.6 (w), 751.9 (m), and 630.1 (m) cm^{-1}, which is tentatively identified as tetramethyl-1,2,3,4-tetraoxane (TMT), as will be discussed in section 4.4.2. TMT was the sole product for the excitation at >500 and 406 nm. No reaction occurred for

the excitation at 579 and >620 nm. Acetone, CO_2, CO and O_3 start to appear at 364 nm but remain as minor products even at 297 nm as shown in Fig.4.4 (c). The product distribution changed drastically at 254 nm; the above fragment compounds become major products and TMT is seen only as a minor product. Apparently, secondary photolysis of TMT also contributed to the formation of acetone. As seen from the comparison of the product spectra with Fig.4.4 (d), tetramethyl-1,2-dioxetane was not formed at all as a product.

Fig.4.5 demonstrates the relative quantum yield of 2,3-dimethyl-2-butene photolysis as a function of exciting wavelength compared with the absorption spectrum. The relative quantum yield was obtained from the rate of decrease of 2,3-dimethyl-2-butene divided by the photon flux and the absorbance value at each wavelength. As shown in Fig.4.5, the relative quantum yield increases drastically at <400 nm and reaches an approximately constant value below 334 nm.

Table IV-I. Relative Reaction Rates and Products Observed in the Irradiation of Alkenes in Cryogenic Oxygen Matrices

Alkene	Reaction Threshold[a] nm	Relative Reaction Rates[b] 254 nm	297 nm	Products
ethene	237 ~ 220[c]	---	---	CO_2, CO, HO_2, O_3
propene	254 ± 17	0.032	---	CH_3CHO, HCHO, CO_2, CO, HO_2, O_3
2-methylpropene	297 ± 17.5	---	0.003	$(CH_3)_2CO$, HCHO, CO_2, CO, O_3
c-2-butene	322 ± 12	0.43	0.045	t-2-C_4H_8, CH_3CHO, CO_2, CO, O_3
t-2-butene	333 ± 19.5	0.41	0.005	c-2-C_4H_8[d], CH_3CHO, CO_2, CO, O_3
2-methyl-2-butene	364 ± 20	---	0.088	$(CH_3)_2CO$, CH_3CHO, CO_2, CO, O_3
2,3-dimethyl-2-butene	500 ~ 532	0.27	0.27	TMT[e], $(CH_3)_2CO$, CO_2, CO, O_3

a) Specified by the center wavelength and bandwidth of the interference filter and by the wavelength of 10% transmittance of the long-pass filter.
b) Defined as a first order decrease rate of the integrated absorbance of a reactant IR band being normalized to the photon flux at each wavelength. Apparent decrease of integrated absorption coefficient due to photochemical annealing has not been corrected. See text.
c) The slow reaction due to the oxygen atom or $O_2(^3\Sigma_u^+)$ was observed at 254 nm. See text.
d) c-2-C_4H_8 was a sole product at 297 and 334 nm.
e) TMT(tetramethyl-1,2,3,4-tetraoxane) was a sole product at 406 and >500 nm.

Table IV-II. Distributions (%) of Reactant and Products after the Irradiation of cis-2-Butene in Solid Oxygen Referenced to the Amount of the Reactant before Irradiation[a]

Irradiation wavelength/nm	time/min	Reactant and Products cis[a]	trans[a]	CH_3CHO	O_3	CO_2	CO
322	180	54	13	trace[b]	trace	trace	ND[c]
297	15	70	12	0.5	1.0	0.1	ND
254	10	77	6	0.2	0.2	trace	ND
254	30	48	11	1.1	1.6	0.2	trace

a. Decrease of the integrated absorption coefficients of the bands of c- and t-2-butene due to photochemical annealing has not been corrected giving underestimated values for these compounds.
b. Lower than 0.1%.
c. Not detected.

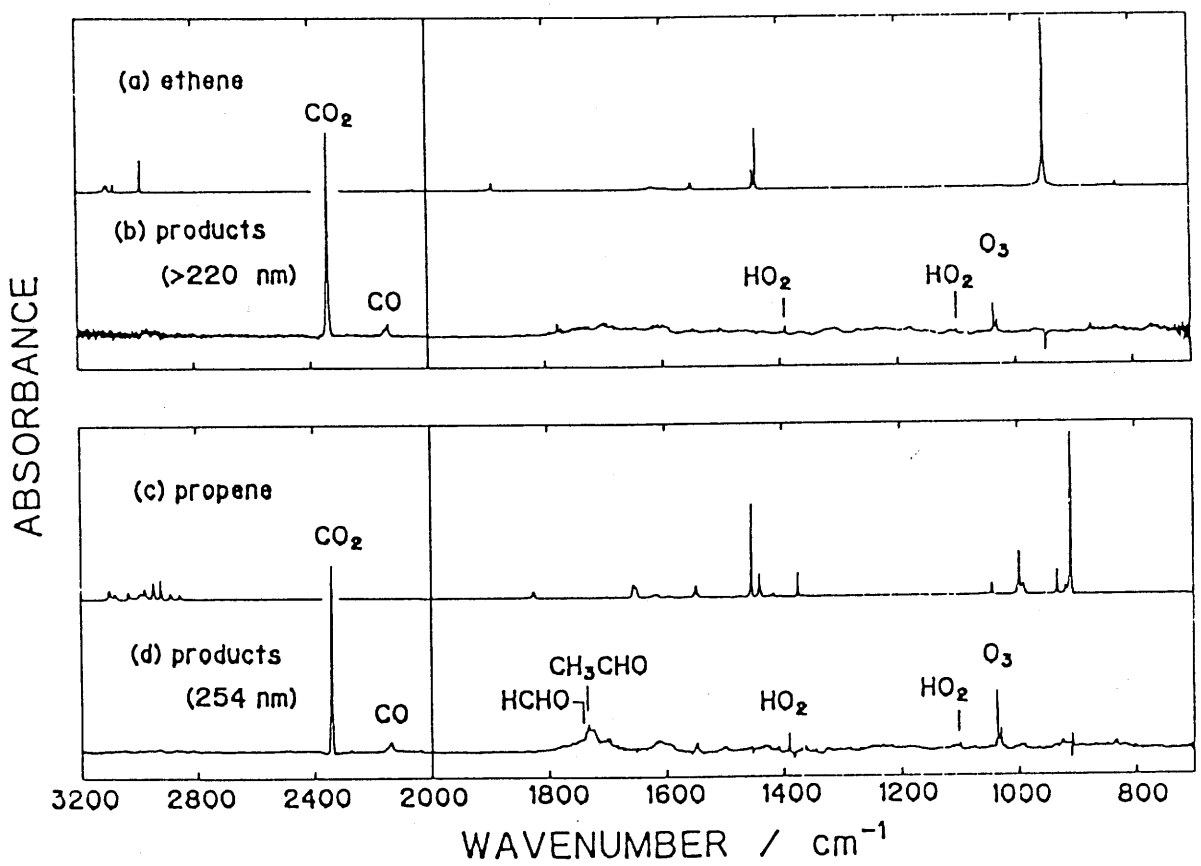

Fig.4.1 IR absorption spectra of (a) ethene in O_2 matrix (M/R = 250/1); (b) the photochemical reaction products after the irradiation at >220 nm for 120 min; (c) propene in O_2 matrix (M/R = 250/1) and (d) the photochemical reaction products after the irradiation at 254 nm for 190 min.

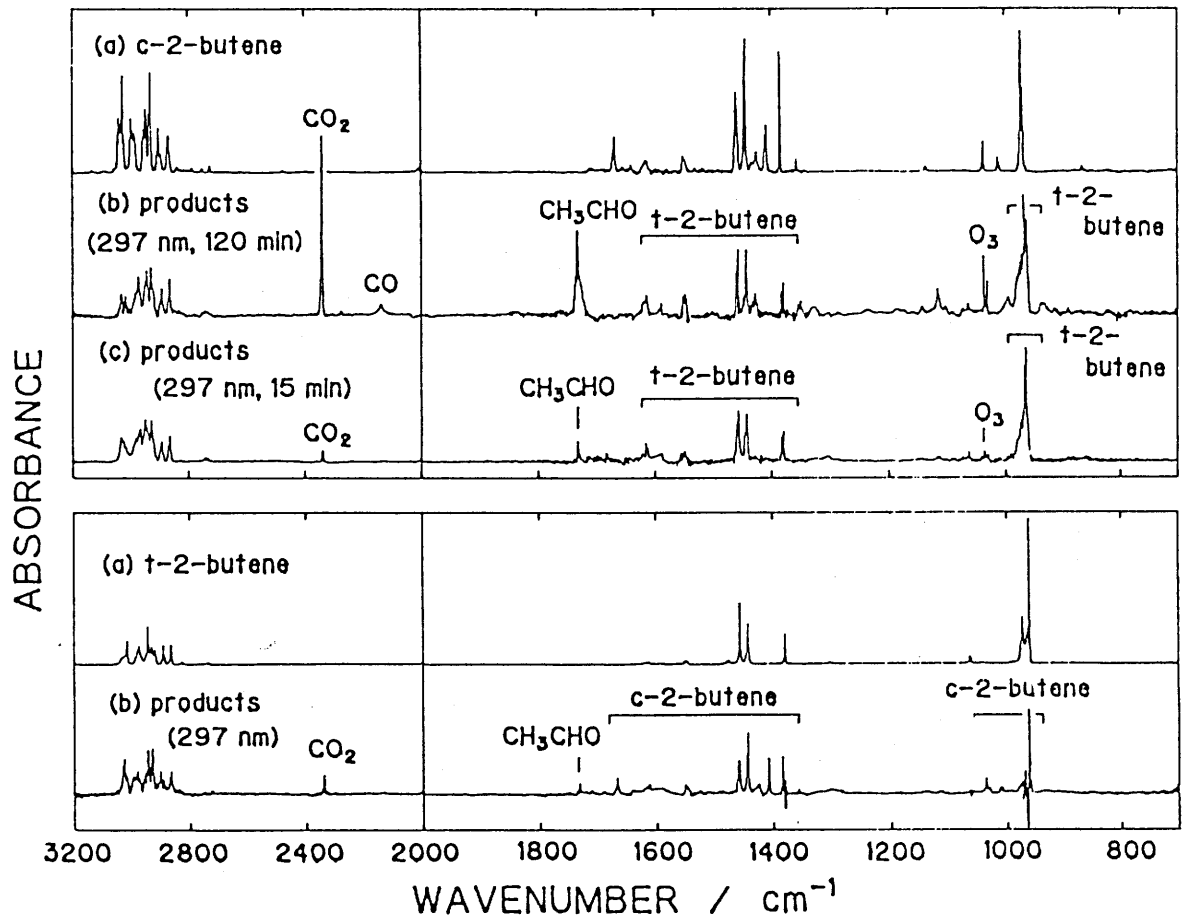

Fig.4.2. IR absorption spectra of (a) c-2-butene in O_2 matrix (M/R = 250/1); (b) the photochemical reaction products after the irradiation at 297 nm for 120 min; (c) at 297 nm for 15 min; (d) trans-2-butene in O_2 matrix (M/R = 250/1) and (e) the photochemical reaction products after the irradiation at 297 nm for 140 min.

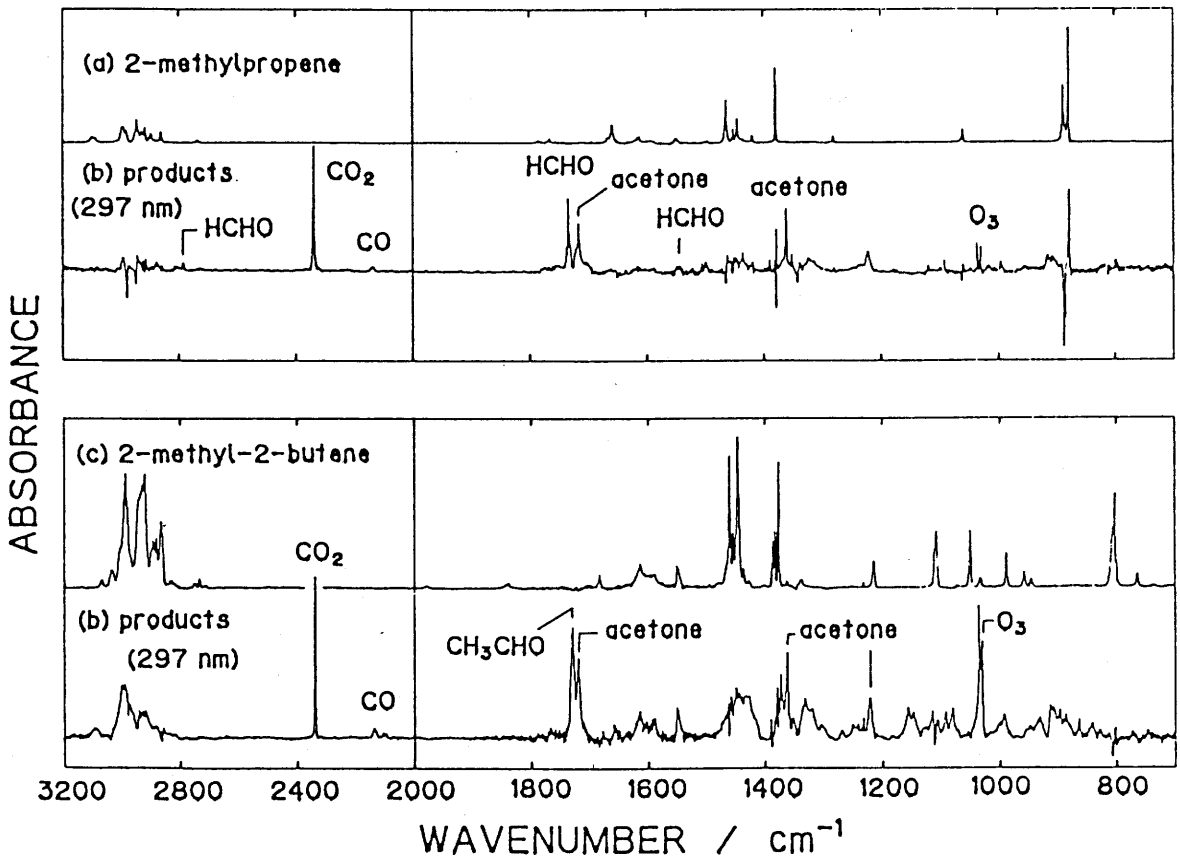

Fig.4.3. IR absorption spectra of (a) 2-methylpropene in O_2 matrix (M/R = 250/1); (b) the photochemical reaction products after the irradiation at 297 nm for 180 min; (c) 2-methyl-2-butene in O_2 matrix (M/R = 250/1) and (d) the photochemical reaction products after the irradiation at 297 nm for 15 min.

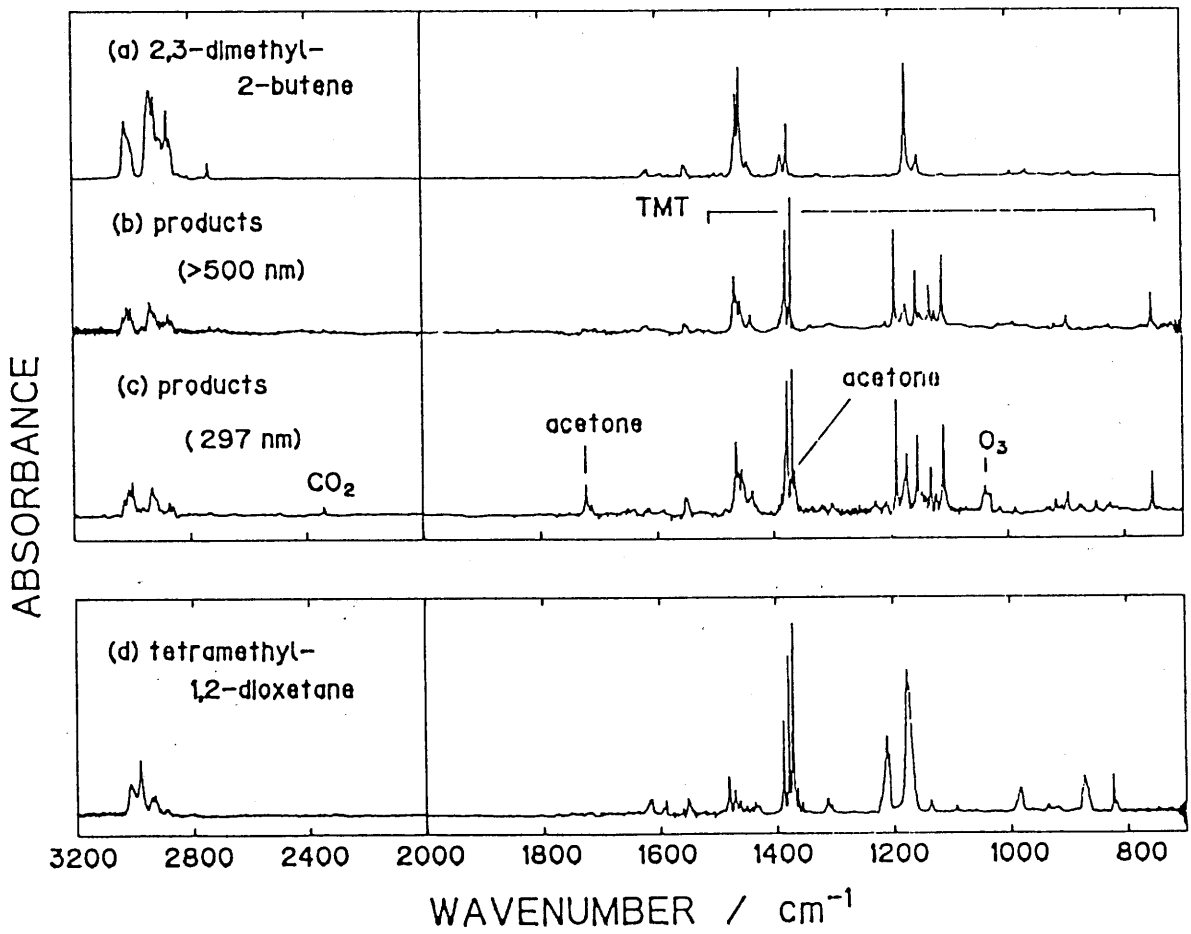

Fig.4.4. IR absorption spectra of (a) 2,3-dimethyl-2-butene in O_2 matrix (M/R = 250/1); (b) the photochemical reaction product (TMT) after the irradiation at >500 nm for 30 min; (c) products after the irradiation at 297 nm for 2 min; (d) reference spectra of tetramethyl-1,2-dioxetane in O_2 matrix.

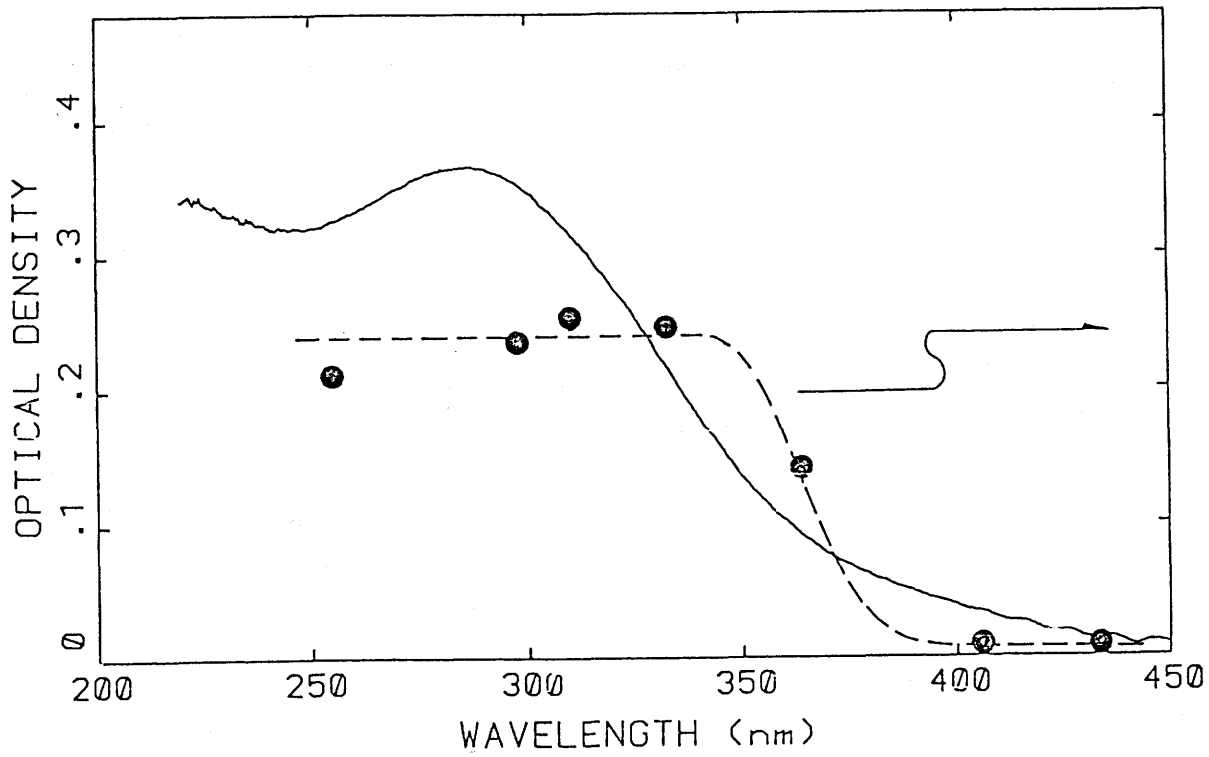

Fig.4.5. The CCT absorption spectrum of (2,3-dimethyl-2-butene)-O_2 system and relative quantum yield of the photochemical reaction at specified irradiation wavelengths calculated from apparent first order decay rate of the reactant, the optical density, and the irradiance.

(b) Simple Arenes

Excitation of benzene and methyl substituted benzenes in the oxygen matrices within the absorption bands shown in Fig.3.5 induced a decrease in the infrared absorption bands of the parent molecules. The thresholds on the long wavelength side were found to coincide approximately with the absorption thresholds within the bandwidth of the interference filters. However, the reaction thresholds of styrene and naphthalene were shorter than the absorption thresholds shown in Fig.3.4. Table IV-III shows the relative photolytic first order decay rate constant calculated from the decrease of IR absorbance and normalized to the photon flux through the optical filter at each excitation wavelength. These values are relative to that for p-xylene at 297 nm. Ionization potentials for these compounds are also cited. Values in brackets are the relative quantum yields calculated as $R/(1-10^{-A})$ and normalized to p-xylene, where R is the photolytic decay rate constant and A is the UV absorbance. The relative quantum yield is not given in Table IV-III when the UV absorbance is smaller than 0.01. Table IV-III also cites the data for 2,3-dimethyl-2-butene for comparison.

Figs.4.6~9 show the IR spectra sets of reactants and products for benzene, toluene, naphthalene, and styrene, respectively. Irradiation of benzene at 297 nm for 1h caused a 4% decay of the reactant (the photon flux was 1.32 of that used for p-xylene at 297 nm). Fig.4.6 (b) shows the product spectrum of benzene in the oxygen matrix following irradiation. Reaction products are identified as CO_2 (2342 cm^{-1}), CO (at 2139 cm^{-1},

broad). Fig.4.6 (b) also shows two strong carbonyl peaks at 1701 and 1690 cm^{-1} and many small peaks between 1150 to 900 cm^{-1}. Further irradiation at 254 nm with relative photon flux of 0.16 for 1h caused 10% additional decay of benzene. Fig.4.6 (c) shows that the intensity of the small peaks decreased while other new small peaks appeared in the same spectrum region. CO_2 increased markedly, with the increment being twice as big as it was for the case of irradiation at 297 nm with about 8 times the photon flux. Broad absorption bands around 2900 to 2700 cm^{-1} appeared to be distinct. The strong peak at 1701 cm^{-1} increased while the 1690 cm^{-1} peak did not.

Strong IR absorption bands around 1700 cm^{-1} can be noted in the product spectrum of toluene as shown in Fig.4.7 (b). Irradiation at 297 nm for 1h, with the relative photon flux being 1.0, caused a 14% reactant decay. A peak at 2342 cm^{-1} of CO_2 also appeared. Weak product bands can also be seen between 1600 and 800 cm^{-1}.

Spectra of photochemical products for other methyl substituted benzenes are very much like those for toluene. For p-xylene, new absorption peaks at 1707, 1695, and 1688, appeared together with many peaks between 1650 and 600 cm^{-1}. Irradiation at 297 nm for 30 min, with unit relative photon flux, caused a 32% reactant decay. CO_2 also appeared but the relative intensity compared to the band around 1700 cm^{-1} was lower than that for toluene under similar irradiation conditions. For p-xylene, the yield of CO_2 relative to that for carbonyl compounds increased as the excitation wavelength was decreased from 313 to 297 nm.

Irradiation of naphthalene in the oxygen matrix gives a product spectrum similar to benzene as shown in Fig.4.8 (b). Absorption bands of CO_2, CO and multiple peaks around 1710 cm^{-1} were observed. Irradiation at 297 nm for 2h, with a relative photon flux of 0.54, gave 25% reactant decay.

In contrast, styrene in the oxygen matrix forms benzaldehyde and formaldehyde as major photochemical products together with smaller amount of CO_2 and CO. Fig.4.9 (b) shows the product spectrum after irradiation at 297 nm for 1h, with the relative photon flux being 1.0, caused 30% reactant decay. Carbonyl peaks at 1711 cm^{-1} and 1737~1732 cm^{-1} for benzaldehyde and formaldehyde are shifted from those of authentic samples at 1718 and 1740 cm^{-1}, respectively, suggesting that both carbonyl compounds formed from the same styrene molecule make a molecular complex. Irradiation at 313 nm gave nearly the same spectrum as 297 nm, but with a lower product yield. At 254 nm the ratio of CO_2 and CO to benzaldehyde increased. Fig.4.9 (c) shows a reference spectrum of benzaldehyde in oxygen matrix (M/R = 1000/1).

Fig.4.10 compares the IR spectra of carbon dioxide formed from Ph-$^{13}CH_3$. Fig.4.10 (a) shows a part of Fig.4.7 (b) from unlabeled toluene. The band of $^{13}CO_2$ at 2274 cm^{-1} can be seen in the expanded curve. The ratio of integrated absorption of $^{13}CO_2$ to that of $^{12}CO_2$ is 0.013. Fig.4.10 (b) and 8c show the spectra from Ph$^{13}CH_3$ after the irradiation at 297 nm (relative photon flux was 0.87) for 1 and 2h, respectively. The $^{13}CO_2/^{12}CO_2$ ratio is 0.023 and 0.036, respectively.

TABLE IV-III. Ionization Potential, Relative Photo-oxidation Rates and Relative Quantum Yields of Selected Arenes and 2,3-Dimethyl-2-butene

Compound	IP_D/eV[a]	Excitation Wavelength / nm 254	297	313	333	364
		Relative Decay Rate[b] [Relative Quantum Yield][b]				
Benzene	9.24	0.86 [0.39]	0.04	-	NR	NR
Toluene	8.82	1.8 [0.82]	0.22 [1.2]	0.04	NR	NR
p-Xylene	8.44	-	1.0 [1.0]	0.29 [1.2]	NR	NR
Mesitylene	8.4	1.9 [1.1]	1.1 [0.89]	-	NR	NR
Durene	8.03	-	1.5 [0.9]	-	0.64 [1.1]	0.11
Styrene	8.47	1.5 [0.66]	0.46 [0.58]	0.19 [0.54]	NR	NR
Naphthalene	8.12	0.56 [0.36]	0.36 [0.45]	0.18 [0.34]	NR	NR
2,3-dimethyl-2-butene[c]	8.30	9.5 [4.6]	11.1 [5.0]	-	7.2 [4.7]	1.8 [2.5]

a. R.C.West Ed., CRC Handbook of Chemistry and Physics, 68th Edition, 1988, Pp.72-73.
b. Normalized to the values of p-xylene at 297 nm.
c. Ref.2
NR No reaction.
- Not studied.

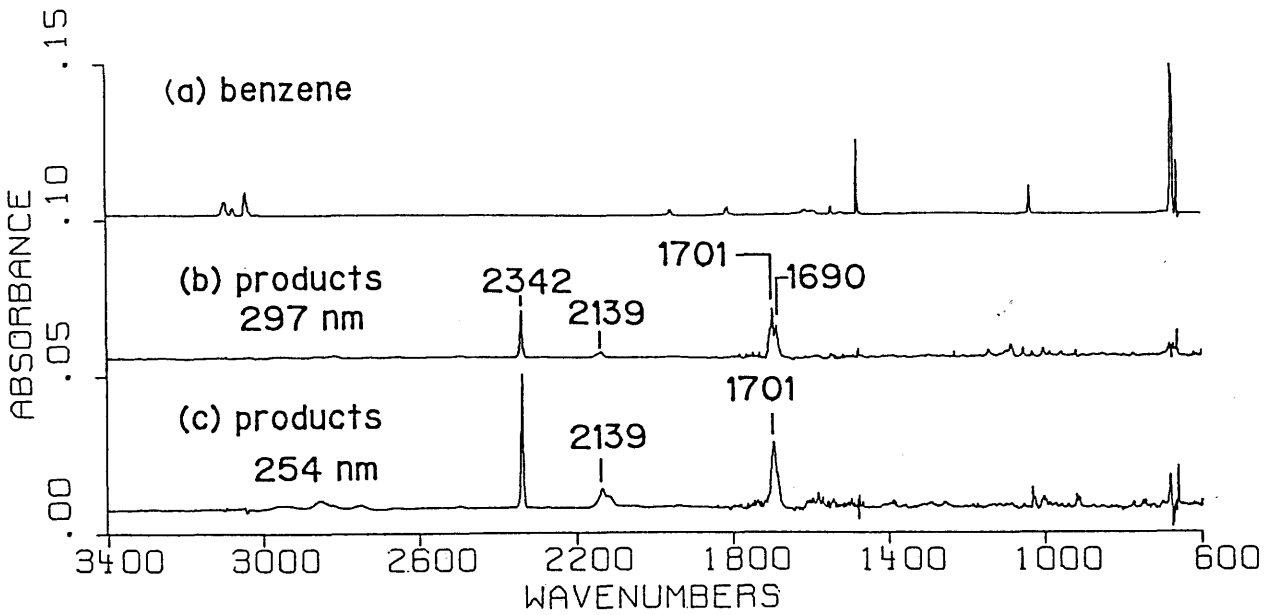

Fig.4.6. (a) IR absorption spectrum of benzene in oxygen matrix with the M/R = 250/1 at 11K; (b) product spectrum after irradiation at 297nm for 1h; (c) product spectrum after further irradiation at 254 nm for 1h. Vertical scale of curve (a) is reduced by a factor of 10.

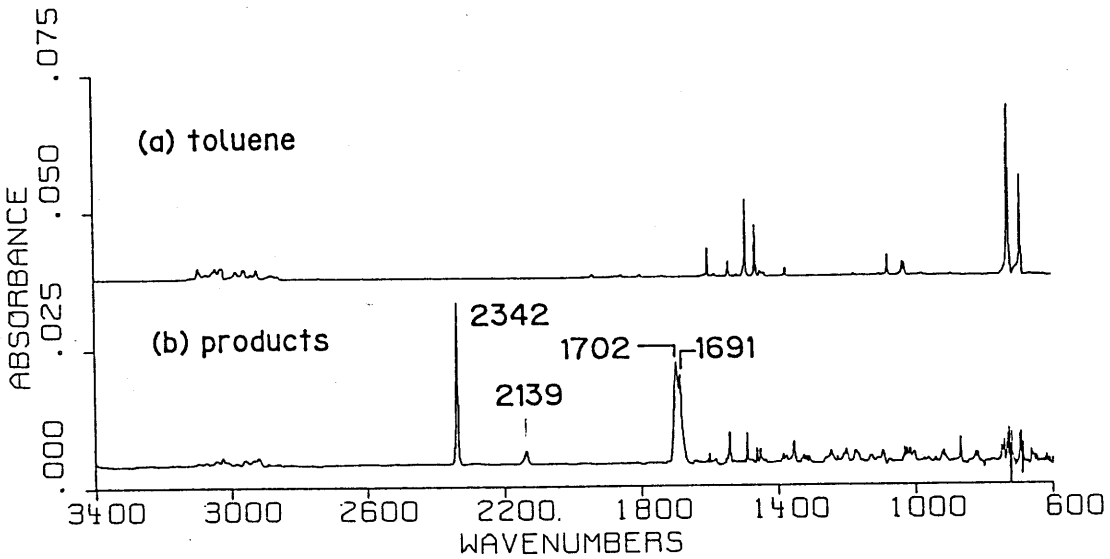

Fig.4.7. (a) IR absorption spectrum of toluene in oxygen matrix with the M/R = 250/1 at 11K; (b) product spectrum after irradiation at 297 nm for 1h. Vertical scale of curve (a) is reduced by a factor of 5.

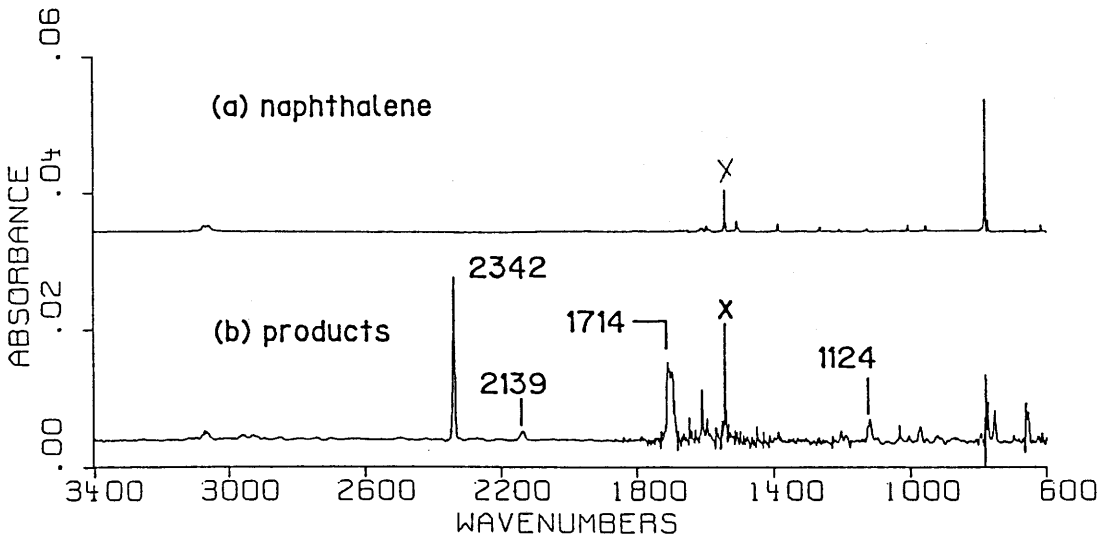

Fig.4.8. (a) IR absorption spectrum of naphthalene in oxygen matrix with the M/R = 1000/1 at 11K; (b) product spectrum after irradiation at 297 nm for 2h. Peak marked by X is due to oxygen; vertical scale of curve (a) is reduced by a factor of 5.

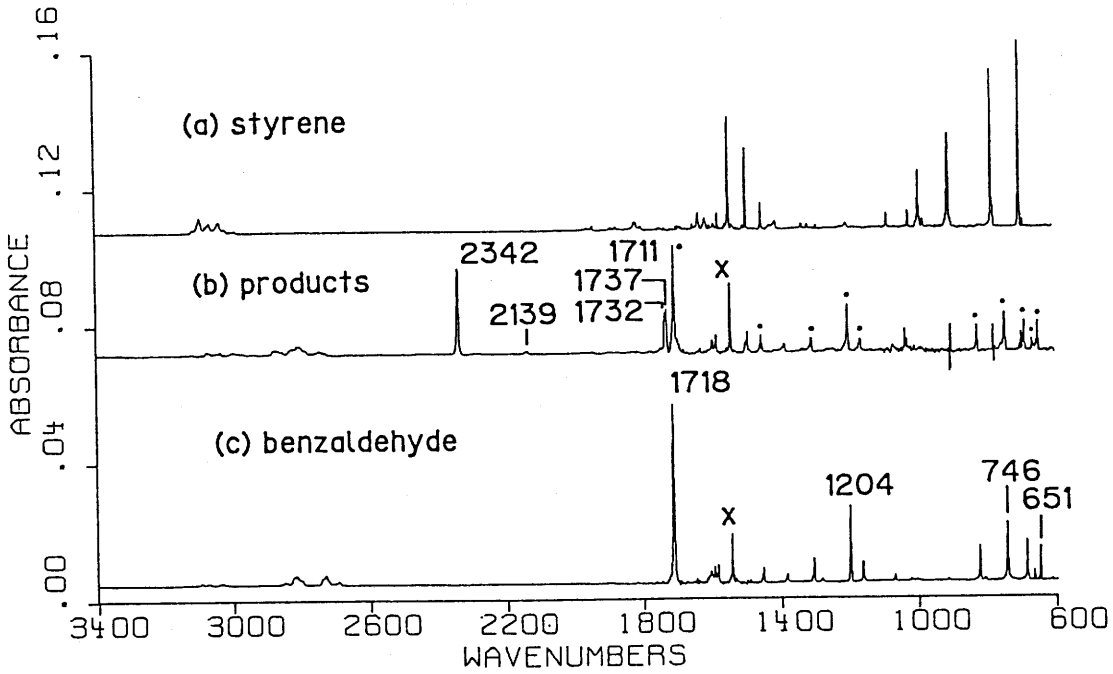

Fig.4.9. (a) IR absorption spectra of styrene in oxygen matrix with the M/R =1000/1 at 11K; (b) product spectrum after irradiation at 297 nm for 1h. Peaks denoted by • is due to benzaldehyde. (c) standard spectrum of benzaldehyde in oxygen matrix with M/R = 1000/1. Peak marked by X is due to oxygen. Vertical scales of curves (a) and (c) reduced by factors of 2 and 4, respectively.

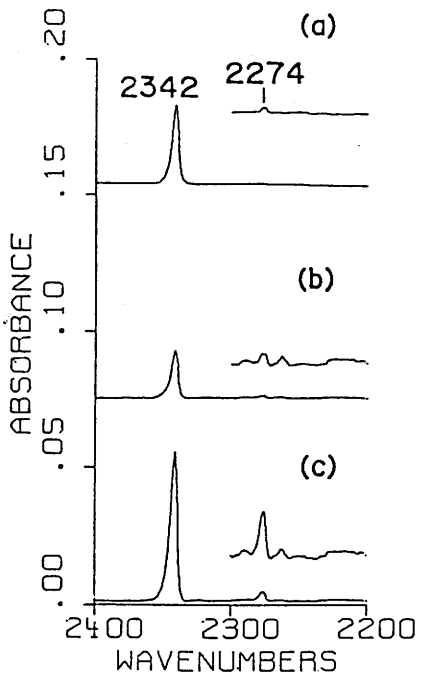

Fig.4.10. IR absorption spectra of $^{12}CO_2$ and $^{13}CO_2$ formed from the irradiation of toluene at 297 nm in the oxygen matrices. (a) spectrum from the irradiation of unlabeled toluene for 1h; (b) spectrum from the irradiation of $Ph^{13}CH_3$ for 1h; (c) spectrum from the further irradiation of $Ph^{13}CH_3$ for 1h.

(c) Methyl Substituted Ketenes

Excitation of ketene-O_2 systems within the CCT absorption bands shown in Fig.3.7 induced photochemical reaction in all the cases. The long-wavelength thresholds of the reactions as expressed by the central wavelengths of optical filters were 333 and 434 nm for methylketene and dimethylketene respectively. These were found to coincide approximately with the CCT absorption threshold within the range of the bandwidth of the interference filters. This tendency is same as alkenes. It should be noted that no reaction observed in methylketene-O_2 system by irradiation at 406 nm which matches the intrinsic $n\rightarrow\pi^*$ band of methyl ketene and longer than the absorption threshold of the CCT band.

Figs.4.11 (a)~(c) shows IR absorption spectrum of dimethylketene in oxygen matrix (M/R = 250/1) at 10K, product spectrum after irradiation at 434 nm for 2h, and also after irradiation at 406 nm for 1h. Many new absorption bands are appeared in these product spectra. Relatively strong bands appeared at 1724.1, 1363.0, and 1219.0 cm^{-1}. These are easily identified as bands of acetone by comparison of the standard spectrum in oxygen matrix (M/R = 1000/1, shown in Fig.4.11 (d)) with the product spectra (b) and (c). Acetone is not only the main product. Absorption bands of CO and CO_2 are also found at around 2150 and 2340 cm^{-1} respectively, and conspicuous absorption bands at 1880.0 and 1852.6 cm^{-1} with side band at 1849.4 cm^{-1} are obviously appeared in (b) and (c). Band at 3509.2 is also appeared in the product spectra as shown in Fig.4.12. (b) and (c). Difference in the

relative peak intensity in different irradiation condition, spectrum (b) against (c), means the species for the peak at 1880.0 cm^{-1} is different that for the peak at 1852.6 cm^{-1}. The peak at 3509.2 cm^{-1} could be of the same species as at 1852.6 cm^{-1} and should not as at 1880.0 cm^{-1} since the ratio of each peak intensity of in figure (b) over (c) (b/c) is 0.74 (3509.2 cm^{-1}), 0.50 (1880.0 cm^{-1}) and 0.82 (1852.6 cm^{-1}), respectively. The spectrum obtained in the experiment for $^{18}O_2$ matrix in the similar condition shows isotope shifted peaks corresponding to these three, at 3496.8 (3509.2), 1876.6 (1880.0) and 1850.7/1847.6 (1852.6/1849.4) cm^{-1}. These values of shift are relatively small, 2~3 cm^{-1}, while obvious shift was found for acetone, whose C=O st. band appeared at 1696.4 cm^{-1}. Any peak in the spectrum obtained from the experiment for $^{16}O_2$-$^{18}O_2$ (1:1) matrix could found in experiments for $^{16}O_2$ or $^{18}O_2$, no new peak was found.

In the case of methylketene, acetaldehyde was the main product as shown in Fig.4.13 (b), which is a product spectrum after irradiation at 333 nm for 5h. The intrinsic bands of acetaldehyde at 1731.3, 1427.8, 1350.5 and 1111.4 cm^{-1} in the reference spectrum, Fig.4.13 (c), are also found in the product spectrum with negligible difference at 1731.3, 1427.4, 1350.7 and 1112.3 cm^{-1}. Small amount of O_3 was also formed. CO and CO_2 were formed as common product for other CCT excited reaction in oxygen matrices. Remarkable but unknown peak at 1778.3 cm^{-1} also appeard as in the product spectrum.

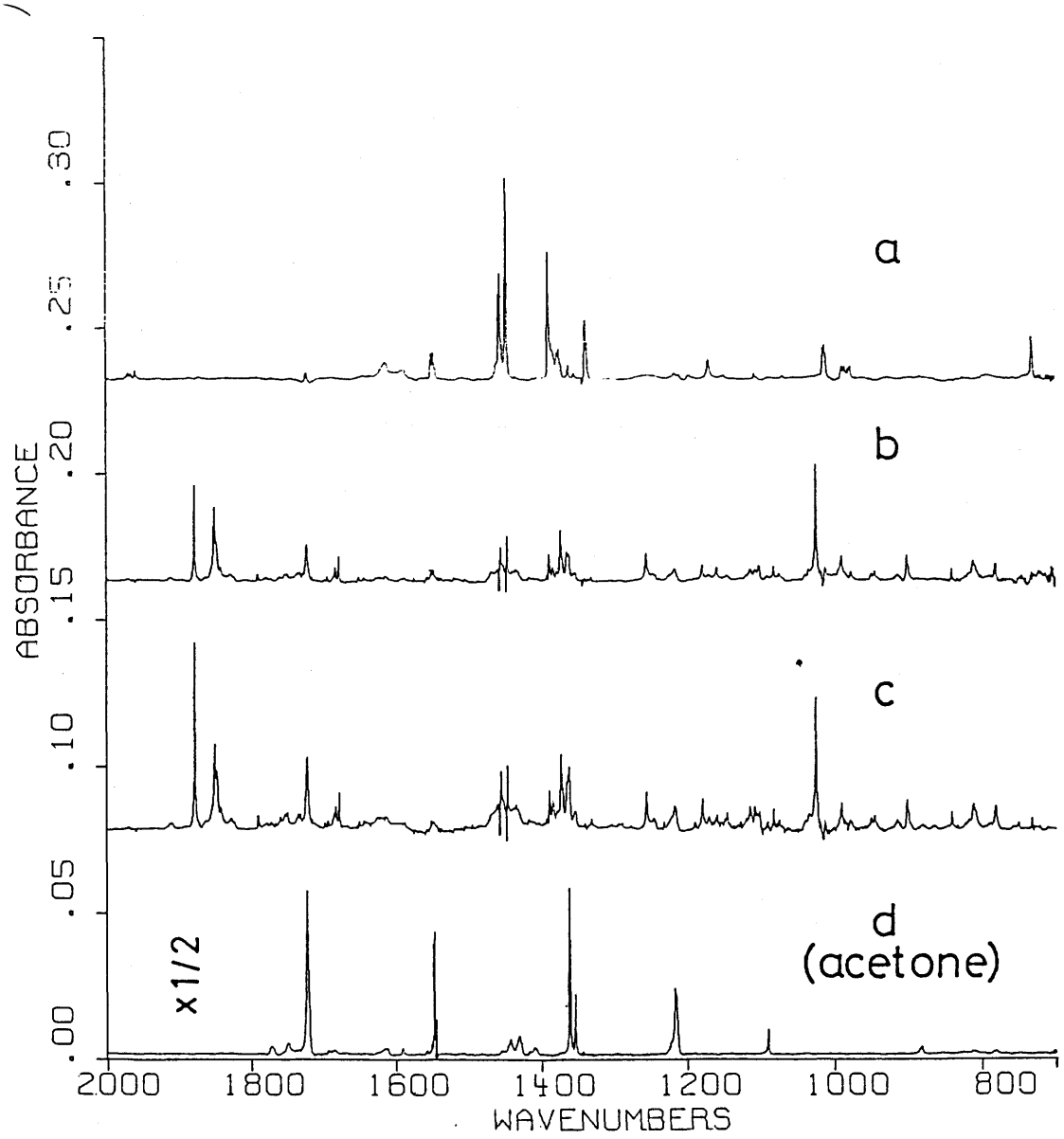

Fig.4.11. (a) IR absorption spectrum of dimethylketene in oxygen matrix (M/R = 250/1) at 10K; (b) product spectrum after irradiation at 434 nm for 2h; (c) product spectrum after irradiation at 406 nm for 1h. (d) Standard spectrum of acetone in oxygen matrix (M/R = 1000/1).

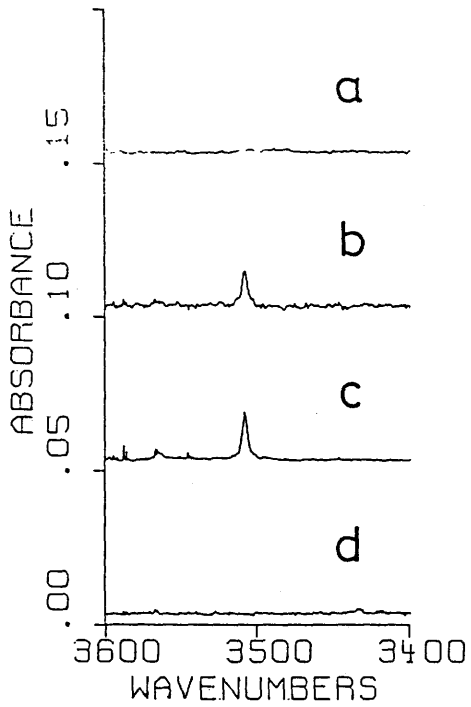

Fig.4.12. IR absorption spectra around 3400~3600 cm^{-1} region: (a) spectrum of dimethylketene in oxygen matrix (M/R = 250/1) at 10K; (b) product spectrum after irradiation at 434 nm for 2h; (c) product spectrum after irradiation at 406 nm for 1h. (d) Standard spectrum of acetone in oxygen matrix (M/R = 1000/1).

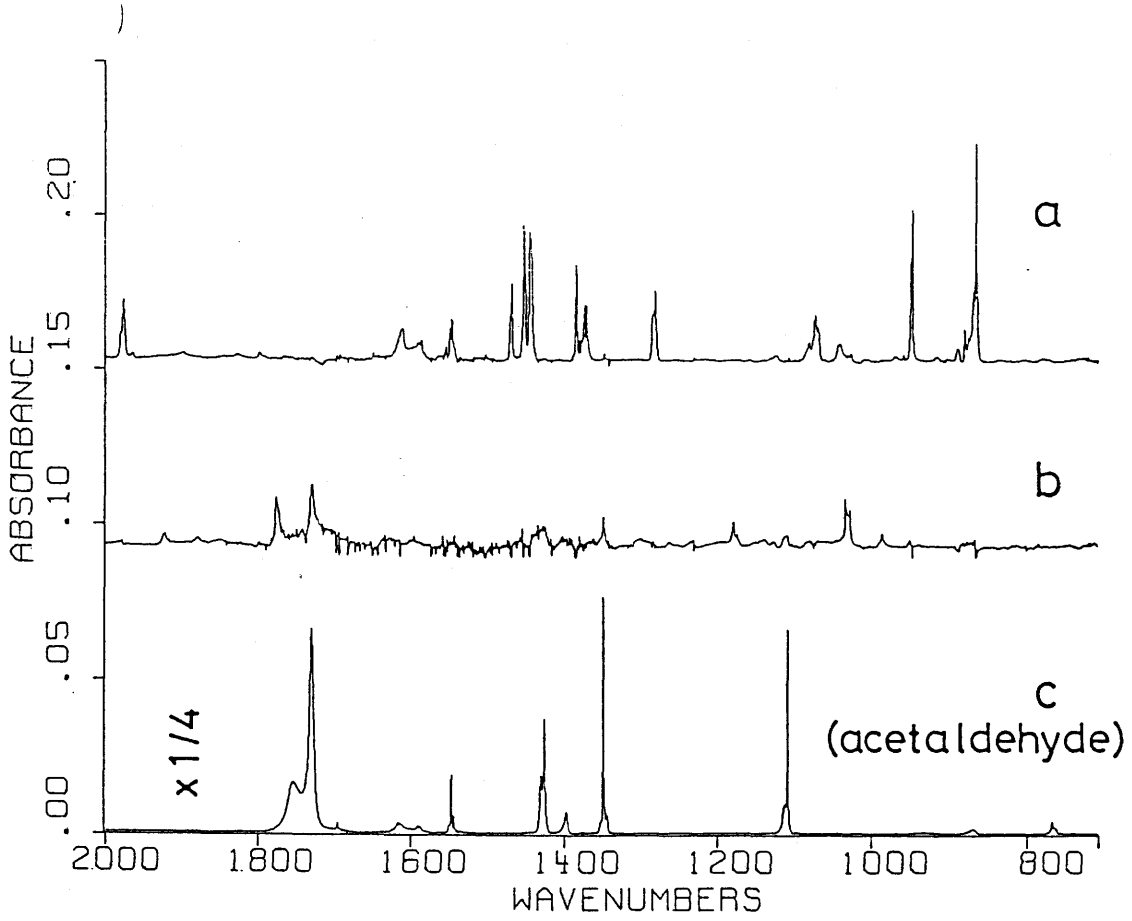

Fig.4.13. (a) IR absorption spectrum of methylketene in oxygen matrix (M/R = 250/1) at 10K; (b) product spectrum after irradiation at 333 nm for 5h. (c) Standard spectrum of acetaldehyde in oxygen matrix (M/R = 1000/1).

CHAPTER IV

4. CT Excited Photochemical Reactions in the Oxygen Matrices

(a) Photochemical Property of Simple Alkenes

The type of the photooxygenation of the simple alkenes in solid oxygen depends on the type of alkene molecule and also on the excitation energy. The reaction can be classified into the following four pathways.

(i) Photooxygenation to give an oxygen adduct. This type of reaction was observed only for the (2,3-dimethyl-2-butene)-O_2 system. The product, the oxygen adduct, has been identified tentatively as tetramethyl-1,2,3,4-tetraoxane (TMT) as discussed in the next section. Absence of the reaction at >620 nm and 579 nm implies that the photochemistry induced by the direct excitation of the singlet oxygen bands is negligible under our experimental conditions since the excitation wavelength of 579 nm matches well with the (1 ← 0) band of the transition $2O_2(^1\Delta_g) \leftarrow 2O_2(^3\Sigma_g^-)$ and the irradiation at >620 nm covers the fundamental band of that transition.

(ii) cis-trans isomerization. The cis-to-trans and trans-to-cis isomerization was observed for c-2-butene and t-2-butene at the excitation wavelength region of 250~300 nm as a major reaction channel. The observation suggests that the triplet alkene was formed after the CCT excitation. The cis-trans isomerization of simple alkenes via triplet state in which two methylene planes are twisted by 90 degrees, has long been known[7], while the isomerization does not occur in the ionic state[8] since the planes are twisted only by ~25 degrees[9]. Therefore, the cis-trans isomerization would be ascribed to the formation of the

triplet state of alkene. For other alkenes, the change in the spectral band shape of reactants after the irradiation, particularly noticed for 2-methylpropene and 2-methyl-2-butene, is suggestive of the internal rotation about the double bond, which in turn would indicate the formation of triplet alkenes. It is also interesting to note that the reaction rate of c-2-butene was much faster than that of t-2-butene at 297 nm, but they are very close at 254 nm as shown in Table IV-I. This fact would be ascribed to the higher barrier of t-2-butene for the crossing from the CCT state to the alkene triplet state.

(iii) Double bond scission to give carbonyl compounds. The C=C double bond scission to give corresponding two carbonyl compounds was observed for all alkenes studied. The wavelength of the reaction threshold for the double bond scission was shorter than that for the photooxygenation and cis-trans isomerization in case of 2,3-dimethyl-2-butene and t-2-butene, respectively. In the reaction of c-2-butene, acetaldehyde formation was observed only in a trace amount at the threshold energy of the cis-trans isomerization as shown in Table IV-II. For other alkenes the double bond scission was observed at any excitation wavelengths within the CCT bands. For 2-butenes, the scission process is much slower than isomerization at all the wavelengths studied.

(iv) Formation of CO_2, CO, HO_2 and O_3. Fragmentation to give CO_2, CO and HO_2 was observed at the shorter excitation wavelengths than the reaction threshold to form the carbonyl compounds, and its importance increases as the excitation energy

increases. This mode was the most important reaction pathway observed for ethene. A part of CO_2 and CO are apparently secondary products via the photooxidation of carbonyl products as judged from the increased yield ratio of CO_2 and CO against the carbonyl compounds for increased irradiation time. However, CO_2 and CO has also been seen in a short reaction time for ethene, propene, 2-methylpropene and 2-methyl-2-butene. The possibility of initial formation of these products can not be excluded in these cases. Ozone was also produced when this type of fragmentation was observed. The initial yield of ozone is in general much higher than that of CO_2. About twice as much of acetaldehyde was formed in the reaction of c-2-butene at 297 nm as shown in Table IV-II. Formation of ozone has been reported in almost all photooxidation studies[1,2] of organic molecules in solid oxygen.

(b) A Hyperoxide: Tetramethyl-1,2,3,4-tetraoxane

All the IR absorption bands in the product spectrum (Fig.4.4 (b)) obtained by the longer wavelength excitation would belong to a single product since the relative intensity among the peaks do not change for all the spectra obtained under different conditions of irradiation time and excitation wavelength. This product was found to be stable for the annealing at ~25 K for ~3 min at least. Comparison of the IR spectra of the product with that of 2,3-dimethyl-2-butene (Fig.4.4 (a)) reveals some similarity suggesting that the main framework of the molecular structure of 2,3-dimethyl-2-butene is retained in the product.

The most possible candidate of the product is tetramethyl-1,2-dioxetane. It was synthesized[4] and its matrix spectra was obtained as reference (Fig.4.4 (d)). The IR spectra in the Ar and O_2 matrix are almost identical, and these also close to that of the standard spectrum in the liquid as reported by Aroca and Menzinger[10]. Most characteristic bands of the dioxetane are at 1175 and 872 cm^{-1} due to ring stretching and breathing. Comparison of the reference spectrum with the product spectrum Fig.4.14 (b), however, no identical peak was found. Thus, the major product cannot be dioxetane.

The product can not be 2,3-dimethyl-3-hydroperoxy-1-butene, which is a specific product[11,12] known in the 2,3-dimethyl-2-butene-$^1O_2$ reaction both in the gas and liquid phase; neither characteristic band of the hydroperoxide at 3530 cm^{-1} (OO-H st.) nor at 906 cm^{-1} (CH_2 out of plane) are seen in our product spectrum.

In order to explore the possibility of containing two oxygen molecules in the product, photochemical experiments were carried out in the matrix containing ^{18}O-isotope labeled oxygen at 406 nm. Fig.4.14 (a) depicts the product spectrum obtained in the $^{16}O_2$-$^{18}O_2$ (1:1) matrix. Reactions in pure $^{16}O_2$ and $^{18}O_2$ matrices gave the reference spectrum as shown in Fig.4.14 (b) and (c), respectively. Comparing these spectra, substantial isotope shifts can be noted for the 750 and 630 cm^{-1} bands as well as several bands between 1050 and 1200 cm^{-1}. It should be noted in Fig.4.14 (a) that the bands at 750 and 630 cm^{-1} appears as triplet peaks with the intensity ratio close to 1:2:1. This

evidence strongly indicates that the compound does contain oxygen atoms from two O_2 molecules, $^{16}O_2$ and $^{18}O_2$, with a statistical distribution. Subtraction of Fig.4.14 (b) and (c) from (a) gives the spectrum shown in (d), which should be ascribed to the product molecule containing both of $^{16}O_2$ and $^{18}O_2$. Almost complete subtraction at the 750 and 630 cm^{-1} band leaving a single peak at the center for each band indicate that no other isotope-scrambling species than the $^{16}O_2$-$^{18}O_2$ (1:1) product are formed. The IR spectrum of the product is much different from that of tetramethyl-1,2,4,5-tetraoxane[13], which is also called "acetone peroxide dimer".

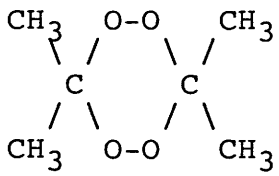

Acetone Peroxide Dimer

(Tetramethyl-1,2,4,5-tetraoxane)

All the evidence indicates that the product is an oxygen adduct containing oxygen atoms from two O_2 molecules in a statistical ratio but is neither of a known product such as dioxetane, hydroperoxide, nor 1,2,4,5-tetraoxane. A possible but tentative identification is that the adduct is tetramethyl-1,2,3,4-tetraoxane (TMT, hereafter), which contains four oxygen atoms successively chained in a six-membered ring.

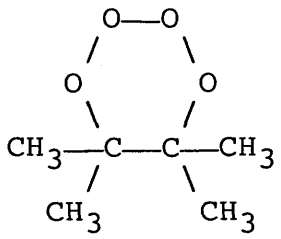

TMT

(Tetramethyl-1,2,3,4-tetraoxane)

The IR absorption bands at 3050~2800, 1465.6, 1377.1~1367.9, and 1173.1~1155.1 cm^{-1} (see Fig.4.14 (b)) which did not show any distinct isotope shift when the matrix was changed from $^{16}O_2$ to $^{18}O_2$, should be assigned to the C-H stretching, asymmetric CH_3 deformation, symmetric CH_3 deformation, and C-C-C stretching mode, respectively. The bands at 1132.0 and 1110.3 cm^{-1} in the $^{16}O_2$ matrix shifts to 1115.8 and 1065.5 cm^{-1} in the $^{18}O_2$ matrix as shown in Fig.4.14 (b) and (c). The isotope shift expected for the stretching mode of a localized O-O and C-O bonds are 5.72 and 2.41 %, respectively. Although one could assign the bands at 1132.0 and 1065.5 cm^{-1} to the O-O stretching of the C-^{16}O-^{16}O and C-^{18}O-^{18}O moiety since the isotope shift of 67 cm^{-1} is close to that expected for the localized O-O stretching (65 cm^{-1} at 1132 cm^{-1}), yet the blue shift of the remaining band at 1110.3 cm^{-1} can not be explained. Thus, we conclude that those bands near 1100 cm^{-1} showing distinct isotope shift are the mixed stretching modes of C-C-O-O frame of TMT. The bands at 751.9 and 630.1 cm^{-1} showing the isotope shift of 21 and 10 cm^{-1}, respectively, may be assigned to the deformation modes of the six-membered ring of TMT rather than the stretching mode of the weaker O-O bond since the

isotope shift is much smaller than that expected for the latter mode.

Thus, although the identification of the product as TMT is rather speculative at this stage, the IR bands are in accord with the identification. This is the first evidence for existence of a molecule which has O-O-O-O bonding in the structure.

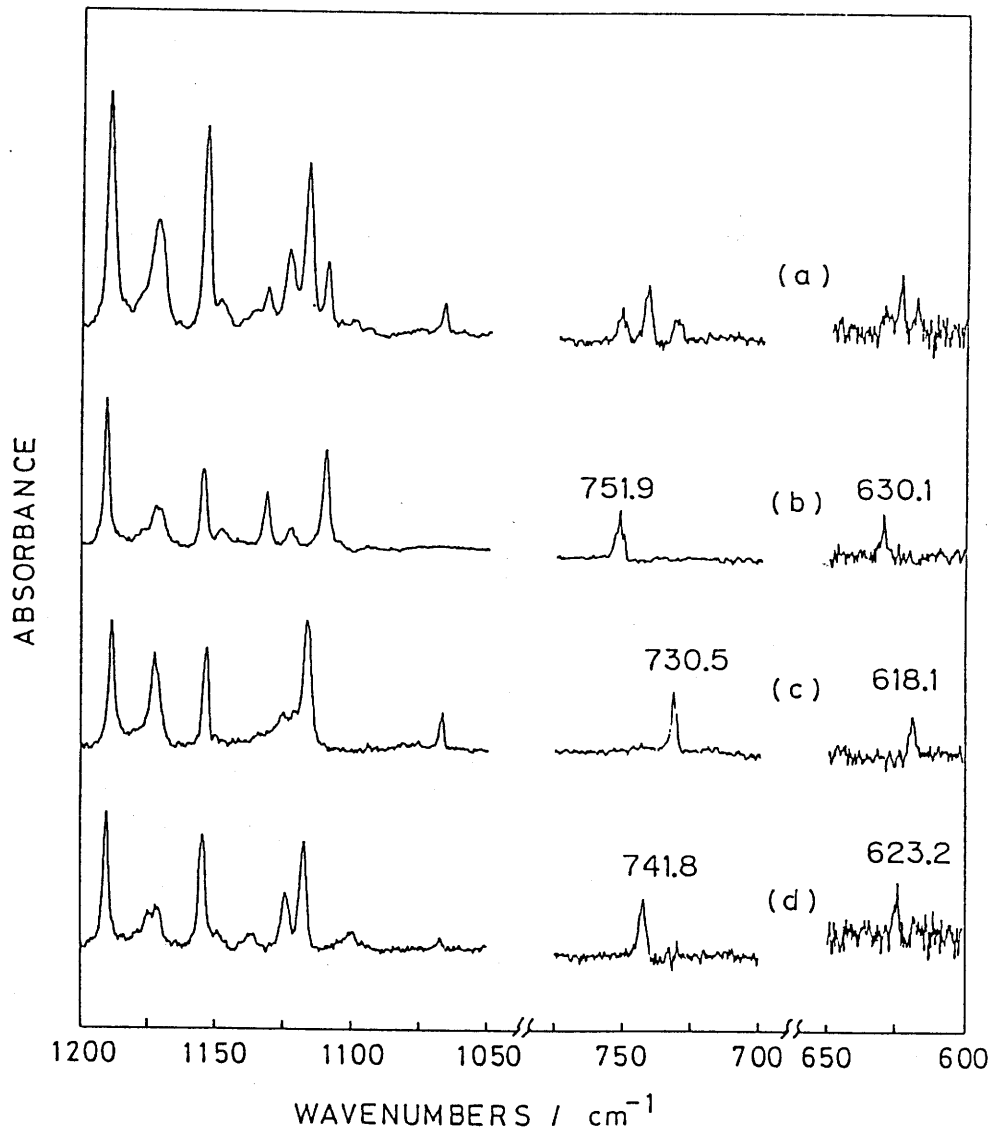

Fig.4.14. IR absorption spectra of the photochemical product (TMT) formed by irradiations of 2,3-dimethyl-2-butene in the oxygen matrix at 406 nm for 2 h: (a) in the 1:1 mixture of $^{16}O_2/^{18}O_2$; (b) in pure $^{16}O_2$; (c) in pure $^{18}O_2$; (d) the difference spectrum obtained by subtraction of (b) and (c) from (a).

(c) Excitation and Reaction Mechanism of Alkenes

Photochemistry of simple alkenes in solid oxygen via excitation of the CCT bands is proposed to be as follows according to the observation described so far.

SCHEME IV-I

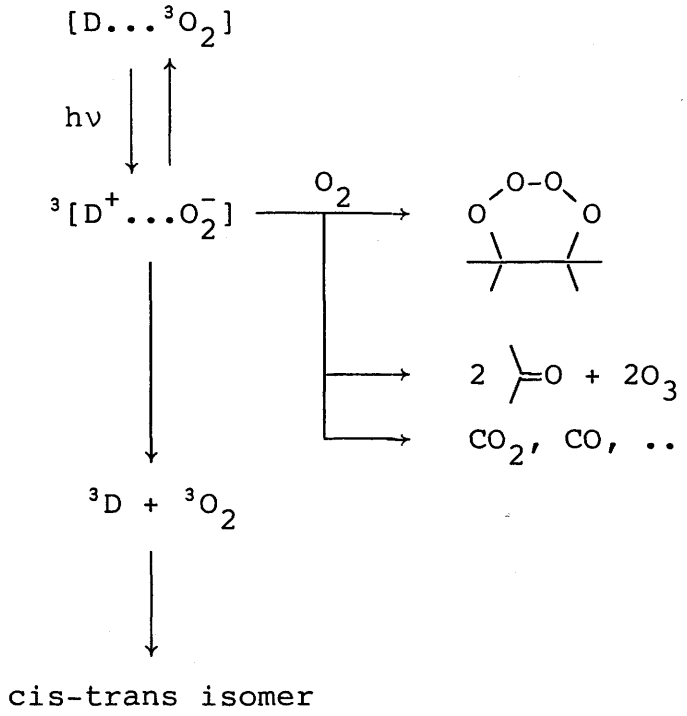

The energy diagram of the system can be visualized as shown in Fig.4.15.

As shown in Fig.4.15, the triplet state of simple alkenes lie at ~3.4 eV above the ground state.[14,15] The potential surface correlating to ^{3}[alkene] + $^3O_2$ would cross the ion pair state (excited charge transfer state) at a certain level whose energy ranges between the above value and ~1 eV higher than this depending on the twisting angle of the methylene-methylene

planes. For the alkenes with sufficiently low ionization potential, excitation to the ion pair state lower than the crossing point to the alkene triplet is possible. This is the case only for 2,3-dimethyl-2-butene (DMB), and the excitation at 406 and >500 nm gave TMT as a sole product. Although intersystem crossing from the triplet CT surface to the singlet surface correlating to 2,3-dimethyl-2-butene + $^1O_2$ should not be excluded, the relevance of the singlet oxygen reaction has been excluded by the fact that no reaction was occur by the direct excitation to the singlet states of $(O_2)_2$. Therefore, it can be concluded that the formation of the adduct containing two O_2 molecules is a reaction pathway specific to 2,3-dimethyl-2-butene from the triplet CT state in solid oxygen. Other than the adduct formation, deactivation to the ground state of triplet pair is expected[16] since the ion pair state lies close to the ground state. Low quantum yield of photochemical reaction of 2,3-dimethyl-2-butene at >400 nm as demonstrated in Fig.4.5 verifies this is actually the case. As the excitation energy increases, double bond scission to form two carbonyl compounds starts to occur. This process is thought to proceed through the triplet CCT state rather than after crossing to the triplet state of alkene. The reasoning is as follows: in the case of 2,3-dimethyl-2-butene, a rather sharp increase of the quantum yield of the photochemical decay of reactant at $\leq$364 nm (see Fig.4.5) accompanies the increased yield of TMT and the appearance of acetone, but no evidence of triplet formation verified by the change in the band shape was observed. The increase in the

reaction quantum yield can be interpreted as the decrease of deactivation process; in the case of trans-2-butene, the reaction thresholds of the cis-trans isomerization (333 nm) and the acetaldehyde formation (297 nm) do not coincide.

No adduct was observed except for 2,3-dimethyl-2-butene. TMT type compound would not be stabilized for the smaller alkenes and further degradation via this type of intermediate would cause double bond scission to give two carbonyl compounds. Here, it should be noted that ozone formation was observed in many cases of this study. Since the (0-0) transition of the Herzberg bands of O_2 ($A^3\Sigma_u^+ \leftarrow X^3\Sigma_g^-$) lies at 280.0 nm and the convergence limit of this transition lies at 5.116 eV (242.3 nm)[17], ozone formation through the processes (4-1)~(4-4)

$$O_2(X^3\Sigma_g^-) \xrightarrow[\lambda<280nm]{h\nu} O_2(A^3\Sigma_u^+) \qquad (4\text{-}1)$$

$$\xrightarrow[\lambda<242nm]{h\nu} 2O(^3P) \qquad (4\text{-}2)$$

$$O_2(A^3\Sigma_u^+) + O_2(X^3\Sigma_g^-) \longrightarrow O_3 + O(^3P) \qquad (4\text{-}3)$$

$$O(^3P) + O_2(^3\Sigma_g^-) \longrightarrow O_3 \qquad (4\text{-}4)$$

are possible only for excitation at wavelengths shorter than those discussed above. Therefore, ozone formation wavelengths longer than 297 nm as observed in c-2-butene, t-2-butene, 2-methylpropene, 2-methyl-2-butene and 2,3-dimethyl-2-butene cannot be explained by the excitation of matrix O_2 molecule. Even for the excitation at 254 nm, ozone yield in the presence of alkene

is much higher than that for oxygen alone, so that the contribution of the process (4-3) is minimal at this wavelength. Since the ozone formation in the present study always accompanies the double bond scission, one possible process could be conceived as follows,

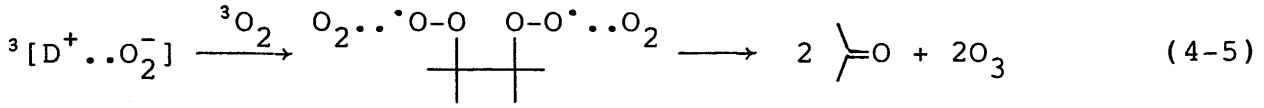

(4-5)

Only in the case of ethene, the CCT absorption at >220 nm would not be strong enough as compared to the Herzberg transition judged from the absorption spectra in liquid argon presented by Buschmann[18]. Formation of a trace amount of an unidentified product with bands at 1779.6, 1138.3 and 872.9 cm^{-1} at 254 nm suggests that this compound may be a product of the oxygen atom or $O_2(A^3\Sigma_u^+)$ reaction.

For alkenes with the CCT bands starting at 3.9±0.2 eV, i.e., 2-methylpropene, c-2-butene and t-2-butene, excitation at 334~254 nm (3.7~4.9 eV) leads to the ^{3}[alkene] + $^3O_2$ state followed by cis-trans isomerization as a major reaction pathway. Direct reaction from the CCT state to form carbonyl compounds, CO_2, CO and O_3 occurs in parallel with the isomerization as a minor reaction pathway. The photochemistry of 2-methylpropene would be an intermediate case between 2-butenes and 2,3-dimethyl-2-butene.

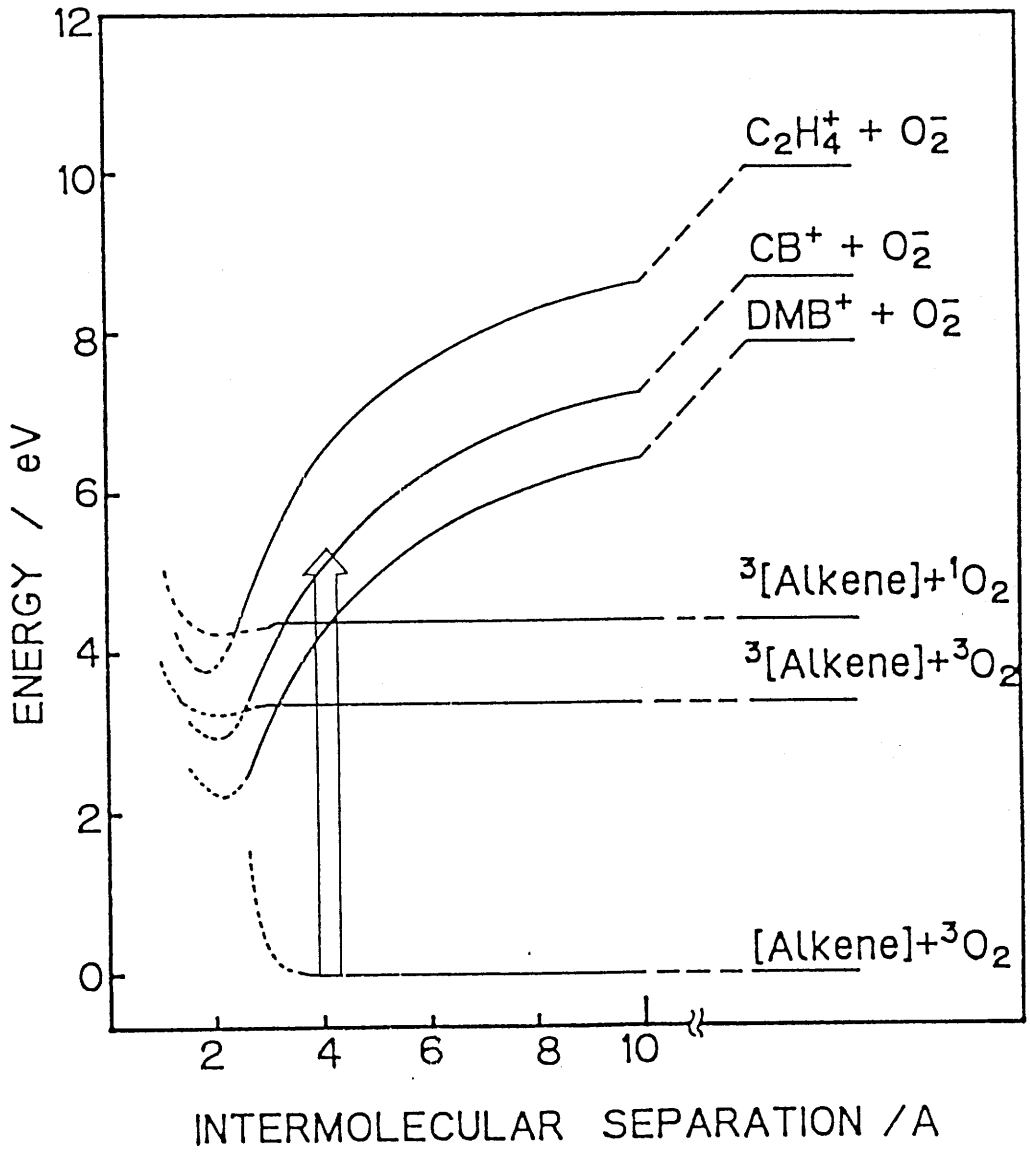

Fig.4.15. Energy diagram of the alkene-O_2 systems. $C_2H_4^+$, CB^+ and DMB^+ denote cation radicals of ethene, c-2-butene and 2,3-dimethyl-2-butene, respectively.

(d) Photochemical Property of Simple Arenes

Excitation of benzene and methyl substituted benzenes in the oxygen matrices within the CCT absorption bands caused photochemical reaction to form CO_2, CO, and some unsaturated carbonyl compounds as will be discussed later (see Figs.4.6~9). It is very interesting to note in Table IV-III that the relative quantum yields (normalized to p-xylene at 297 nm) of toluene, p-xylene, mesitylene, durene at 254 and 297 nm fall into nearly the same range of 1.0 ± 0.2, whereas those of styrene at 254~313 nm are 0.6 ± 0.06 and of benzene at 254 nm and naphthalene at 254~313 nm are 0.4 ± 0.05. In contrast the relative quantum yield of 2,3-dimethyl-2-butene is 4.8 ± 0.2 between 254 and 333 nm. Thus, the quantum yields of photochemical reaction for benzene and naphthalene are more than 10 times smaller, and those for methyl substituted benzenes are about a factor of 5 smaller than that for 2,3-dimethyl-2-butene. This fact suggests that the non-reactive deactivation channels are much more efficient for arenes than the alkene. This would be due to the more efficient intersystem crossing to the T_1 state from the CT state for the former compounds. This also suggests that the T_1 states of the arenes are non-reactive in the oxygen matrices.

Benzene. Excitation of benzene in the oxygen matrix at 297 nm, close to the absorption threshold (see Fig.3.3 (1a)), induced photochemical reaction to form CO_2, CO and carbonyl compounds giving IR peaks at 1701 and 1690 cm^{-1} as shown in Fig.4.6 (b). Phenol was never observed either at 297 nor 254 nm as evidenced by the absence of the OH stretching band[19] around 3600 cm^{-1}.

This result leads to a conclusion that the reaction sequence (4-10)~(4-13) (see section 4.5.1) is not initiated by the excitation of the benzene-O_2 pair directly to the CT state. The carbonyl compound observed in Fig.4.6 (b) is most probably 2,4-hexadiendials (isomers of mucondialdehyde) since the absorption frequencies at around 1700 cm^{-1} is characteristic of the conjugated carbonyl bonds[19]. Thus, an unsaturated dicarbonyl compound, CO_2 and small amount of CO are the product from the benzene-O_2 pair excitation. The formation of these compounds can be ascribed to the oxidative scission of double bond analogous to the CCT photochemistry of simple alkenes in oxygen matrices, which have been discussed in section 4.4.3.

The CCT photochemistry of benzene in the oxygen matrix is proposed to proceed as follows,

$$[C_6H_6..O_2] \xrightarrow[O_2]{h\nu} \text{(OO}^{\bullet}\text{-cyclohexadienyl-OO}^{\bullet}\text{)} \longrightarrow HCO(CH=CH)_2CHO, \text{ etc.} \quad (4\text{-}6a)$$

$$\text{(OO}^{\bullet}\text{-cyclohexadienyl-OO}^{\bullet}\text{)} \longrightarrow CO_2, CO, \text{ etc.} \quad (4\text{-}6b)$$

while CT excited reaction of 2,3-dimethyl-2-butene could be ascribed as,

$$[CH_3CH=CHCH_3..O_2] \xrightarrow[O_2]{h\nu} CH_3CH(OO^{\bullet})-CH(OO^{\bullet})CH_3 \longrightarrow 2CH_3CHO, \text{ etc.} \quad (4\text{-}7a)$$

$$CH_3CH(OO^{\bullet})-CH(OO^{\bullet})CH_3 \longrightarrow CO_2, CO, \text{ etc.} \quad (4\text{-}7b)$$

Formation of CO_2 is observed from the beginning of irradiation suggesting that it is at least partly a primary product. As shown in Fig.4.6 (c), successive irradiation of benzene at 254 nm

after the irradiation at 297 nm caused the decrease of the intensity of the carbonyl band at 1690 cm^{-1} and the small bands around 900~1150 cm^{-1}, accompanying the spectral change of the 1700 cm^{-1} band. Secondary photooxidation of the unsaturated aldehyde apparently contributes to the secondary formation of CO_2 and another carbonyl product.

Formation of CO and CO_2 and unidentified organic products has been reported by Lin and Tevault[20] in the $Ar/C_6H_6/O_2$ matrices (100/1/x, x=0.5~2) irradiated by a full arc of high-pressure mercury lamp (VUV radiation eliminated). Both CO and CO_2 were believed to be formed by secondary photolysis of O_2-adducts produced by the reaction of $C_6H_6(^3B_{1u})$ and O_2. Although their finding that both absolute and relative yields of CO and CO_2 depends on the O_2 ratio is very interesting, it is hard to assess the relative importance of the reaction via the CCT and direct excitation, since no UV absorption spectrum has been reported.

Toluene. Product spectrum depicted in Fig.4.7 (b), shows strong IR absorption band of CO_2 and bands at 1702 and 1691 cm^{-1} which could be assigned as unsaturated carbonyl compounds formed by the cleavage of the aromatic ring as seen in the reaction of benzene. Benzaldehyde is not found in the product spectrum. This result is in contrast to those observed[21,22] in the photo-oxidation of oxygen-saturated neat toluene at 254 and 313 nm, where benzaldehyde, benzyl alcohol and benzylhydroperoxide are reported to be main products. Those products are apparently formed by radical reactions initiated by abstraction of hydrogen from the methyl substituent. None of these products are

identified in the CCT band excitation photochemistry in the oxygen matrix.

Contribution of methyl carbon atom to the product CO_2 was evaluated in the present study using $Ph^{13}CH_3$. The ratio of integrated absorbance of $^{13}CO_2$ to that of $^{12}CO_2$ from unlabeled toluene, 0.013 agrees well with the natural abundance of ^{13}C within error limit. The $^{13}CO_2/^{12}CO_2$ ratios from $Ph^{13}CH_3$ after the irradiation for 1 and 2h are 0.023 and 0.036 as depicted in Fig.4.10 (b) and (c), respectively. Thus, the contribution of methyl carbon atom to CO_2 is only 1~2% as compared to ring carbon atoms. This evidence also supports the conclusion that the oxidative cleavage of an aromatic ring similar to the reactions (4-6a) and (4-6b) is the major pathway of the excited charge transfer state of toluene-O_2 pair, and the reaction on the methyl group is of little importance. Fig.4.10 (b) and (c) also show the increments of both $^{12}CO_2$ and $^{13}CO_2$ are larger for the later irradiation time, which suggests that the secondary photo-oxidation of the products also contributes to the formation of carbon dioxide.

p-Xylene, Mesitylene and Durene. The main feature of the products from the methyl substituted benzenes is the same as those of benzene and toluene, i.e. CO_2 and possible unsaturated carbonyl compounds are the main products. Unknown bands around 3300 cm^{-1} were found in the product spectra of p-xylene, mesitylene and durene. The bands appear at the beginning of the irradiation suggests that they are primary products. The frequency is much lower than typical value (3640~3600 cm^{-1})[19] of

O-H stretching mode of phenol, alcohol or hydroperoxide, and could be assigned to hydrogen bonded O-H stretching mode. A possible candidate is a difunctional acid or alcohol in which hydrogen bonding to another functional C=O group is exerting. It is also noted that the initial CO_2/carbonyl ratio is higher for the excitation at higher energy for a specific reactant. This tendency could be explained if the reaction intermediate retains the excitation energy and decomposes unimolecularly to form CO_2 before losing the excess vibrational energy.

Styrene and Naphthalene. Styrene has an olefinic double bond as well as an aromatic ring. It is of interest to see which site is more reactive with reference to the CCT band excitation in oxygen matrix. The experimental result manifests the olefinic type of reaction by giving benzaldehyde and formaldehyde as the main products.

$$[Ph\text{-}CH{=}CH_2 \ldots O_2] \xrightarrow{h\nu} Ph\text{-}CHO + HCHO \qquad (4\text{-}8)$$

Formation of benzaldehyde and formaldehyde has been reported by Kodaira[23] et al. in the liquid phase photo-copolymerization of styrene with oxygen by the excitation of a CT band.

The spectral feature of the product from naphthalene is similar to that of benzene and toluene suggesting that oxidative cleavage of aromatic ring to form aromatic dicarbonyl compounds and CO_2 is the major pathway. Formation of the 1,4-endo-peroxide such as that reported[16] in the excitation of the CCT pairs of 2,3-dimethyl-naphthalene and 1,2,3,4-tetramethyl-naphthalene with oxygen in various solvents is not observed since an expected

absorption band of cis-olefinic C-H out-of-plane mode at 730-665 cm^{-1} is not found in the product spectrum. This implies the absence of $O_2(^1\Delta_g)$ in the reaction of the CCT pairs of arenes and O_2 as was the case of alkenes.

Comparison with alkenes. In the excitation of the arene-O_2 pair, reactions of type (iii) and (iv) in alkene-O_2 system are commonly observed for all the compounds studied here. It can be concluded that the oxidative cleavage of double bond, either olefinic or aromatic, is the most characteristic type of reaction in the excited charge-transfer or ion-pair state of the pairs of unsaturated organic compound with O_2. The cis-trans isomerization is indicative of the formation of the triplet alkene. Although there is no direct evidence of the formation of the triplet state for arenes, lower reactivity of these than alkenes would be attributable to more efficient quenching process to form the triplet state; quenching of the fluorescence of benzene by O_2 has long been thought[24] to proceed by producing the triplet state via the CT state.

e) Photochemical Property of Methyl Substituted Ketene

It has been well known[25] that ketene is induce photofragmentation into CH_2 and CO by excitation at the $n\rightarrow\pi^*$ band in gas phase. Zabransky and Carr[25a] proposed the following scheme for the near ultraviolet photochemistry of ketene:

$$CH_2CO(\tilde{X}^1A_1) \xrightarrow{h\nu} CH_2CO(^1A'') \xrightarrow{\tau<0.4ns} CH_2CO^{\dagger}(\tilde{X}A_1) \qquad (4\text{-}9)$$

$$CH_2CO^{\dagger}(\tilde{X}A_1) \longrightarrow {}^1CH_2 + CO \qquad (4\text{-}10a)$$

$$\xrightarrow{M} CH_2CO(\tilde{X}A_1) \qquad (4\text{-}10b)$$

$$\longrightarrow CH_2CO({}^3A') \qquad (4\text{-}10c).$$

The $^1A''$ state is formed initially by excitation in ultraviolet, and the state crosses over to the ground state by internal conversion within 0.4 ns (4-9). Where $CH_2CO^{\dagger}$ denotes ground state ketene with excess vibrational energy. The fate of the vibrationaliy excited ketene molecule is represented as three reactions 4-10a~c: the dissociation into $^1CH_2$ + CO (4-10a), the deactivation to ground state by collision with third body (4-10b), and inter system crossing to $^3A'$, from which ketene will dissociate into $^3CH_2$ + CO. The quantum yield[25b] of dissociation into CH_2 + CO at low-pressure limit is unity at 313 nm, which is near the absorption maximum of $n\rightarrow\pi^*$ bands of ketene in gas phase as shown in Fig.3.7a(g).

On the other hand, Bandow and Akimoto[2] reported that no reaction was found in ketene in argon matrix by excitation around 310 ~ 410 nm (high pressure Hg-arc lamp with Corning 7-51 filter). They also study the photochemistry of ketene in oxygen and O_2-Ar matrices. The photochemical products observed in solid oxygen were HO_2, CO, CO_2, H_2O and O_3. When the ratio of O_2/Ar decrease, the oxidation rate efficiently decreased. They concluded that the photooxidation of ketene in the O_2 and also O_2-Ar matrices occurs via the reaction of the excited state of ketene surrounded by O_2 molecules, not via the photo-dissociation

reaction (4-10a) followed by the reaction of CH_2 with O_2. In present study, no reaction observed for methylketene even in O_2 matrix by irradiation at 406 nm which is near the center of the intrinsic $n\rightarrow\pi^*$ band (see Fig.3.7b(g)) and is at longer wavelength than the absorption threshold of the CCT band. Thus the dissociation reaction is not found in O_2 and/or Ar matrices for ketene and methyl ketene, and also possibly dimethylketene. The contrast of in gas phase and in matrix could be explained that the vibrational energy transfer from the guest to the matrix lattice should be very efficient in these system, i.e., the vibrational relaxation of $CH_2CO^{\dagger}$ is very rapid in cryogenic matrices, so the dissociation could not occur.

However, in oxygen matrices, excitation within the CCT absorption bands induced photochemical reaction for methylketene and dimethylketene, and within the $n\rightarrow\pi^*$ for ketene. Matching of the long-wavelength threshold for the reaction and that for CCT absorption band of each methyl substituted ketene in oxygen matrix suggests the reaction occur from the CT state, $[D^+..O_2^-]$. This is also supported by formation of the carbonyl compound from each ketene; acetone and acetaldehyde for dimethylketene and methylketene. These compounds can form from oxidative cleavage of C=C bonding with CO_2, which was indeed formed. This mechanism is similar to that of the reaction of alkenes in oxygen matrices. Reaction types of dimethylketene and methylketene could correspond to that of alkene's type (iii) of 2-butene and of 2,3-dimethyl-2-butene. Thus, it can be concludes that the photochemical reaction of methylketene and dimethyl ketene in oxygen

matrices are the same as alkene type (iii) in 300 ~ 400 nm region. In the case of ketene, when the excitation performed at more shorter wavelength the CT photochemistry, whose contribution thought to be a little in the the excitation at 310 ~ 410 nm, will increase of its importance.

There is an attractive explanation but no proof for that no reaction occur in the methylketene-O_2 system by excitation at $n\rightarrow\pi^*$ band while reaction occur in the ketene-O_2. The hypothesis is as follows. A specific configuration for O_2-ketene pear is required for to react by $n\rightarrow\pi^*$ excitation. The configuration should be a linear form as $O{=}O\cdots CH_2{=}C{=}O$. Electronically excited ketene can attack the partner oxygen molecule only by the vibrational motion parallel to its molecular axis, symmetric or anti-symmetric motion of C=C=O. This is a kind of mode selective reaction. In Ar-O_2 matrices, if the ratio of Ar/O_2 is low, only a few of O_2-ketene pear which has the linear configuration can form, so the ratio very efficient to the decrease of the reaction rate. In the case of methylketene, none of the pear has a linear configuration because of the existence of the methyl group. This is the reason that no reaction was found in methylketene-O_2 system by excitation at $n\rightarrow\pi^*$ band.

Several unknown peaks were found in the product spectra from dimethylketene-O_2 system (see Fig.4.12). Band at 1880.0 showed isotope shift when $^{18}O_2$ was used for matrix material. The value 2 ~ 3 cm^{-1} means the shift is secondary. From the mixing ($^{18}O_2$-$^{16}O_2$), it is expected that the product for the band was formed from a reaction with one oxygen molecule. On the other hand, the

frequency, 1880 cm^{-1}, is a special value which is only found in several compounds[26]. Stretching mode of C=O in α-lactone[26a] and α-peroxylactone[26b] were found around 1900 cm^{-1}. Considering all these above, the most possible compound is dimetyl-α-peroxy-lactone[26b] whose C=O stretching mode appears at 1874 cm^{-1}. This compound could form form O_2 addition to C=C bonding of dimethyl-ketene.

Band at 1852.6 cm^{-1} appeared with a band at 1849.4 cm^{-1} is thought to be of the same product as at 3509.2 cm^{-1}. One possible candidate is a peracid, CH_2=CH(CH_3)-C(=O)-OOH, whose O-H st. mode could reduce the wavenumber form ordinal acidic O-H by intramolecular hydrogen bonding. However, 1852.6 cm^{-1} is too higher value for ordinal peracid (1734 cm^{-1} for C=O st. of HC(O)OOH in oxygen matrix[27]), so these peaks are remain as unassigned. Peak at 1778.3 cm^{-1} found in the product spectrum from methylketene-O_2 system is at too higher to assign as acetaldehyde dimer appears around 1755 cm^{-1} which is shown in the reference spectrum. This also remains as unknown.

5. Comparison with Other Photooxygenation Reactions of Organic Compounds with Oxygen

(a) Comparison with the Reaction in Liquid and Gas Phase

Photolysis of C_2H_4/O_2 mixtures in liquid Ar at 87K has been reported by Buschmann[18], which is apparently most closely related to ours. Although the CCT photochemistry was studied in this system, only ozone production by the irradiation at 206.2 nm was reported, so no further comparison is possible.

Onodera et al.[16] summarized their results of the CCT photochemistry of a series of (organic molecule)-O_2 pairs in conventional oxygen-saturated organic solution and classified the possible processes into three types: (1) formation of a pair of the substrate cation radical and the superoxide ion; (2) conversion to the triplet substrate and singlet oxygen; and (3) deactivation to the starting materials. The first process, formation of a completely separated ion pair ($D^+ + O_2^-$) is possible only in the polar solvents and is impossible in solid oxygen from energetics in the near UV region. Thus, while the formation of a certain type of product was interpreted as a result of a radical cation-solvent reaction in their study, our study demonstrated the alkene-O_2 reactions can be directly ascribed to the excited CCT pair in solid oxygen. The second process of triplet alkene formation was assessed by its cis-trans isomerization in the present study while the singlet oxygen molecule formation due to the processes,

$$^3(D^+..O_2^-) \longrightarrow {}^3D + {}^1O_2 \qquad (4\text{-}9a)$$

$$\text{or } ^3(D^+..O_2^-) \longrightarrow {}^3D + {}^3O_2 \longrightarrow D + {}^1O_2 \qquad (4\text{-}9b)$$

was assessed by its specific reaction products in their study. The third process of deactivation to the ground state has been observed both in the present cryogenic system and in the room temperature organic solvent. Although the 2,3-dimethyl-2-butene is the species studied commonly in both media, direct comparison of the results is difficult since the excitation of the CCT pair at 313 nm (3.96 eV) in methanol produced $(CH_3)_2C(OCH_3)C(CH_3)_2OH$

and $CH_2=C(CH_3)-C(CH_3)_2OOH$, which were ascribed[16] to the reaction of the radical cation. In solid oxygen, TMT formation was the major process in this energy range.

Only for benzene among arenes discussed above, a fair amount of photooxidation studies have been reported[28~32] in the gas and liquid phase. Excitation of benzene with 248~254 nm radiation in the presence of high pressure of oxygen has been known[29,30] to result in photooxygenation. The major product appears to be phenol and mucondialdehyde in the gas phase although no clear information on yields is yet available. Irina and Kurien[29] reported that the major product from the irradiation at 254 nm changed from phenol to mucondialdehyde when the rate of oxygen flow bubbled through benzene was increased. It is interesting to note that other than polymeric products, only mucondialdehyde, was found[28] in liquid phase photo-oxidation of O_2-saturated benzene. The formation of phenol reveals the presence of $O(^3P)$ atom which is known[33] to react with benzene to give the product. Hunter et al.[30] proposed the following processes to explain the formation of phenol.

$$C_6H_6(^1A_{1g}) + h\nu(248\sim254nm) \longrightarrow C_6H_6(^1B_{2u}) \longrightarrow C_6H_6^{\ddagger}(^3B_{1u}) \quad (4\text{-}10)$$

$$C_6H_6^{\ddagger}(^3B_{1u}) + O_2(^3\Sigma_g^-) \longrightarrow C_6H_6(^1A_{1g}) + O_2(^1\Sigma_u^-) \quad (4\text{-}11)$$

$$O_2(^1\Sigma_u^-) \longrightarrow 2O(^3P) \quad (4\text{-}12)$$

$$O(^3P) + C_6H_6(^1A_{1g}) \longrightarrow C_6H_5OH \quad (4\text{-}13)$$

Formation of phenol with a quantum yield of 0.01 by the

excitation at 193 nm as observed by Nakashima and Yoshihara[32] may also proceed via the reaction of $O(^3P)$ atom. On the other hand, mucondialdehyde could be formed from the excited charge transfer state of a benzene-O_2 pair.

$$C_6H_6(^1B_{2u}) + O_2(^3\Sigma_g^-) \longrightarrow {}^3[C_6H_6^+ \ldots O_2^-] \qquad (4\text{-}14)$$

$$^3[C_6H_6 \ldots O_2] + h\nu \longrightarrow {}^3[C_6H_6^+ \ldots O_2^-] \qquad (4\text{-}15)$$

$$^3[C_6H_6^+ \ldots O_2^-] \longrightarrow HCO(CH{=}CH)_2CHO$$

$$\longrightarrow C_6H_6(^1A_{1g}) + O_2(^3\Sigma_g^-) \qquad (4\text{-}16)$$

The triplet charge transfer exciplex state can be reached either by the collisional deactivation of $^1B_{2u}$ state of a benzene or directly by the excitation of the CCT absorption of a benzene-O_2 pair. The relative importance of the two pathways depends on the relative intensity of the intrinsic and CCT absorption bands which is a function of the concentration of O_2.

Photooxidation of oxygen-saturated neat toluene has also been studied, and oxidative chain reaction to form benzaldehyde, benzyl alcohol and benzylhydroperoxide has been reported by Wei and Adelman[22], and by Chien[21]. This is a remarkable contrast that the contribution of methyl substituent for photooxygenation is thought to be negligible in the CT excited photochemistry of toluene in the cryogenic oxygen matrix.

(b) Comparison with the Reactions on Surfaces

Formation of the radical ion pair ($D^+..O_2^-$) has been postu-

lated[34,35] during the course of photooxidation of organic molecules on n-type semiconductor surfaces, e.g. TiO_2, Z_nO, CdS etc, in the presence of oxygen. Although the reaction mechanism on the surfaces could be more complex due to the incorporation of metal ions and oxygen atoms of metal oxides, it is very interesting to note that in these reactions double bond scission of alkenes to form carbonyl molecules followed by rapid secondary photooxidation to yield CO_2 is often observed[35~37].

Efficient CO_2 formation (mineralization) in the photooxidation of toluene on TiO_2 has also been reported by Ibusuki and Takeuchi[38]. Nearly complete oxidation of all the carbon atoms in toluene to CO_2 may proceed via successive oxidative cleavage of the double bonds besides the unimolecular fragmentation of the carbonyl oxide type biradical in equation (9b). Relevance to ozone chemistry has been pointed out by Martinez[39] since both processes are thought to involve similar biradical ($\diagdown\!\!\diagup C^{\bullet}\text{-}OO^{\bullet}$) state as an intermediate.

The marked similarity of the products from photooxidation on semiconductor surfaces and those from CCT pair photochemistry in solid oxygen suggests the importance of the reaction of the radical ion pair state or excited charge transfer state as a common process. Sancier et al.[34] reported that irradiation of sand adsorbing organic compounds emits CO_2 very efficiently. Such a process might also involve the ion-pair state and would be relevant to the CCT photochemistry studied here.

6. Conclusion

Photochemical reaction of simple alkenes, arenes, and ketenes in the excitation within the CCT bands were studied by using FT-IR.

The reaction of alkene can be classified into the following four pathways: (i) photooxygenation to give an oxygen adduct, which is observed only for 2,3-dimethyl-2-butene; (ii) cis-trans isomerization, which is the major reaction path for cis and trans-2-butene, suggesting the crossing to the alkene triplet state; (iii) double bond scission to give two corresponding carbonyl compounds, which is observed for all alkenes studied with the energy threshold higher than the photooxygenation and cis-trans isomerization; (iv) formation of CO_2, CO, and O_3, which occurs at still shorter wavelength than the double bond scission. In case of ethene and propene, HO_2 was also produced. No evidence was found formation of singlet oxygen molecule in the photochemical reaction.

Photochemical properties of benzene, toluene, p-xylene, mesitylene, durene, styrene and naphthalene in solid oxygen at 11K have also been studied. Photochemical excitation at the CCT absorption band for all the compounds studied except styrene cause oxidative cleavage of the aromatic ring to form corresponding dicarbonyl compounds and CO_2 as main products. Styrene reacts as an alkene giving benzaldehyde and formaldehyde specific for the oxidative cleavage of side chain rather than an aromatic ring.

Reaction through CT state in oxygen matrices have been found

in methyl substituted ketenes. The main reaction was oxidative cleavage of C=C double bond to form carbonyl compounds and CO_2, that is similar to that of alkene type (iii). A product expected to be dimethyl-α-peroxylactone formed from dimethylketene-O_2 system.

It can be concluded that the oxidative cleavage of a double bond is the common for alkenes, arenes and methyl substituted ketenes, and the reaction pathway characteristic to the ion-pair state of $[D^{+\cdot\cdot\cdot}O_2^-]$.

Reference

1) (a) Diem, M; Lee, E.K.C. J. Phys. Chem. **1982**, 86, 4507.
(b) Tso, T-L; Lee, E.K.C.; J. phys. Chem. **1984**, 88, 5465.
(c) Tso, T-L; Lee, E.K.C.; J. Phys. Chem. **1984**, 88, 2781.

2) Bandow, H; Akimoto, H; J. Phys. Chem. **1985**, 89, 845.

3) Frei, H; Pimentel, G.C. J. Chem. Phys. **1983**, 79, 3307.

4) Kopecky, K.R,; van de Sande, J.H.; Mumford, C. Can. J. Chem. **1968**, 46, 25.

5) Hanford, W.E.; Sauer J.C. Organic Reactions Vol. 3, pp. 108, John Wiley & Sons, London, **1946**.

6) Tso, T-L.; Diem, M.; Lee, E.K.C. Chem. Phys. Lett. **1982**, 91, 339.

7) Cundall, R.B. Prog. Reaction Kinet. **1964**, 2, 165.

8) Fujisawa, J.; Sato, S.; Shimokoshi, K.; Shida, T. J. Phys. Chem. **1985**, 89, 5481.

9) Köppel, H.; Domcke, W.; Cederbaum, L.S.; Niessen, W.V. J. Chem. Phys. **1978**, 69, 4252.

10) Aroca, R; Menzinger, M. Spectrosc. Lett. **1983**, 16, 945.

11) Gleason, W.S.; Broadbent, A.D.; Whittle, E; Pitts Jr., J.N. J. Am. Chem. Soc. **1970**, 92, 2068.

12) Foote, C.S. Science, **1968**, 162, 963.

13) Criegee, R.; Paulig, G. Chem. Ber. **1955**, 88, 712.

14) Itoh, M.; Mulliken, R.S. J. Phys. Chem. **1969**, 73, 4332.

15) Evans, D.F. J. Chem. Soc. **1960**, 1735,

16) Onodera, K.; Furusawa, G.; Kojima, M.; Tsuchiya, M.; Aihara, S.; Akaba, R.; Sakuragi, H.; Tokumaru, K. Tetrahedron, **1985**, 2215.

17) Huber, K.P.; Herzberg, G. "Molecular Spectra and Molecular Spectroscopy, IV Constants of Diatomic Molecules", Van Nostrand Reinhold Co., New York, 1979.

18) Buschmann, H.W. Ber. Bunsenges. Phys. Chem. 1974, 78, 1344.

19) Colthup, N.B.; Daly L.H.; Wiberley, S.E. "Introduction to Infrared and Raman Spectroscopy", Academic Press, London, 1964.

20) Lin, M.C.; Tevault, D.E. Combust. Flame, 1981, 42, 139.

21) Chien, J.C.W. J. Phys. Chem. 1965, 69, 4317.

22) Wei, K. S.; Adelman, A. H. Tetrahedron Lett. 1969, 3297.

23) Kodaira, T.; Hashimoto, K.; Sakanaka, Y.; Tanihata, S.; Ikeda, K. Bull. Chem. Soc. Jpn. 1978, 51, 1487.

24) Brown, R.G.; Phillips, D. J. Chem. Soc. Faraday 2, 1974, 70, 630.

25) (a) Zabransky, V.; Carr Jr., R.W. J. Phys. Chem., 1975, 79, 1618. (b) Porter, G.B.; Connelly, B.T. J. Chem. Phys., 1960, 33, 81.

26) (a) Chapman, O.L.; Wojtkowski, P.W.; Adam, W.; Rodriguez, O.; Rucktaschel, R. J. Am. Chem. Soc. 1972, 94, 1365. (b) Adam, W; Alzérreca, A.; Leu, J.C.; Yany, F. J. Am. Chem. Soc. 1977, 99, 5768.

27) Diem, M; Lee, E.K.C J. Phys. Chem. 1982, 4507.

28) Wei, K.; Mani, J-C.; Pitts Jr., J.N. J. Am. Chem. Soc. 1967, 89, 4225.

29) Irina, J.; Kurien, K.C. J. Chem. Soc. Chem. Commun. 1973, 738.

30) Hunter, T.F.; Rumbles, D.; Stock, M.G. Chem. Phys. Lett.

1977, 45, 145.

31) Knee, J.L.; Otis, C.E.; Johnson, P.M. J. Phys. Chem. 1982, 86, 4467.

32) Nakashima, N.; Yoshihara, K. Bull. Chem. Soc. Jpn. 1982, 55, 2783.

33) Bonnano, R.A.; Kim P.; Lee, J.; Timmons, R.B. J. Chem. Phys. 1972, 57, 1377.

34) Sancier, K.M.; Morrison, S.R. Surf. Sci. 1979, 83, 29.

35) Kanno, T.; Oguchi, T.; Sakuragi, H.; Tokumaru, K. Tetrahedron Lett. 1980, 21, 467.

36) Takeuchi, K.; Yazawa, T.; Ibusuki, T. Atmos. Environ. 1983, 17, 2253.

37) Pichat, P.; Herrmann, J-M.; Disdier. J.; Mozzanega, M.-N. J. Phys. Chem. 1979, 83, 3122.

38) Ibusuki, T.; Takeuchi. K. Atmos. Environ. 1986, 20, 1711.

39) Martinez, R.I. J. Phys. Chem. 1987, 91, 1354.

CHAPTER V

INFRARED SPECTROSCOPIC DETECTION OF THE HSO_X RADICAL USING MATRIX ISOLATION TECHNIQUE

1. Introduction

Bisulfite (also called hydroxysulfonyl, i.e. $HOSO_2$) radical is recognized[1] as an important intermediate in the atmospheric oxidation of SO_2 initiated by OH radicals. The oxidation process has been discussed on the basis of the recognition that the reaction (5-1) is the major rate-controlling step in the gas phase homogeneous oxidation of SO_2 in the troposphere, and the subsequent reaction (5-2) and/or (5-3) produce SO_3 and/or $HOSO_4$, and finally, the formation of sulfuric acid aerosol is the goal of the oxidation reaction[1].

$$OH + SO_2 + M \longrightarrow HOSO_2 + M. \qquad (5\text{-}1)$$

$$HOSO_2 + O_2 \longrightarrow HO_2 + SO_3 \qquad (5\text{-}2)$$

$$HOSO_2 + O_2 + M \longrightarrow HOSO_4 + M. \qquad (5\text{-}3)$$

Stockwell and Calvert[2] have presented evidence in their study of photooxidation of the $CO/HONO/NO/NO_2/SO_2$ mixture in air that reaction (5-2) may be the dominant channel for the reaction of $HOSO_2$ radicals with oxygen. Further evidence supporting the predominance of reaction (5-2) has been reported in more recent direct kinetic studies[3-6]. On the other hand, thermochemical estimates by Benson[7] put the enthalpy changes for reactions (5-2) and (5-3) to be 8 ± 2 kcal $mole^{-1}$ endothermic and 16 kcal $mole^{-1}$ exothermic, respectively, thus favoring reaction (5-3) in

contrast to the experimental evidence. Since reaction (5-2) followed by the reaction

$$HO_2 + NO \longrightarrow OH + NO_2 \qquad (5\text{-}4)$$

constitutes chain sustaining steps while reaction (5-3) does not, the experimental observations for the predominance of reaction (5-2) are of great importance in atmospheric chemistry of both troposphere[1] and stratosphere[8].

In spite of the atmospheric significance the intermediate radical, bisulfite, have not been directly detected by any opto-spectroscopic method either in gas or condensed phase. Only two other kind of spectroscopic detection have been reported. One is an ESR detection by Flockhart et al[9], who assigned the signal observed in the reaction between H_2O_2 and SO_2 in aqueous solution /to $HOSO_2$. The other is the mass spectral observation[6] converting to SO_3^- in gas phase. As for the peroxybisulfate no experimental data is available in either gas or condensed phases.

In this study, a matrix isolation method was used to detect the $HOSO_2$ radical from a reaction of SO_2 and hydroxyl radical produced by the photolysis of H_2O_2 or H_2O. $HOSO_2$ was trapped in the Ar matrix at 11 K and its infrared spectrum was measured as it were to 'freeze' the reaction (5-1) and to look directly the reaction intermediate. Here, it will be reported that the first direct detection of $HOSO_2$ by an opto-spectroscopic method. More, detection of $HOSO_4$ was also examined.

Additionally, in order to get better insight, ab initio calculations of the molecular geometries, and vibrational fundamental frequencies for the ground states of the $HOSO_2$ and

$HOSO_4$ radicals were carried out at the 3-21G(*) level. The comparison of the calculated and experimental results will be discussed.

2. Experimental

The $HOSO_2$ radicals were produced by the reaction of hydroxyl with SO_2. Photolysis of H_2O_2 at 185/254 nm by a Hg resonance lamp with CaF_2 window or photolysis of water vapor at 147 nm by a Xe resonance lamp with CaF_2 window was used as a source of hydroxyl radicals. Both electrode-less lamps were actuated by a 2.45 GHz microwave generator.

Gas mixture of SO_2 in Ar (1:250) was introduced into the vacuum vessel through one of the stainless steel tubing of the deposition line. Separately, H_2O_2 in Ar (M/R = 250/1) was introduced thorough the an all-glass deposition line with a PTFE nozzle at the end in the vessel in order to minimize the decomposition of hydrogenperoxide. These sample mixtures were jetted simultaneously and effusively about 10 mm before contacting the CsI sample plate surface. The photolysis lamp irradiates the cold surface through the gas flow in the mixing zone so that photolysis can occur in the gas phase when the irradiation is made during deposition. Fig.2.4 shows the optional setup of the cryostat for this experiment. Typically, about 0.5 mmol of each gas mixture was first deposited simultaneously without irradiation to obtain reference IR spectra and then additional about 1.5 mmol of each gas mixture was deposited under irradiation by the Hg lamp with a flow rate of 1 mmol/h each.

Similar conditions were employed for the experiments using $H_2{}^{16}O$ or $H_2{}^{16}O$-$H_2{}^{18}O$ mixture (1/1) in Ar as an hydroxyl radical source. The deposition temperature employed was 11K for all runs. After taking the infrared spectrum, the reaction mixture was annealed at 20~28 K (28K is about 30 % of the melting point of Ar) for about 15 min and another spectrum taken after re-cooling to 11K. In some runs photolysis was made on the deposited mixtures instead of during the deposition in order to check the efficiency of the production of the radicals.

In order to sort out the absorption bands due to the hydroxyl radical reaction from those due to the H-atom reaction, a matrix isolation experiment coupled with a discharge flow reactor was also carried out. In this experiment, a discharge flow tube with a sampling pinhole of ca. 0.3 mm in diameter was installed on the cryostat. A mixture of H_2/Ar (M/R = 100/1) was discharged though a microwave cavity and a SO_2/Ar (M/R= 250/1) mixture was added downstream. A part of the reaction mixture was collected on the CsI cold surface through the pinhole. Typical total pressure of the discharge region was 0.2 Torr and the flow rate was about 1 mmol/h.

To detect the $HOSO_4$ radical, a similar experiment using oxygen instead of Ar matrix gas was also carried out. A mixture of SO_2/O_2 (M/R = 250/1) and a mixture of H_2O_2/O_2 (M/R = 250/1) were co-deposited on the CsI sample plate at 11 K with irradiation by the Hg resonance lamp. Spectra of the reaction mixture were also measured by the FT-IR in the same manner.

Samples, H_2O_2 (90% pure, Mitsubishi Gas-Chemicals Co. Ltd.),

$H_2{}^{18}O$ (99% pure, B.O.C. Ltd.) and SO_2 (99.98%, Matheson Co. Ltd.) were used after trap-to-trap distillation for degassing. All infrared spectra were measured by the FT-IR under the condition of 0.24 cm^{-1} resolution and 512 times accumulation with a narrow band (high D*) HgCdTe detector. The spectral range observed was 4000~700 cm^{-1}.

3. Computational Details

Geometries were fully optimized at the spin-unrestricted Hartree-Fock (HF) level with the split-valance 3-21G(*) (polarization functions only on sulfur) basis set[11]. The computed expectation value of the spin-squared operator $\langle S^2 \rangle$ from the unrestricted HF wave function was 0.76 for $HOSO_2$ radical, this was close to the correct value of 0.75 for a pure doublet. Harmonic vibrational frequencies were calculated by using the HF/3-21G(*) analytical energy derivatives. Force constant matrix and normal coordinates (not presented here) are available upon request.

In order to obtain more reliable energies, single-point calculations were carried out at the HF/3-21G(*) optimized geometries; with the larger 6-31G** (polarization functions on all atoms) basis set[12], the effect of electron correlation was incorporated by means of Møller-Plesset (MP) perturbation theory up to fourth-order(MP4SDTQ)[13]. In these calculations, all single (S), double(D), triple(T), and quadruple(Q) excitations were included, with the constraint that core-like orbitals were doubly occupied. This will be denoted by MP4SDTQ/6-31**//3-21G(*), the

// symbol meaning "at the geometry of". Zero-point correction was made with harmonic vibrational frequencies at the HF/3-21G(*) level.

4. Spectroscopic Detection of HSO_X Radicals

(a) $HOSO_2$ Radical

To detect the $HOSO_2$ radical from a reaction of SO_2 and hydroxyl radical produced by the photolysis of H_2O_2 or H_2O, the photochemical reactivity of these compounds were examined first. Photolysis of H_2O_2/Ar at 185 nm during deposition produced matrix isolated hydroxyl radical the bands at nearly the same wavenumber (3452 and 3427 cm^{-1}) with a slightly broader bandwidth than those obtained in the photolysis of H_2O. The absorption bands of HO_2 radical[14,15] were not observed in the photolysis of H_2O_2/Ar during deposition. Photolysis of H_2O/Ar at 147 nm during deposition produced matrix isolated hydroxyl radicals as confirmed by the absorption bands at 3452.2 and 3428.2 cm^{-1} agreeing well with the data of Acquista et al.[16] The origin of the two bands has not been clarified but might be due to the species at different matrix sites. Photolysis of SO_2/Ar alone by the Hg and Xe resonance lamps during deposition gave no absorption peak due to SO[17], SO_3[18,19] and SO_4[20].

When H_2O/Ar or H_2O_2/Ar was photolyzed during co-deposition with SO_2/Ar mixture, the hydroxyl bands disappeared and new bands appeared. Figs 5.1 (a) and (b) compare the matrix infrared absorption spectra of the $H_{2O}2$/Ar-SO_2/Ar system at 11K obtained without and with irradiation by the Hg lamp. Absorption bands

observed after unphotolyzed deposition is assigned to H_2O_2[21], H_2O[22~24], SO_2[25] and gas phase H_2O lines due to unremoved water vapor in the spectrometer. Fig.5.1 (b) shows six new absorption peaks, and the same six bands were observed at the same frequencies within ± 0.1 cm^{-1} when H_2O/Ar was used as an hydroxyl radicals source. From the different behavior of the peak intensity toward annealing these absorption bands can be ascribed to two or three different species. The band intensities of the peaks at 3539.9, 1309.2, 1097.3 and 759.5 cm^{-1} always vary in parallel while those of two bands at 1286.8 and 1285.4 cm^{-1} vary independently of the other four peaks when the reaction mixture was annealed or prepared from a different radical source. TABLE V-I shows the absolute and relative absorbance of the former four bands observed in the present study, showing constancy of the relative intensity for these bands. When the reaction mixture obtained in the 1:1 flow ratio of H_2O_2/Ar and SO_2/Ar, run.1, was annealed at 23 K for 15 min, the peak heights of the former four bands decreased in parallel to about two-thirds of the peak heights before annealing, whereas those of the latter two bands remained almost unchanged. In another run, run.2, the former four bands decreased to two-thirds while the other bands decreased to one-third in absorbance after annealing at 28 K for 15 min. It has been noted that when the reaction mixture obtained at the flow rate of H_2O_2/Ar begin in excess of that of SO_2/Ar, an absorption band of the hydroxyl radical was observed at 3452.2 cm^{-1}, and under these conditions all of the peaks of the transient species increased 30~50% in absorbance after

annealing at 20 K for 20 min. When the same matrix sample annealed again at 30 K for 15 min, the former four peaks increased to about twice the intensity whereas the peaks at 1286.8 and 1285.4 cm^{-1} decreased to about the same intensity as in the original spectrum before annealing.

All the evidence suggests that the four bands at 3539.9, 1309.2, 1097.3 and 759.5 cm^{-1} can be ascribed to a single transient species which we assign to the $HOSO_2$ radical according to the discussion below. The transient peaks at 1286.8 and 1285.4 cm^{-1} are apparently due to other species, which will be discussed in latter section. The $HOSO_2$ radical is thought to be produced by the reaction of SO_2 with hydroxyl radical generated by the photolysis of either H_2O_2 or H_2O in the gas phase, since the irradiation of the H_2O/Ar-SO_2/Ar mixture after deposition for 3 h gave no new transient absorption peaks. Irradiation of the H_2O_2/Ar-SO_2/Ar mixture after deposition gave only trace peak at 1309 and 1097 cm^{-1}, suggesting a negligible contribution of photochemical reaction within the matrix to produce the radical. The reaction of hydroxyl with SO_2 could occur mostly within the surface and shallow part of the developing matrix since the pressure between the mixing jet and the surface should be too low to enhance the gas phase third-body reaction[26,27]. Significant increase of the $HOSO_2$ peaks when the matrix of the reaction mixtures containing hydroxyl radicals were annealed supports the view.

In order to give the assignment of the observed IR bands, the $H_2{}^{16}O$-$H_2{}^{18}O$(approximately 1:1 mixture)/Ar mixture was used as

a hydroxyl radical source. Fig.5.1 (c) shows the absorption spectrum obtained after annealing. As depicted in Fig.5.1 (c), isotope shifted peaks appears at 3528.6 (3539.8), 1308.7 (1309.2), 1096.0 (1097.2), and 735.1 (759.4) cm^{-1} corresponding to the unlabeled peaks shown in parentheses. These eight absorption bands behaved in parallel after annealing suggesting that the new peaks should be assigned to the ^{18}O-labeled species of the same kind. The isotope shifts of the band at 3540cm^{-1} and 759 cm^{-1} are 0.32% and 3.2%, respectively. These value of the isotope shift are in accord with those expected for the ^{18}O-H and S-^{18}OH stretching modes for which ^{18}O-isotope shifts of 0.33% and 3.5%, respectively, are expected based on simple diatomic approximation[28]. The frequencies of the S-^{16}OH and S-^{18}OH stretching modes of HSOH, 763 and 735 cm^{-1}, reported by Pinchas et al.[29], are very close to 759 and 735 cm^{-1} obtained for unlabeled and labeled species in the present study. Thus, we could assign these two bands at 3540 and 759 cm^{-1} to the O-H and single bonded S-OH stretching modes of $HOSO_2$ radical. Then the bands at 1309 and 1097 cm^{-1} can be assigned to the asymmetric and symmetric stretching modes of the double bonded O=S=O moiety of the $HOSO_2$ radical. Small isotope shifts of 0.5 and 1.2 cm^{-1} are consistent as secondary isotope effects due to the adjacent ^{18}O. More, $HOSO_2$ radical have been characterized by use of ab initio calculations as discussed next section, the analysis of the calculated vibrational modes will strongly support this assignment.

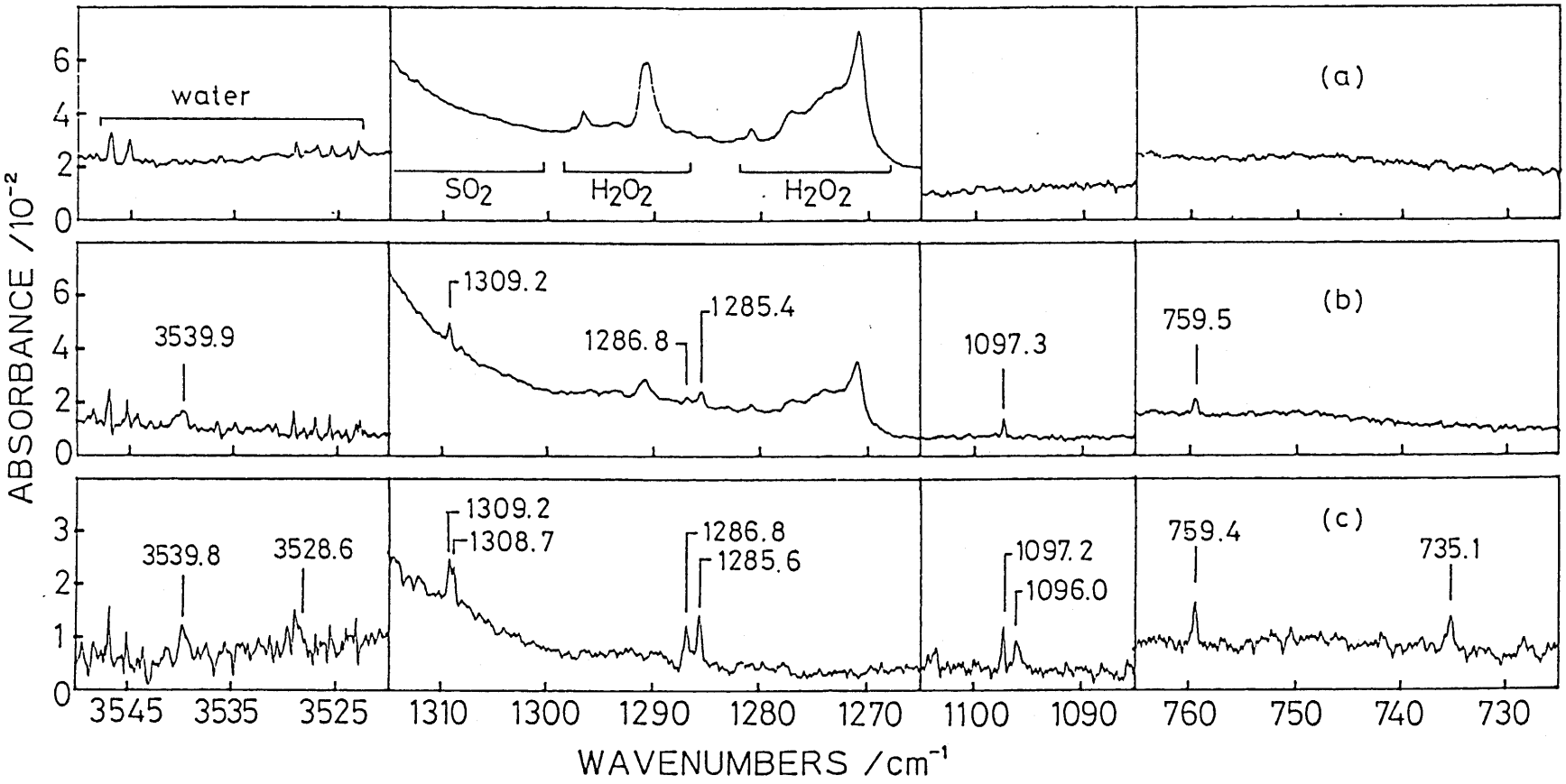

Fig.5.1 Infrared spectra of reaction mixtures after annealing. M/R ratio of all gas mixture is 250/1. (a) Un-photolyzed mixture of H_2O_2/Ar and SO_2/Ar. (b) H_2O_2/Ar and SO_2/Ar, 1.6 mmol for each, co-deposited with irradiation by the Hg resonance lamp after 0.5 mmol each co-deposition in dark; spectrum of water vapor subtracted partially. (c) $H_2{}^{18}O$-$H_2{}^{16}O$(about 1:1 mixture)/Ar, 1.2 mmol, and SO_2/Ar, 1 mmol, co-deposited with irradiation by the Xe resonance lamp after about 1 mmol each co-deposition in dark; spectrum of water vapor subtracted partially also.

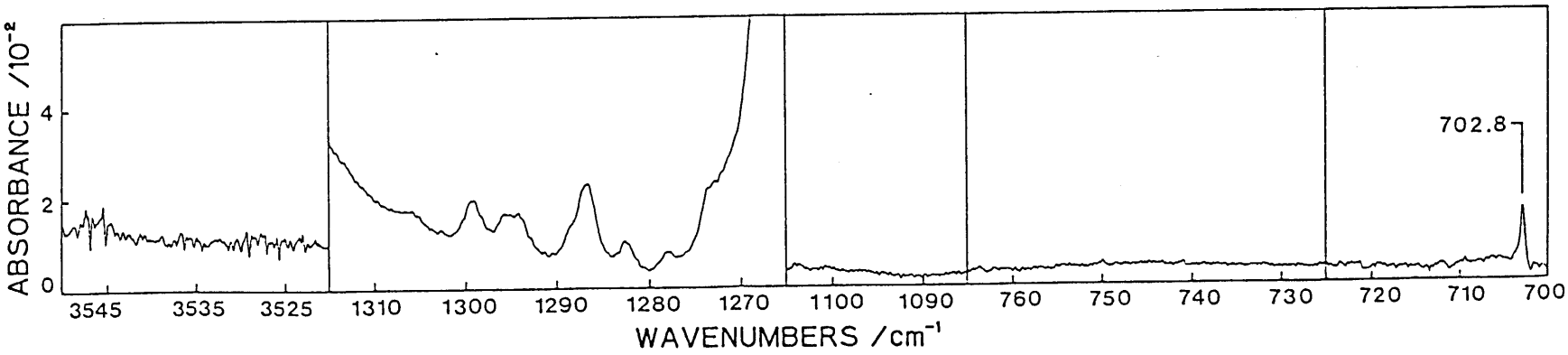

Fig.5.2. Infrared spectra of reaction mixtures of H_2O_2/O_2 and SO_2/O_2 (M/R = 250/1 each) co-deposited with irradiation by the Hg resonance lamp after 0.5 mmol each co-deposition in dark; spectrum of water vapor subtracted partially.

TABLE V-I. Observed Absorption Peak Intensity of the Bands Assigned as $HOSO_2$

Run	OH source		Annealing[b] temperature	Intensity[c] / 10^{-3} O.D. unit			
	compound	/SO_2[a]	/K	3539.9	1309.2	1097.3	759.5 cm^{-1}
1	H_2O_2	0.98	--	6 [0.55]	11 [unity]	10 [0.91]	10 [0.91]
			23	4 [0.57]	7 [unity]	6.5[0.93]	6.5[0.93]
2	H_2O_2	0.84	--	7 [0.38]	18.5[unity]	17.5[0.95]	13 [0.70]
			28	5 [0.36]	14 [unity]	12.5[0.86]	10.5[0.75]
3	H_2O	1.27	--	2 [0.50]	4 [unity]	4 [1.00]	3.5[0.88]
			20	2.5[0.50]	5 [unity]	5 [1.00]	4.5[0.90]
4	H_2O	1.00	--	5 [0.56]	9 [unity]	8 [0.89]	8 [0.89]
			21	4 [0.57]	7 [unity]	6 [0.86]	6.5[0.93]
5	H_2O[d]	1.04	--	2.5[0.56]	4.5[unity]	4 [0.89]	4 [0.89]
			20	2 [0.50]	4 [unity]	3.5[0.88]	3.5[0.88]
Average of Relative Intensity[e]				[0.51±0.15]	[unity]	[0.39±0.09]	[0.85±0.17]
				[0.50±0.17]	[unity]	[0.91±0.12]	[0.88±0.15]

(a) Ratio of the flow rate of H_2O_2/Ar or H_2O/Ar to SO_2/Ar.
(b) About 15 min annealing in each run.
(c) For each run and average, the upper and lower figures indicate the values before and after annealing, respectively. Relative intensity normalized by the peak intensity at 1309.2 cm^{-1} is also listed in brackets.
(d) A 1:1 mixture of $H_2{}^{16}O$ and $H_2{}^{18}O$ was used as OH radical source.

(b) $H-SO_2$ Radical

When discharged H_2/Ar was mixed with SO_2/Ar, the observed spectrum does show two peaks at 1287.5 and 1285.5 cm^{-1} which agree well with the unidentified peaks noted above, thus confirming that these two peaks are not due to the reaction of hydroxyl radical but the reaction of H atom with SO_2. All the bands which were assigned to the $HOSO_2$ radical did not appear in the reaction of atomic hydrogen(s) and SO_2.

Since excess amount of SO_2 against that of atomic H presented in the reaction mixture of the experiment of $HOSO_2$, importance of reactions of SO_2 + 2H and $HOSO_2$ + H are thought to be negligible. So the molecules to show peaks at 1287.5 and 1285.5 cm^{-1} could be products of the reaction of H + SO_2. Two structure is possible for the product. One is $H-S(=O)_2$ and the other is H-O-S=O. If the spices has former structure, these two bands could be assigned as asym. st. of $-S(=O)_2$ part. The reason of appearance of doublet peak is expected to be the species is in two different sites of the Ar matrix. Strong absorption of SO_2 around 1050 cm^{-1} could hide the sym. st. of $-S(=O)_2$ of $H-S(=O)_2$. However, possibility of the latter structure could not be removed. Although no infrared absorption bands in the spectra of all experiments could be assigned as O-H st. of H-O-S=O observed, there is an attractive explanation for appearance of two absorption bands if the species are H-O-S=O. These two are could be absorption bands of S=O st. of cis and trans structure of H-O-S=O, as observed in HONO[30]

There are no conclusively evidence in this stage. Further

study should be done to identify the spices.

(c) $HOSO_4$ Radical

Under the optimized conditions for observing $HOSO_2$ by co-depositing SO_2/Ar and H_2O_2/Ar under irradiation, a fraction of Ar in the SO_2 mixture was replaced by O_2. The $HOSO_2$ band intensity decreased drastically when only 4% of Ar was substituted by O_2 ($SO_2/O_2/Ar$ = 1/10/250). All the absorption bands of $HOSO_2$ disappeared for the codeposition of SO_2/O_2 and H_2O_2/O_2 during irradiation, but no new band was recognized except for the weak diffuse bands of unidentified products in the range of 1300~1280 cm^{-1} and the bands of O_3 at 2108, 1034 and 702 cm^{-1} as shown in Fig.5.2. Bands ascribed to SO_3 (1385.8 cm^{-1} in O_2 matrix)[31] and HO_2 (1391.6 cm^{-1})[14,15] were not observed either.

The disappearance of $HOSO_2$ suggests occurrence of the reaction with O_2, and $HOSO_4$ expected to be formed. But the absorption bands of the $S(=O)_2$ asym. and sym. stretching modes of $HOSO_4$ might be located in the very strong absorption band of SO_2. An ab initio calculation, as discussed in next section, predicts the frequencies of the $S(=O)_2$ asym. and sym. stretching modes are very close to those for SO_2, 1573 and 1341 cm^{-1}, respectively. Other absorption bands of $HOSO_4$ are thought to have weaker intensity than that of these two modes. The band overlapping could be the reason of the unobservation of $HOSO_4$ radical.

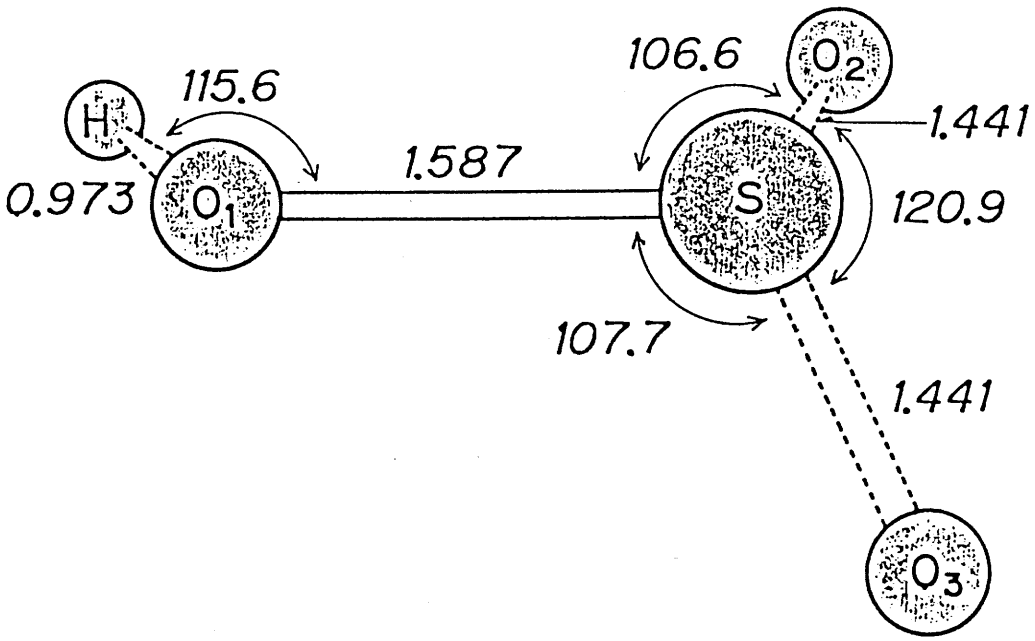

Fig.5.3. Optimized geometry of the $HOSO_2$ radical at the HF/3-21G(*) level. Distances are in A and angles are in degree. $\angle HO_1SO_2 = 1.3$.

5. Comparison with ab initio Calculations

(a) Molecular Structure of $HOSO_2$

TABLE V-II compares the observed vibrational frequencies of the $H^{16}OS^{16}O_2$ and $H^{18}OS^{16}O_2$ radicals with the calculated values obtained at the HF/3-21G(*) level. As shown in TABLE V-II, the calculated vibrational frequencies were 7.8, 0.7, 2.5 and 21.4 % higher than the observed ones for the H-O st., $S(=O)_2$ asym. st., $S(=O)_2$ sym. st. and S-OH st. mode, respectively. An uneven ratio of the calculated to observed frequencies of different vibrational modes has been noted[11] in the compounds containing hypervalent sulfur atoms. An important point to be noted in TABLE V-II is that the values and the trend of the ^{16}O-^{18}O isotope shift are reproduced satisfactorily for all the observed vibrational modes. TABLE V-III cites the vibrational fundamentals calculated for three isotopic species of $H^{16}OS^{16}O_2$, $H^{18}OS^{16}O_2$ and $H^{18}OS^{18}O_2$. The H-O-S bending mode as calculated at 1181 and 1175 cm^{-1} for the $H^{16}OS^{16}O_2$ and $H^{18}OS^{16}O_2$, respectively, would be overlapped by the strong absorption of SO_2 centered at ca. 1150 cm^{-1}. All other low frequency modes should appear out of observation range. Thus, the identification of the infrared bands of the $HOSO_2$ radical has been strongly supported by the additional experimental evidence and the theoretical prediction.

Fig.5.3 presents the HF/3-21G(*) optimized geometry of the $HOSO_2$ radical. As shown in Fig.5.3, the structure of $HOSO_2$ is non-planar, as found by Boyed et al.[10] with the smaller STO-3G(*) basis set. The S=O bond length of 1.441A in $HOSO_2$ is appreciably longer than the calculated (1.419A) and experimental

(1.431A)[32] values in SO_2. This should explain the lowered experimental frequencies of the $S(=O)_2$ asym. and sym. stretching mode, 1309 and 1097 cm^{-1}, respectively, as compared to those for SO_2, 1356 and 1153 cm^{-1} in the Ar matrix.[31] The calculated HO-S bond length of 1.587A is close to the observed value of 1.574A[33] for H_2SO_4, which would represent a typical single bond.

The nature of the radical is better understood from the atomic spin densities and net atomic charges shown in TABLE V-IV. The spin densities are delocalized on all three atoms of the $-SO_2$ group. It should also be noted that the S, H, O_1, O_2, and O_3 atoms are highly charged implying a substantial polarization in all the associated bonds. This gives a large dipole moment of 2.88D (3-21G(*)) and 2.91D (6-31G**//3-21G(*)) to the radical. The characteristics of the electronic structure of $HOSO_2$ may be represented by the following resonance structures;

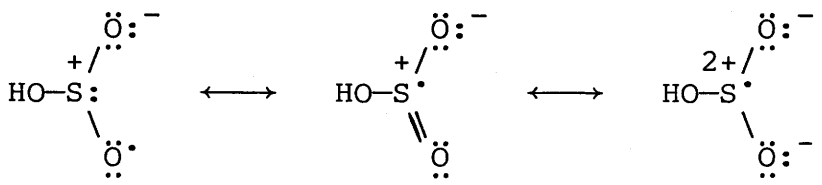

(I) (II) (III)

where the counterpart of the equivalent structures for (I) and (II) are omitted.

It would be interesting here to compare the results to those reported by Boyed et al.[10] with the STO-3G(*) basis. It can be seen that the greatest spin density resides on the S atom, and the extent of the charge polarization is more pronounced at the

6-31G** and 3-21G(*) levels than at the STO-3G(*) level, suggesting more significant contribution of the resonance structures (II) and (III) at the higher calculation levels. The $S-O_1$, $S-O_2$, $S-O_3$ and $H-O_1$ bond lengths by the STO-3G(*) basis set are 1.629, 1.474, 1.465 and 0.994A, respectively, and are all longer by 3~4% than those given in Fig.5.3.

TABLE V-II. Observed and Calculated Fundamental Frequencies of $H^{16}OS^{16}O_2$ and $H^{18}OS^{16}O_2$

Vibrational Mode	$H^{16}OSO_2$ $H^{18}OSO_2$	Wavenumber (cm^{-1}) Calc.	Exp.	Ratio Calc./Exp.
H-O st.	^{16}O	3818	3539.9	1.078
	^{18}O	3805	3528.6	1.078
	shift(a)	13	11.3	-
SO_2 asym.st.	^{16}O	1319	1309.2	1.007
	^{18}O	1318	1308.7	1.007
	shift	1	0.5	-
SO_2 sym.st.	^{16}O	1125	1097.3	1.025
	^{18}O	1122	1096.0	1.024
	shift	3	1.3	-
S-OH st.	^{16}O	921.9	759.5	1.214
	^{18}O	889.3	735.1	1.210
	shift	32.6	22.4	-

(a) Isotope shift (cm^{-1}).

TABLE V-III. Calculated Vibrational Frequencies of Isotopically Labeled $HOSO_2$ Radicals

Vibrational Mode	Vibrational Frequencies (cm^{-1})		
	$H^{16}OS^{16}O_2$	$H^{18}OS^{16}O_2$	$H^{18}OS^{18}O_2$
1 H-O st.	3818	3805	3805
2 SO_2 asym. st.	1319	1318	1280
3 H-O-S in-plane bend	1181	1175	1162
4 SO_2 sym. st.	1125	1122	1084
5 S-OH st.	922	889	883
6 SO_3 deform.	544	542	528
7 SO_2 sciss.	491	485	468
8 SO_3 deform.	437	430	419
9 H-O-S out-of-plane bend	252	250	250

TABLE V-IV. Calculated Electronic Properties of $HOSO_2$

Atom	Atomic Spin Densities			Net Atomic Charges		
	STO-3G(*)	3-21G(*)	6-31G**	STO-3G(*)	3-21G(*)	6-31G**
H	-0.01	0.01	0.00	0.23	0.45	0.41
O_1	0.12	0.08	0.07	-0.24	-0.71	-0.65
S	0.18	0.34	0.42	0.42	1.33	1.39
O_2	0.38	0.24	0.22	-0.21	-0.57	-0.61
O_3	0.33	0.34	0.29	-0.20	-0.50	-0.54

(b) $HOSO_4$ radical

The $HOSO_4$ radical is located as a minimum on the potential energy surface. The HF/3-21G(*) optimized geometry of the $HOSO_4$ radical is shown in Fig.5.4. As depicted in Fig.5.4, the S-O bond configuration around the S atom is similar to that of H_2SO_4. The S=O bond distances (1.414 and 1.406 A) are appreciably shorter than those in the $HOSO_2$ discussed before and are close to the calculated value for SO_2 (1.419A) and also to the experimental value[33] in H_2SO_4 (1.422A). The calculated HO-S and S-OO bond distances (1.549 and 1.620A, respectively) are slightly shorter and appreciably longer than the observed HO-S bond length[33] in H_2SO_4 (1.574A), respectively, suggesting a lower bond energy for the S-OO than for HO-S. Calculated electronic properties of the $HOSO_4$ radical are given in TABLE V-V. The spin density is almost localized on the terminal oxygen atom giving the features of a more common peroxy radical to the $HOSO_4$ radical. The S atom is highly, positively charged and the four surrounding O atoms are all negatively charged. Thus, the bonds in the $HOSO_4$ radical are highly polarized as in the case of $HOSO_2$ giving an even larger dipole moment of 3.16D(3-21G(*)) and 3.22D(6-31G**//3-21G(*)).

The calculated vibrational frequencies are: 3835, 1588, 1349, 1184, 1025, 929, 680, 626, 564, 552, 449, 416, 312, 233 and 107 cm^{-1}. Apparently, the first five frequencies correspond mainly to the H-O stretching, $S(=O)_2$ asymmetric and symmetric stretching, H-O-S in plane bending, and S-OH stretching mode, respectively. All the lower frequency modes reflect mixed motion

of molecules and the exact assignment is not possible without potential energy analysis, which were not made in the present study. The predicted frequencies of the $S(=O)_2$ asym. and sym. stretching modes are very close to those for SO_2 (1573 and 1341 cm^{-1}, respectively) calculated with the same basis set[11], reflecting the close S=O bond distances.

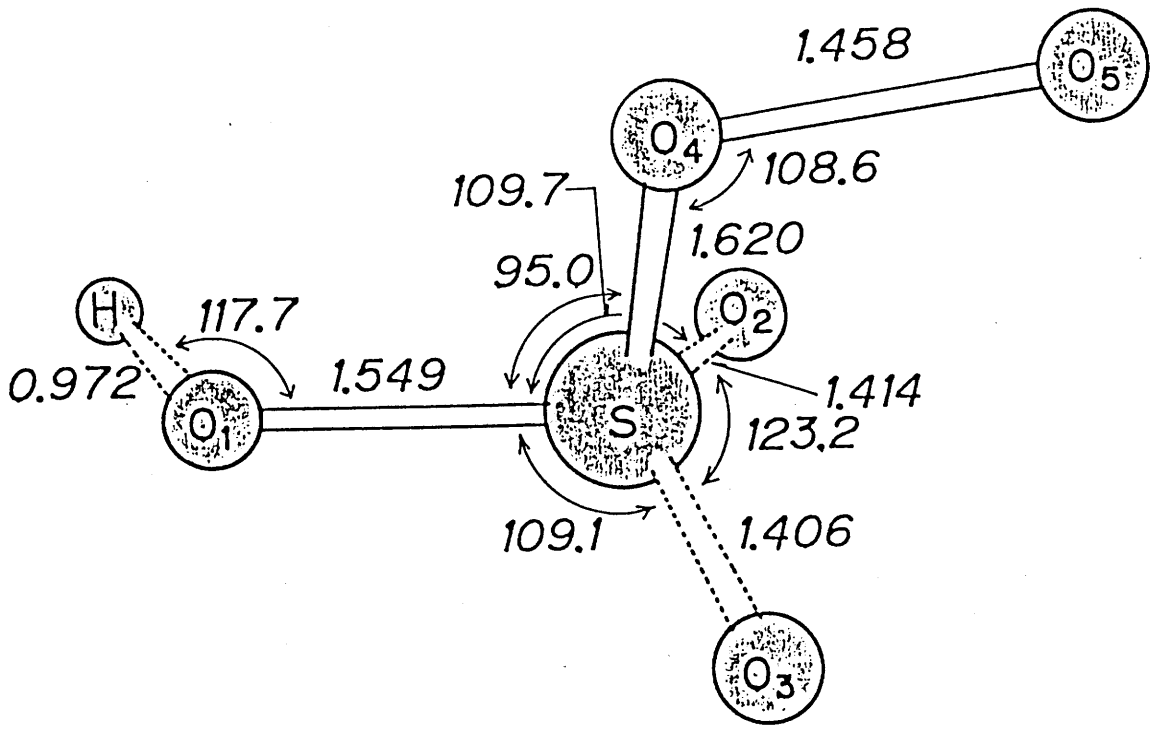

Fig.5.4 Optimized geometry of the $HOSO_4$ radical at the HF/3-21G(*) level. Distances are in A and angles are in degree. $\angle HO_1SO_2 = 0.5$; $\angle O_5O_4SO_1 = 179.1$; $\angle O_4SO_1O_2 = 89.4$.

TABLE V-V. Calculated Electronic Properties of $HOSO_4$

Atom	Atomic Spin Densities		Net Atomic Charges	
	3-21G(*)// 3-21G(*)	6-31G**// 3-21G(*)	3-21G(*)// 3-21G(*)	6-31G**// 3-21G(*)
H	0.00	0.00	0.47	0.42
O_1	-0.01	0.00	-0.69	-0.63
S	0.00	0.00	1.65	1.73
O_2	0.00	0.00	-0.56	-0.61
O_3	0.00	0.00	-0.52	-0.57
O_4	-0.20	-0.18	-0.42	-0.39
O_5	1.21	1.18	0.08	0.06

6. Conclusion

The IR absorption spectrum of sulfo ($HOSO_2$) radical, an important intermediate of atmospheric oxidation of SO_2, was obtained in argon matrix at 11K in the reaction of SO_2 and OH prepared by the photolysis of H_2O_2 or H_2O during deposition. The IR absorption bands of $H^{18}OSO_2$ were also obtained by using $H_2{}^{18}O$ as a hydroxyl radical source. Observed vibrational frequencies at 3539.9 (3528.6), 1309.2 (1308.7), 1097.3 (1096.0) and 759.5 (735.1) cm^{-1} were assigned as the O-H st., $S(=O)_2$ asym. st., $S(=O)_2$ sym. st. and S-OH st. modes of the $H^{16}OS^{16}O_2$ ($H^{18}OS^{16}O_2$) radical, respectively. Absorption bands at 1286.8 and 1285.4 cm^{-1} were also appeared. These could be assigned as $H-S(=O)_2$ which is a reaction product of H + SO_2. Sulfo radical was characterized by use of ab initio calculations at the HF/3-21G(*) level. The calculated vibrational frequencies and the isotope shift support the assignment of the observed infrared absorption bands in the Ar matrix. The same calculation was attempted to the peroxybisulfate ($HOSO_4$) radical. It was found to be located as a minimum on the potential surface. The fully optimized geometry and vibrational frequencies was obtained, although the detection of the radical in the O_2 matrix was not successful.

References

1) Calvert, J.G.; Stockwell, W.R. "SO_2, NO and NO_2 Oxidation Mechanism: Atmospheric Consideration", Butterworth: Boston, 1984: Chapter 1 and references therein.

2) Stockwell, W.R.; Calvert, J.G. Atmos. Environ. 1983, 17, 2231.

3) Margitan, J.J. J. Phys. Chem. 1984, 88, 3014.

4) Schmidt, V.; Zhu, G.Y.; Becker, K.H.; Fing, E.H. Ber. Bunsenges. Phys. Chem. 1985, 89, 321.

5) Martin, D.; Jourdain, J.L.; Le Bras, G. J. Phys. Chem.1986, 90, 4143.

6) Gleason J.F.; Sinha A.; Howard, C.J. J. Phys. Chem. 1987, 91, 719.

7) Benson, S.W. Chem. Rev. 1978, 78, 23.

8) Mckeen, S.A.; Liu, S.C.; Kiang, C.S. J. Geophys. Res. 1984, 89, 4873.

9) Flockhart, B.D.; Ivin, K.J.; Pink, R.C.; Sharma, B.D. J. Chem. Soc. Chem. Commun. 1971, 339.

10) Boyed, R.J.; Gupte, A.; Langler, R.F.; Lownie, S.P.; Pinock, J.A. Can. J. Chem. 1980, 58, 331.

11) Pietro, W.J.; Francl, M.M.; Hehre, W.J.; DeFrees, D.J.; Pople, J.A.; Binkley, J.S. J. Am. Chem. Soc. 1982, 104, 5039.

12) Francl, M.M.; Pietro, W.J.; Hehre, W.J.; Binkley, J.S.; Gordon, M.S.; DeFrees, D.J.; Pople, J.A. J. Chem. Phys. 1982, 77, 3654.

13) MP2: Binkley, J.S.; Pople, J.A, Int. J. Quantum Chem., Symp. 1975, 9, 229. MP3: Pople, J.A.; Binkley, J.S.; Seeger, R.

Int. J. Quantum Chem., Symp. **1976**, 10, 1. MP4: Krishnan, R.; Frisch, M.J.; Pople, J.A. J. Chem. Phys. **1980**, 72, 4244.

14) **a.** Jacox, M.E.; Milligan, D.E. J. Mol. Spectry. **1972**, 42, 495. **b.** Milligan, D.E.; Jacox, M.E. J. Chem. Phys. **1963**, 38, 2627.

15) Smith, D.W.; Andrews, L. J. Chem. Phys. **1974**, 60, 81.

16) Acquista, N.; Schoen, L.J.; Lide, D.R. J. Chem. Phys. **1968**, 48, 1968.

17) Hopkins, A.G.; Brown, C.W. J. Chem. Phys. **1975**, 62, 2511.

18) Thomas, R.K.; Thompson, H. Proc. Roy. Soc. **1970**, A314, 329.

19) Sodeau, J.R.; Lee, E.K.C. J. Phys. Chem. **1980**, 84, 3358.

20) Hopkins, A.G.; Daly, F.P.; Brown, C.W. J. Phys. Chem. **1975**, 79, 1849.

21) Lannon, J.A.; Verderame, F.D.; Anderson Jr., R.W. J. Chem. Phys. **1971**, 54, 2212.

22) Glasel, J.A. J. Chem. Phys. **1960**, 33, 252.

23) Redington, R.L.; Milligan, D.E. J. Chem. Phys. **1962**, 37, 2162.

24) Ayers, G.P.; Pullin, A.D.E. Spectrochem. Acta, **1976**, 32A, 1629.

25) Allavena, M.; Rysnik, R. White, D.; Calder, V.; Mann, D.E. J. Chem. Phys. **1969**, 50, 3399.

26) Lew, M.T. J. Phys. Chem. **1982**, 86, 4558.

27) Harris, G.W.; Atkinson, R; Pitts Jr. J.N. Chem. Phys. Lett. **1980**, 69, 378.

28) Pinchas S.; Laulicht, I. Infrared Spectra of Labelled Compounds", Academic Press, London, **1971**.

29) Swardzewski, R.R.; Lin, M.C. J. Chem. Phys. 1977, 66, 3197.

30) Baldeschwieler, J.D.; Pimentel, G.C. J. Chem. Phys. 1960, 33, 1008.

31) Tso, T-L.; Lee, E.K.C. J. Phys. Chem. 1984, 88, 2776.

32) Morino, Y.; Kikuchi, Y.; Saito, S.; Hirota, E. J. Mol. Spectrosc. 1984, 13, 95.

33) Kuczkowski, P.L.; Suenram, R.D.; Lovas, F.J. J. Am. Chem. Soc. 1981, 103, 2561.

APPENDIX: List of Publication

(a) CT Excited Photochemical Reactions of Unsaturated Organic Molecules in Cryogenic Oxygen Matrices

1) "Visible light photooxygenation of 2,3-dimethyl-2-butene at the contact charge transfer band in the cryogenic oxygen matrix"
Satoshi Hashimoto and Hajime Akimoto, J. Phys. Chem., **1986**, 90, 529-532.

2) "Absorption spectra of contact charge transfer bands and photochemical reactions of simple alkenes in the cryogenic oxygen matrix"
Satoshi Hashimoto and Hajime Akimoto, J. Phys. Chem., **1987**, 91, 1347-1354.

3) "UV absorption spectra of contact charge transfer bands and photochemical reactions of simple aromatic hydrocarbons in the cryogenic oxygen matrix"
Satoshi Hashimoto and Hajime Akimoto, submitted to J. Phys. Chem. in press.

4) "Contact charge transfer excited reaction of ketene, methylketene, dimetylketene and acetone in the cryogenic oxygen matrices"
Satoshi Hashimoto and Hajime Akimoto, Should be published.

(b) The Direct Spectroscopic Detection of HSO_x Radicals as Reaction Intermediates of Atmospheric Importance

5) "Infrared spectroscopic detection of the $HOSO_2$ radical in argon matrix at 11K"
Satoshi Hashimoto, Gen Inoue and Hajime Akimoto, Chem. Phys. Lett., **1984**, 107, 198-202.

6) "$HOSO_2$ and $HOSO_4$ radicals studied by ab initio calculation and matrix isolation technique"
Shigeru Nagase, **Satoshi Hashimoto** and Hajime Akimoto, J. Phys. Chem., **1988**, 92, 641-644.